

MECHANICS OF DILATANCY AND ITS APPLICATION TO LIQUEFACTION  
PROBLEMS

By

NAVARATNARAJAH SASIHARAN

A dissertation submitted in partial fulfillment of  
the requirements for the degree of

DOCTOR OF PHILOSOPHY

WASHINGTON STATE UNIVERSITY  
Department of Civil and Environmental Engineering

December 2006

To the Faculty of Washington State University:

The members of the Committee appointed to examine the dissertation of  
NAVARATNARAJAH SASIHARAN find it satisfactory and recommend that it be  
accepted.

---

Chair

---

---

---

---

## ACKNOWLEDGEMENT

It is rather difficult to try to express in just few lines, my gratitude to all the people who helped me, in one way or another, to accomplish this work. I hope that those that I have mentioned realize that my appreciation extends far beyond the ensuing paragraphs.

First and foremost, I would like to thank my supervisor and mentor Dr. Muhunthan for persuading me to continue my studies toward PhD degree. I will always be indebted to him for his guidance, motivation and friendship. His enthusiasm and integral view on research and his mission for providing 'only high-quality work and not less', has made a deep impression on me which I will always cherish the rest of my life. I owe him lots of gratitude for having me shown this way of research. He could not even realize how much I have learned from him. I am really glad and proud that I have had an opportunity to work closely with such a wonderful person.

I wish to thank Dr. Adrian Rodriguez-Marek, Dr. William Cofer and Dr. Hussein Zbib for serving on my PhD committee. Special thanks are due to Dr. Rodriguez-Marek for many interesting discussions on dynamic modeling of soils.

My gratitude also goes to my colleagues in GeoTransportation group, especially Senthil, Farid, Mehrdad, Muthu, Suren, Gonzalo and Habtamu.

Financial support by the National Science Foundation (NSF), Federal Highway Administration (FHWA), and Washington State University is acknowledged with gratitude.

Last but certainly not least, I would like to express my deepest gratitude for the continuous support, caring, understanding and love that I received from my wife Lojini. Similar appreciation is extended to my mother, sister, brother-in-law, and nephew. The timely visit of my parent in-laws to Pullman helped recharge my batteries and finish up this dissertation. Thank you all.

# MECHANICS OF DILATANCY AND ITS APPLICATION TO LIQUEFACTION

## PROBLEMS

### Abstract

by Navaratnarajah Sasiharan, Ph.D.  
Washington State University  
December 2006

Chair: Balasingam Muhunthan

A novel conceptual model of the mechanics of sands is developed within an elastic-plastic framework. Central to this model is the realization that volume changes in anisotropic granular materials occur as a result of two fundamentally different mechanisms. The first is purely kinematic, dilative, and is the result of the changes in anisotropic fabric. There is also a second volume change in granular media that occurs as a direct response to changes in stress as in a standard elastic-plastic continuum. Inclusion of the two sources of volume change into the modified Cam Clay dissipation function results in a new anisotropic model which is suitable for sands with pronounced anisotropic granular arrangement. The conditions that lead to features such as phase transition line and ultimate state line that dense sands exhibit are predicted theoretically by the new anisotropic sand model and confirmed with experimental results. The conventional volumetric-shear strain relation obtained from triaxial experiment is used to determine the evolution of fabric anisotropic parameter.

The new anisotropic sand model is generalized to 3-D cases. Bounding surface plasticity theory is used to capture plastic deformation at small strain levels as well as during unloading/reloading. This enables the robust modeling of the accumulation of

plastic strains as well as the buildup of excess pore pressure under cyclic loading of sands. The bounding surface formulation is implemented to the numerical code FLAC3D and used to simulate drained and undrained triaxial tests on Ottawa sand. The FLAC3D model is also used to simulate undrained cyclic triaxial test and predict the liquefaction behavior of Nevada sand observed in centrifuge tests. The analysis shows that the stress induced volumetric strain is the main cause for pore pressure build up leading to initialization of liquefaction whilst the fabric induced volumetric strain influences the post liquefaction behavior of sands.

## TABLE OF CONTENTS

	Page
ACKNOWLEDGEMENTS .....	iii
ABSTRACT .....	iv
LIST OF TABLES .....	ix
LIST OF FIGURES .....	x
CHAPTER 1: INTRODUCTION.....	1
1.1 General.....	1
1.2 Objectives of study .....	4
1.3 Organization of Thesis .....	6
CHAPTER TWO: BACKGROUND .....	8
2.1 Liquefaction .....	8
2.2 Flow liquefaction and cyclic mobility .....	9
2.3 Issues in laboratory testing.....	11
2.4 Schofield's view of liquefaction .....	15
2.5 Plasticity in soil mechanics .....	18
2.6 Granular Dilatancy.....	22
2.7 Cam Clay models.....	26
2.8 Critical state based sand model.....	28
2.8.1 Improved stress-dilatancy rule.....	29
2.8.2 Shear hardening .....	32
2.8.3 Non-associative flow rule .....	33

2.8.4 Double hardening models .....	34
2.8.5 Stored plastic work .....	35
CHAPTER 3: THE NEW ANISOTROPIC SAND MODEL.....	37
3.1 General.....	37
3.2 Fabric measure based on void space.....	38
3.3 Fabric change due to deformation.....	40
3.4 Decomposition of plastic strain .....	44
3.5 Yield loci of anisotropic sand .....	46
3.6 Datum states of dilatancy.....	49
CHAPTER 4: MODEL PARAMETERS .....	53
4.1 Experimental observations.....	53
4.2 Critical state line .....	58
4.3 Evolution of fabric anisotropic parameter .....	60
CHAPTER 5: BOUNDING SURFACE SAND MODEL.....	63
5.1 General.....	63
5.2 Classical plasticity .....	65
5.3 Kinematic hardening models .....	68
5.3.1 Multi – surface plasticity model .....	69
5.4 Bounding surface plasticity.....	71
5.5 New sand model in $q - p$ space.....	74
5.5.1 Elastic strains .....	75
5.5.2 Plastic strains .....	75
5.5.3 Formulation of incremental stress-strain relations.....	77

5.5.4 Model prediction .....	77
5.6 Generalization of new sand model.....	83
CHAPTER 6: MODEL IMPLEMENTATION .....	85
6.1 General.....	85
6.2 Dynamic analysis .....	85
6.3 Modeling dynamic pore pressure generation.....	87
6.4 Explicit, Dynamic Solution (EDS) Scheme.....	87
6.5 Mechanical time step for numerical stability.....	91
6.6 Mixed discretization.....	93
6.6 Model implementation .....	96
CHAPTER 7: FLAC3D ANALYSIS AND RESULTS .....	100
7.1 Monotonic laboratory triaxial test.....	100
7.2 Cyclic laboratory triaxial test.....	108
7.3 Centrifuge testing.....	109
7.3.1 Numerical model of the centrifuge .....	111
7.3.2 Results of numerical analysis.....	113
7.4 Coupled analysis .....	118
CHAPTER 8: CONCLUSIONS AND RECOMMENDATIONS.....	124
7.1 Conclusions.....	124
7.2 Recommendations for further research.....	127
REFERENCES .....	129

## LIST OF TABLES

	Page
Table 4-1: Summary of model parameters.....	62
Table 7-1: Material parameters of Ottawa sand.....	102
Table 7-2: Combinations of mean effective pressure and void ratio for the triaxial monotonic tests .....	102
Table 7-3: Material parameters of Nevada sand .....	110

## LIST OF FIGURES

	Page
Figure 2-1: Schematic diagram of flow liquefaction .....	9
Figure 2-2: Schematic diagram of cyclic mobility .....	11
Figure 2-3: Stress-Strain Response of Undisturbed and Water Pluviated Samples (Vaid et al., 1999) .....	12
Figure 2-4: Influence of Sample Preparation Method on Soil Behavior (Vaid et al., 1999) .....	13
Figure 2-5: Different structures due to the mode of reconstitution of Hostun-RF sand (after Benahmed 2001) .....	14
Figure 2-6: Schematic of limits of stable states of soils (a) normalized $q/p_{crit} - p/p_{crit}$ stress space (b) $v - \ln p$ space (Pillai and Muhunthan, 2002)...	17
Figure 2-7: Taylor's shear box analogy (Deshpande and Cebon, 1999) .....	23
Figure 2-8: Normalized OCC and MCC yield curves .....	27
Figure 3-1: The coordinate system used in the void fabric tensor analysis .....	40
Figure 3-2: Schematic description of volume changes in void and solid skeleton .....	42
Figure 3-3: Yield locus of new anisotropic sand model with different $\alpha$ values .....	48
Figure 3-4: Features of new anisotropic sand model .....	51
Figure 3-5: Dilatancy datum in compressive and extensive sides .....	52
Figure 4-1: Grain Size Distribution for Ottawa F-35 Sand and Glass Beads .....	54
Figure 4-2: Typical drained test results on Ottawa sand .....	56
Figure 4-3: Variation of $\zeta_m$ with shear strain .....	57
Figure 4-4: The relocation of the CSL as a function of the anisotropy parameter $A$ .....	59
Figure 4-5: Variation of maximum anisotropy with $v_k$ .....	62
Figure 5-1: Schematic illustration of the bounding surface in a general stress space .....	73
Figure 5-2: Bounding surface illustration in $q-p$ space for the new sand model .....	76

Figure 5-3: Simulation of drained triaxial test (a) stress path in $q - p$ space (b) shear stress vs. shear strain (c) volumetric strain vs. shear strain .....	79
Figure 5-4: Simulation of undrained triaxial test (a) stress path in $q - p$ space (b) shear stress vs. shear strain .....	80
Figure 5-5: Typical loading-unloading stress path .....	81
Figure 6-1: Calculation loop of EDS scheme in FLAC3D .....	54
Figure 6-2: Deformation model for which mixed discretization would be most efficient .....	95
Figure 6-3: An 8-node zone with 2 overlays of 5 tetrahedra in each overlay .....	96
Figure 6-4: Flow chart for coding the constitutive model .....	99
Figure 7-1: FLAC3D single zone; boundary conditions .....	101
Figure 7-2: Measurements and prediction of drained tests at 100 kPa with different void ratios of 0.637, 0.681, 0.715 (a) shear stress vs. shear strain (b) volumetric strain-shear strain .....	103
Figure 7-3: Measurements and prediction of drained tests at 200 kPa with different void ratios of 0.676, 0.699, 0.739 (a) shear stress vs. shear strain (b) volumetric strain-shear strain .....	104
Figure 7-4: Measurements and prediction of drained tests at 400 kPa with different void ratios of 0.640, 0.679, 0.722 (a) shear stress vs. shear strain (b) volumetric strain-shear strain .....	105
Figure 7-5: Measurements and prediction of drained tests at 600 kPa with different void ratios of 0.670, 0.699, 0.731 (a) shear stress vs. shear strain (b) volumetric strain-shear strain .....	106
Figure 7-6: Measurements and prediction of drained tests at void ratio of 0.640 with different mean effective pressures of 100, 400, 750 kPa (a) shear stress vs. shear strain (b) shear stress vs. mean effective pressure .....	107
Figure 7-7: Measurement of cyclic triaxial test on Nevada sand consolidated at 80 kPa and void ratio of 0.65 .....	108
Figure 7-8: Prediction of cyclic triaxial test on Nevada sand consolidated at 80 kPa and void ratio of 0.65 .....	108

Figure 7-9: Centrifuge model arrangement.....	110
Figure 7-10: FLAC3D model of centrifuge testing .....	112
Figure 7-11: Acceleration input at the base .....	113
Figure 7-12: Shear stress – mean effective pressure variation in zone 1 .....	114
Figure 7-13: Experimental and prediction of pore pressure of transducer P1 .....	114
Figure 7-14: Experimental and prediction of pore pressure of transducer P2 .....	115
Figure 7-15: Experimental and prediction of pore pressure of transducer P3 .....	115
Figure 7-16: Experimental and prediction of pore pressure of transducer P4 .....	116
Figure 7-17: Experimental and prediction of acceleration of accelerometer AH3 .....	117
Figure 7-18: Experimental and prediction of acceleration of accelerometer AH4 .....	117
Figure 7-19: Experimental and prediction of acceleration of accelerometer AH5 .....	118
Figure 7-20: Shear stress – mean effective pressure variation in zone 1 .....	119
Figure 7-21: Experimental and prediction of pore pressure of transducer P1 .....	120
Figure 7-22: Experimental and prediction of pore pressure of transducer P2 .....	120
Figure 7-23: Experimental and prediction of pore pressure of transducer P3 .....	121
Figure 7-24: Experimental and prediction of pore pressure of transducer P4 .....	121
Figure 7-25: Experimental and prediction of acceleration of accelerometer AH3 .....	122
Figure 7-26: Experimental and prediction of acceleration of accelerometer AH4 .....	122
Figure 7-27: Experimental and prediction of acceleration of accelerometer AH5 .....	123

## *Chapter 1*

# **INTRODUCTION**

### **1.1 General**

The cost of remediation of liquefaction damages caused by recent earthquakes often ran into several billions of dollars. This emphasizes the need for the development of better deterministic tools to predict soil liquefaction and assess post-liquefaction stability of structures founded on liquefiable soils.

Liquefaction study has been directed mainly towards three different areas after the two devastating 1964 earthquakes in Niigata in Japan and the Great Alaska earthquake: field observations during and following earthquakes, laboratory experiments, and theoretical studies. Lack of instrumentation on most liquefaction failures observed in the field has made it impossible to obtain recordings of pore pressures and acceleration that induced liquefaction. Therefore, the investigation of liquefaction phenomena has often consisted of laboratory experiments and theoretical models. Laboratory experiments include cyclic triaxial, simple shear, torsional shear testing on samples obtained from the field by freezing or prepared in the laboratory by different methods. Centrifuge model testing has also provided a significant input towards developing a better understanding of liquefaction and related phenomena. Theoretical sand models have also been developed based on fundamental physics of granular soil behavior and applied to boundary value

problems. Realistic constitutive models provide several advantages to liquefaction study. These include better understanding of soil behavior, extrapolation to conditions that cannot be produced in laboratory testing and prediction of soil behavior through finite difference or finite element based numerical techniques so that the liquefaction analysis can be made on a rational basis.

The critical state framework developed by the Cambridge school in the 1960s has contributed immensely to the recent developments of comprehensive scientific approaches to study the shear response of soils. It has also contributed to a fundamental paradigm shift to soil mechanics and helped bring it properly within the ambit of continuum mechanics and plasticity theory. Nevertheless, the original critical state concepts were developed mainly based on the behavior of reconstituted, essentially isotropic, materials. Therefore, it is well appreciated that, whilst the original Cambridge critical state models, Cam Clay (Roscoe et al., 1963) and modified Cam Clay (Roscoe and Burland, 1968) work well for normally consolidated clays, significantly more complex models are required to capture the essential properties of the mechanics of sands as well as anisotropically consolidated clays. Recent experimental information has also shown that the behavior of natural soils, especially sands with pronounced fabric anisotropy, deviate significantly from the fundamental premises of the critical state soil mechanics. Moreover, Vaid et al. (1999) have showed that sample preparation methods (producing different fabric arrangement) greatly influence the stress-strain behavior of sands.

Such deviations have often been attributed qualitatively to the important granular aggregate fabric which was absent at the outset from the foundations of the original critical state theory. The absence of the elements of fabric in the fundamental postulates of the original critical state models has led to many ad hoc proposals relating to critical state concepts. Non-associated flow rules (Lade and Duncan,1975), some form of shear hardening (Nova and Wood, 1979), induced anisotropy (Lade,1979), double hardening concepts (Vermeer,1978), and the improved modeling of dilatancy (Li, 2000), have been added to the basic structure of critical state theory in order to obtain an acceptable degree of realism in soil models. Another approach is to introduce fabric related quantities into the basic structures of critical state soil mechanics. Sand models accounting for fabric anisotropy not only represent its behavior within the continuum framework, but also give more physical intuition to the parameters introduced. The present study falls in this category.

The advances indicated above proved to be successful in modeling the response of sands under static loads. The sand behavior under undrained cyclic loading, however, poses additional complexities in numerical modeling. Significant hysteretic behavior inside the yield surface is a feature of sands under cyclic loading. Moreover, during load reversal in cyclic load In addition, Bauschinger effect has been observed during load reversal in cyclic loading experiments. Isotropic hardening models cannot capture such effects. Moreover, permanent volumetric strains continue to accumulate with each loading-unloading cycle, which has been shown to be the predominant contributor for the build up of excess pore pressure that leads to liquefaction. In addition, the mechanical

response of solid grains is strongly coupled with the flow of the fluid in the pores of sands.

Extended plasticity concepts such as multi-surface (Mroz et al., 1981), bounding surface (Dafalias, 1986), or subloading surface (Hashiguchi, 1989, 1998) plasticity that were inspired by kinematic hardening laws, have been used to improve the applicability of monotonic sand models to cyclic loading. These concepts make it easy to account for the accumulated permanent volumetric strains that occur in sands during cyclic excitation in a unified manner. In order to relax some of the complexities that arise in the numerical formulation due to the coupling between two phases it is usually that the assumed undrained condition prevails during dynamic excitation. However, Seed (1979) reported that most of the liquefaction failures that occurred some time after the passage of the main shock were due to the redistribution of excess pore pressure. Thus, the liquefaction phenomenon is neither fully undrained nor fully drained. Therefore, a fully coupled formulation based on Biot's (1941) theory is needed to analyze liquefaction problems.

Recent advances to account for the complexity of sand behavior in cyclic loading has unfortunately resulted in a rapid increase in model constants where a majority of them defy physical intuition (Scott, 1988). Thus, more insight is needed into the controlling features of the mechanical behavior of granular masses (Scott, 1988). This may only come from a careful interpretation of granular volume changes from a microscopic point of view.

## 1.2 Objectives of study

This study aims to develop a physically based constitutive model for sand along the lines of the critical state soil mechanics. It examines the granular volume changes from a physical and microscopic point of view. It is recognized that plastic volume changes in sand and granular media, occur due to *two* reasons: (a) as a result of stress changes and (b) as a result of changes in fabric during shear deformations (the “Reynolds Effect”).

The two sources of the plastic volume change in granular media are used to develop a constitutive model for sand behavior under monotonic and cyclic loading using bounding surface plasticity theory. The model is subsequently implemented into the finite difference code FLAC3D and used to analyze liquefaction initiation. FLAC3D is a widely used commercial 3-dimensional geotechnical software that provides interfaces to implement user-defined constitutive models. The main objectives of the study are as follows:

### **Objective 1:** Development of a fabric constitutive model for granular soils

The mechanical behavior of granular media is influenced by their anisotropic fabric. The directional distribution of porosity in granular media is characterized here by a functional form. The kinematic relationship between fabric and plastic strain derived using this form results in the coupling of volumetric strain with shear strain through a fabric anisotropy parameter. There is also a second volume change in granular media that occurs as a direct response to changes in stress as in a standard elastic/plastic

continuum. This volumetric strain decomposition is used in the Modified Cam Clay dissipation function and used to develop an anisotropic sand model.

**Objective 2:** Extension of the model to cyclic loading conditions and application

The new sand is extended to cyclic loading 3-D conditions using bounding surface plasticity theory (Dafalias, 1986). Emphasis is placed on capturing the hysteretic behavior of sand and of excess pore pressure build up.

**Objective 3:** Implementation of the model into numerical codes

The new 3-D sand model is then implemented into FLAC3D. It makes use of FLAC3D feature that provides a user interface to implement new constitutive models. External constitutive models can be written in C++ and compiled as DLL (Dynamic Link Library) files that can be uploaded as needed in a FLAC3D simulation.

**Objective 4:** Liquefaction analysis

Implemented sand model is used in the liquefaction analysis. A centrifuge test was simulated and verified with measured test data.

### **1.3 Organization of the Thesis**

Chapter 2 presents a review of the terminologies and the mechanisms that are currently used to explain liquefaction failures. A brief history of plasticity theory as applied to soil mechanics is also presented. The chapter highlights the need to better

understand granular dilatancy and stress-dilatancy relationships. A review of modifications made to critical state theory to model sand behavior is also presented.

The representation of fabric and its changes with deformation is presented in Chapter 3. The developments relating to the decomposition of volumetric strains central to this study is also provided. Application of this volume decomposition into the modified Cam Clay dissipation function produces a new anisotropic sand model. The model produces three important dilatancy datum states. Their importance to sand models is discussed.

A description of the material parameters used in the soil model and their determination are provided in Chapter 4. The model parameters are determined using drained triaxial compression test results. In addition, a function describing the evolution of the fabric parameter is proposed.

Chapter 5 presents details of the classical plasticity theory and kinematic hardening laws used. This chapter introduces to the theory of bounding surface plasticity on which the new anisotropic sand model is formulated for implementation into the numerical code, FLAC3D. Formulation of the new sand model in  $q$ - $p$  space and generalization of it into six dimensions is also provided.

The implementation of the constitutive model into FLAC3D is detailed in Chapter 6. The Explicit, Dynamic Solution (EDS) scheme used in Itasca series software is introduced. Procedures used for dynamic analysis are also provided. The mechanical time step for numerical stability and mixed discretization technique are presented as well.

FLAC3D with the new constitutive model is used in Chapter 7 to simulate monotonic drained and undrained tests, cyclic triaxial tests, and a centrifuge test involving liquefaction. Performance of the new sand model is verified against the measured values.

A summary of the findings of the study as well as some recommendations for further research are presented in Chapter 8.

## *Chapter 2*

### **BACKGROUND**

#### **2.1 Liquefaction**

If loose saturated sand is subjected to ground vibration, it tends to compact and decrease in volume; if drainage is ceased, the tendency to decrease in volume leads to increase in pore water pressure. If the pore water pressure builds to the point at which it becomes equal to the overburden pressure, the sand loses its strength completely, and attains a liquefied state. Although the term liquefaction was first used by Hazen (1920) to explain the mechanism of flow failure of the hydraulic-filled Calaveras Dam in California it has now been used to describe a number of different, though related phenomena. The generation of excess pore water pressure under undrained loading conditions is a hallmark of all liquefaction phenomena.

The Niigata and Alaskan earthquakes of 1964 triggered the onset of earthquake induced liquefaction research. The flow slide of the San Fernando earth dam in the 1971 earthquake added further impetus to seismic liquefaction research. The damaging effects of liquefaction on infrastructure such as roads, buildings, bridges, dams, airports, and port facilities in the earthquakes of Loma Prieta, California, Kobe, Japan, and most recently in Sumatra, Indonesia have sustained research efforts in this area.

The study of liquefaction has consisted mainly of three different areas: field observations during and following earthquakes, laboratory experiments, and theoretical studies. The “critical void ratio” approach suggested by Casagrande (Casagrande, 1936) is perhaps the first scientific hypothesis to delineate conditions under which liquefaction might occur. Based on drained shearing tests in which dense sand expanded whereas very loose sand reduced its volume, he defined the *critical void ratio* as that at which drained shear takes place at constant volume. He supposed that liquefaction as the manifestation of flow failure of sand in states looser than the critical void ratio. The laboratory experiments of Seed and Lee (1966) showed that even dense sand develops positive pore water pressure under cyclic loading that leads to liquefaction. Increased laboratory experimentation and field observation since then has brought forth a number of liquefaction related terminologies. Flow liquefaction and cyclic mobility are the most commonly used among these terms to describe the excessive deformation that ensues as a result of the development of excess pore water pressure.

## **2.2 Flow liquefaction and cyclic mobility**

The typical behavior of saturated loose soils under both monotonic and cyclic undrained shear tests in laboratory experiments is depicted in Fig. (2-1). Loose soil tends to compact when sheared and, without drainage, pore water pressure increases. Shear stress increases monotonically to “peak” stress before it softens and reaches steady state strength. The points at which the softening occurs fall on a straight line called “instability” line (Lade and Pradel, 1990; Ishihara, 1993; Chu and Leong, 2002) or

sometimes the “Collapse” line (Sladen et al 1985). It was proposed that when the stress path reaches the instability line, the soil structure collapses leading to development of high pore pressures. This collapse phenomenon was hypothesized as the main reason for flow liquefaction (Casagrande, 1936, 1975; Castro, 1975).

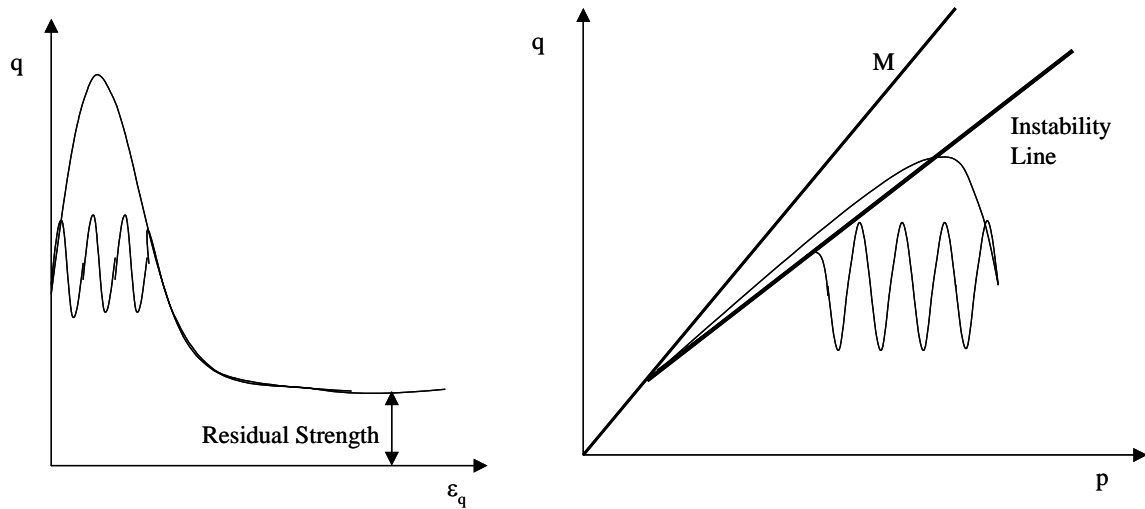


Figure 2-1: Schematic diagram of flow liquefaction

Fig. (2-2) shows the typical behavior of dense sand in monotonic and cyclic undrained loading. These sands initially contract followed by prepeak dilation before they reach the critical state line contrary to the behavior observed in loose sand under monotonic loading. They also develop much higher strength. The point at which the transition from contractive to dilative behavior occurs is termed the phase transition (Ishihara, 1978). Cyclic loading of the same sand, beyond the phase transition line leads to the development of large permanent strains; however, the sand does not collapse. This type of behavior is grouped into cyclic mobility. Lateral spreading, a subclass of cyclic mobility, is the lateral permanent deformation on a gentle slope. Damage caused by

lateral spreading, is severely disruptive and often pervasive. For example, during the Alaska earthquake of 1964, more than 250 bridges were damaged or destroyed by spreading of floodplain deposits toward river channels. Cumulatively, more damage has been reported by lateral spreads than any other form of liquefaction-induced ground failure (NRC, 1985).

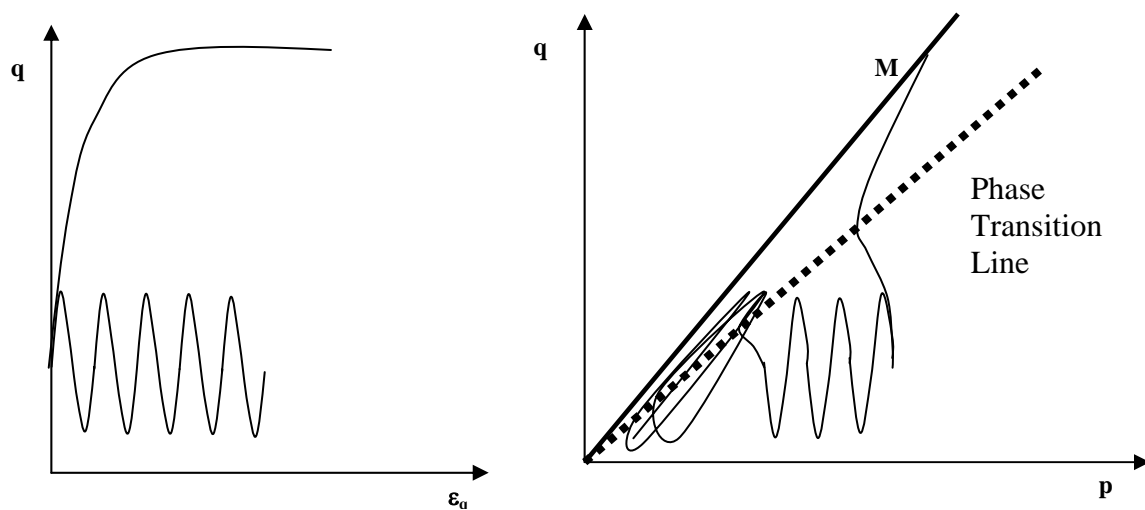


Figure 2-2: Schematic diagram of cyclic mobility

### 2.3 Issues in laboratory testing

Flow liquefaction and cyclic mobility phenomena are defined mainly based on laboratory experimental results. Therefore, the sample must be prepared such as to replicate the soil conditions at the field. There are several methods used to prepare soil sample in the laboratory such as moist tamping, dry deposition, and water sedimentation. Among them, Vaid et al. (1999) have shown that water sedimented specimens tend to

reproduce well field performance of sands. Water sedimented specimens are prepared by pluviating sand into a mold previously filled with water. Figure 2-3 shows the stress-strain response from undrained simple shear tests conducted on relatively “undisturbed” samples obtained from soil freezing and water sedimented samples of Massey and KIDD sands. It can be seen that water deposited specimen simulates the field behavior quite well. Furthermore, water deposited samples tend to show dilative behavior even when prepared in their loosest state (Vaid et al., 1999).

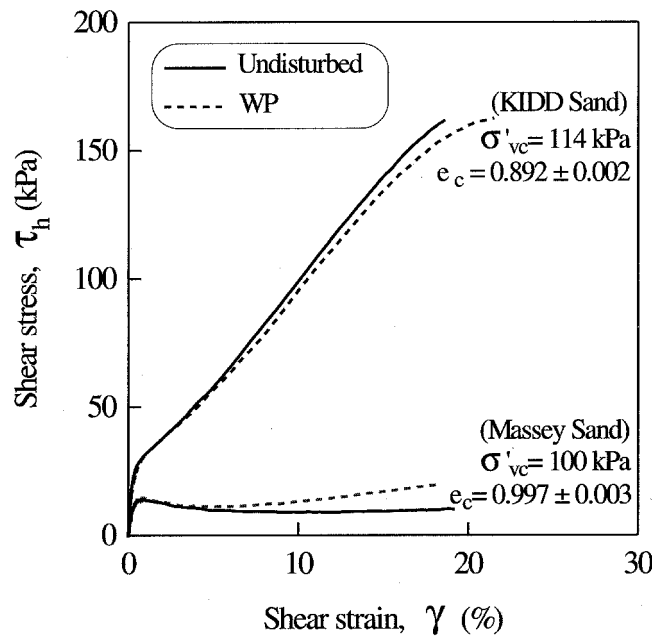


Figure 2-3: Stress-Strain Response of Undisturbed and Water Pluviated Samples (Vaid et al., 1999)

Figure 2-4 shows stress-strain curves obtained from triaxial compression tests on moist compacted and water pluviated samples of Fraser River sand prepared at the same

void ratio. It can be seen that the water pluviated sample shows dilative behavior whilst the moist tamped sample shows contractive behavior. Benahmed (2001) observed different structure formation when a sample of Hostun-RF sand is prepared by moist tamping and dry deposition (See Fig. 2-5). Casagrande (1976) described moist tamped

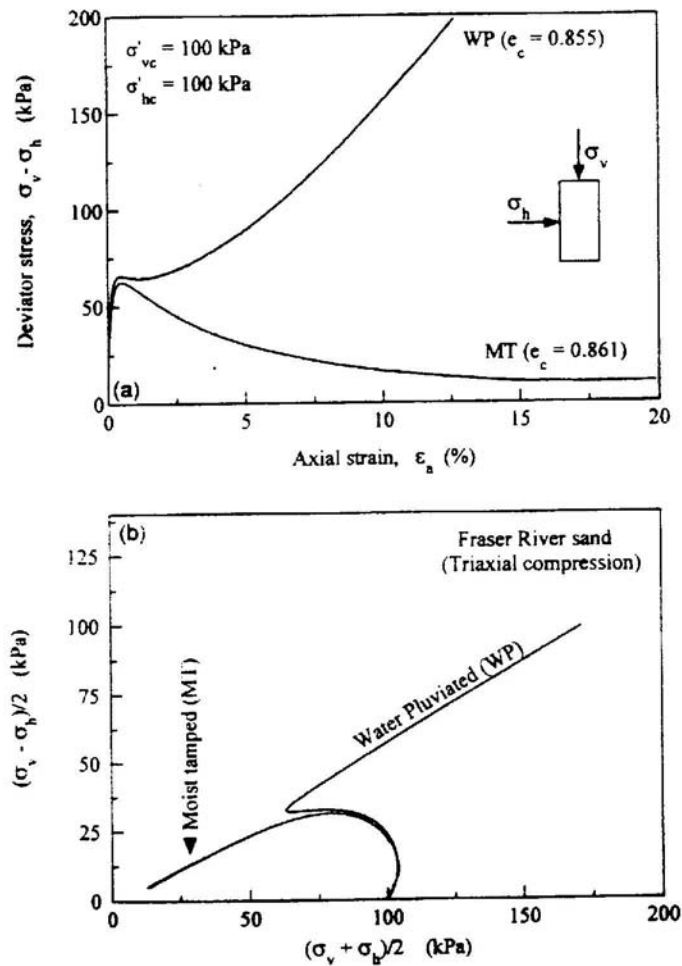
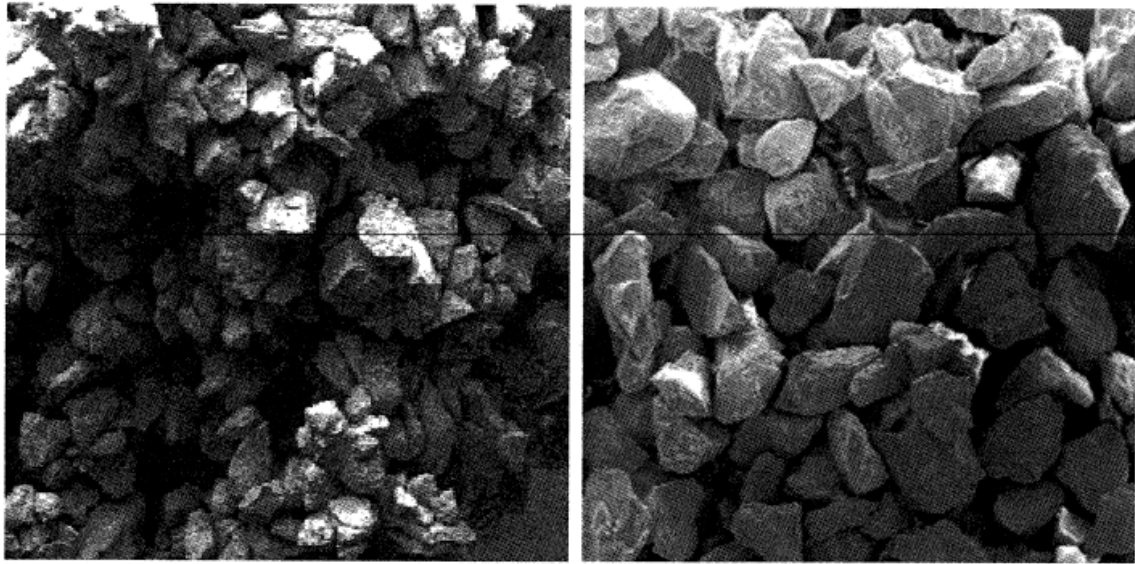


Figure 2-4: Influence of Sample Preparation Method on Soil Behavior (Vaid et al., 1999)

sands as meta-stable due to their honeycomb structure. This structure is reflected in the stress-strain curve from samples prepared at higher void ratios, where a complete collapse of the sample and a significant reduction in strength can often be found (Fig.2-4). The meta-stable structure is most likely due to the small amount of water added to the soil when compacting the soil into the mold. The small amount of water creates menisci in the soil fabric, allowing for higher void ratios than the ASTM maximum, which get destroyed upon final saturation (Terzaghi et al., 1996). The result is a structure that may not be the most favorable, and prone to collapse.

Nevertheless, it is surprising to see the continued interest to simulate static liquefaction of saturated loose sands under undrained loading in laboratory specimens by using moist tamping preparation (e.g. Castro, 1969; Verdugo, 1992, Cubranovski and Ishihara 1998; Yoshimine et al. 1998). Such tests conducted on the behavior of moist tamped specimens have led to many proposals on the nature and existence of the critical state line of sands and liquefaction failures. It is only recently experimental (Vaid et al., 1999) as well as conceptual models (Wood, 2001) that have questioned the validity of the use of such experimentation to geotechnical practice. There is no natural process by which a similar structure as moist tamped specimen would form in the field (Wood, 2001). In addition, the formation of capillary forces with addition of small moisture effectively ensures that such sand is partially saturated and its behavior must be described based on a two pore size model (Wood, 2001).



(a) Moist tamping deposition

(b) Dry deposition

Figure 2-5: Different structures due to the mode of reconstitution of Hostun-RF sand (after Benahmed 2001)

Been and Jefferies (2004) investigated the stress-dilatancy behavior of very loose sand and found that the stress-dilatancy trends of very loose sand are the same as those of dense sand. They also discussed the collapse/instability line in terms of mobilized stress ratio and concluded that there is neither physical basis nor evidence to support the phenomenon of soil structure collapse. They thus proposed that “explanations of sand liquefaction must seek other physical explanations of the soil behavior”. We present here the view of liquefaction by Professor Andrew Schofield of Cambridge University that offers to provide an alternate view of liquefaction.

#### **2.4 Schofield’s view of liquefaction**

Schofield (1980, 2005) has given a new perspective of the liquefaction phenomenon within the framework of critical state theory. He has argued that the

formation of flow structure as suggested by Casagrande (1936) and phenomenon of collapse is impossible in a real situation based on his centrifuge test results (Schofield, 1980). He further hypothesized that liquefaction is the result of rapid transmission of pore water pressures through soil at states near zero effective pressures. At near zero effective pressures, micro cracks form and in the presence of high hydraulic gradient it will lead to catastrophic failure: liquefaction (Schofield, 1982 & 2005).

In the critical state soil mechanics framework, three classes of behavior are recognized; namely, yielding, rupturing, and fracturing (Fig.2-6). On the “wet” or “stable-loose” side of the critical states, the soil yields at lower than critical deviatoric stress, and there may be massive plastic deformation, with rise in pore water pressures. This, however, is not the phenomenon which is described as liquefaction. The test paths that lead to liquefaction are those which exhibit reduction in effective stresses and move away from critical states on the “dry” or “stable-dense” side towards zero effective stress. At near zero effective stress, i.e. when the stress path reaches crack surface (Fig.2-6), there is virtually no contact stress between particles, then micro fissures can open. However, this complete relaxation of effectively stressed particle structure does not mean that the particles are less interlocked geometrically. If at any stage in the test path they are made to undergo a shear distortion they will tend to dilate and develop the full effective stresses that are required to reach a critical state at that packing. By themselves these micro fissures are not too important, but in the presence of an excess pore pressure gradient the approach to zero effective stress leads to one or other of the phenomena given the general name of liquefaction. Therefore, for either flow liquefaction or cyclic

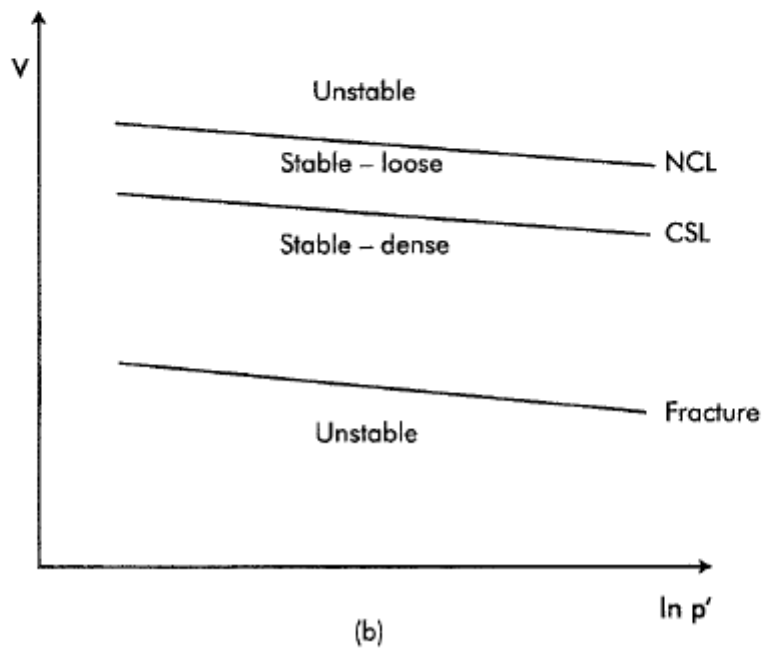
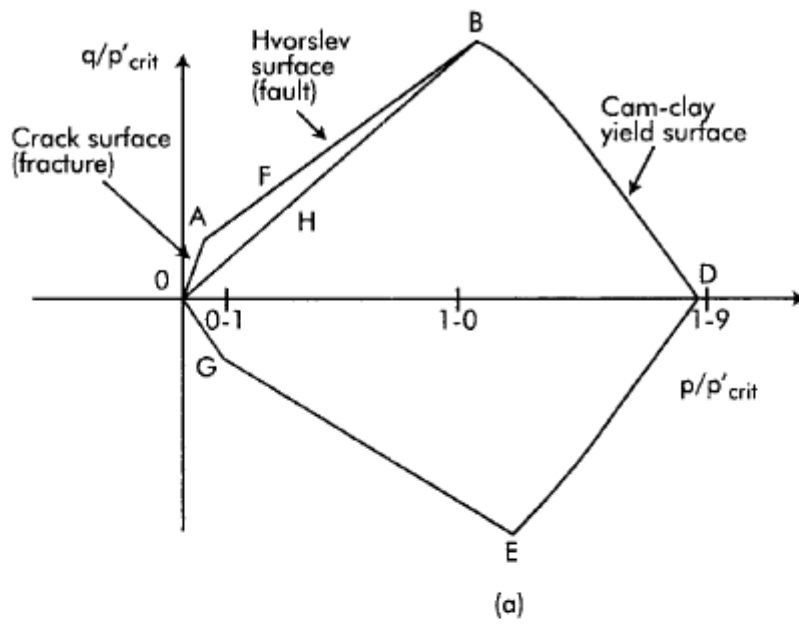


Figure 2-6: Schematic of limits of stable states of soils (a) normalized  $q/p_{crit} - p/p_{crit}$  stress space (b)  $v - \ln p$  space (Pillai and Muhunthan, 2002)

mobility the pore water pressure must necessarily increase and bring the effective mean pressure to near zero.

Muhunthan and Schofield (2000) have re-assessed some of failures of earth dams and reiterated that the failure mechanisms based on flow failure proposed by Casagrande (1936) were not possible and that there should have been excess pore water pressure gradients with fissures at near zero effective stress for their catastrophic failures.

As most of the geotechnical construction is on medium dense to dense soil conditions, it is most likely that soils show the behavior depicted in Fig. 2-2. Moreover, according to Schofield (1980, 1982), for any liquefaction phenomenon to occur, the pore water pressure needs to build up until effective mean stress becomes zero or nearly zero. It is therefore very important that the constitutive models capture this behavior correctly.

There have been several plasticity based constitutive models developed to predict the response of saturated sands under cyclic loading and ensuing liquefaction (Anandarajah, 1994; Yang et al., 2003). Among them the critical state soil mechanics based models have become widely popular. A brief overview of the history of plasticity based soil models and an introduction to the basic concepts of critical state soil mechanics is provided in the following sections.

## **2.5 Plasticity in soil mechanics**

The classical plasticity theory started in 1868 when Tresca presented his yield criterion based on his experimental results on punching and extrusion which led him to

state that a metal yielded plastically when the maximum shear stress attained a critical value. However, Saint-Venant (1797-1886) was the first to set up the fundamental equations of plasticity and to use them in practical problems. In the 1950's major advances were made in the theory of plasticity and the mathematical structure of plasticity was completed. The limit theorem (Drucker et al. 1951, 1952), the concepts of normality and the idea of the stability of a system (Drucker, 1959) are some of the notable advances.

It is interesting to note that the criteria for the yielding of plastic solids, mainly soils, had been proposed by Coulomb (1773) several decades before Tresca published his yield criterion. Nevertheless, application of plasticity to soil mechanics started around 1945. At its beginning, soil plasticity was strictly derived from metal plasticity. But soil, compared to metal, has a different rheological behavior, which depends mainly on mean pressure and density. The Mohr-Coulomb criterion is one of the best known failure criteria in soil mechanics that takes the effect of the hydrostatic pressure on the strength of granular materials into consideration. Because the Mohr-Coulomb criterion is not mathematically convenient in three-dimensional situations due to the existence of corners (singularities), the perfect plasticity model of the Drucker-Prager type (1952) is the simplest model which approximates the Mohr-Coulomb criterion.

Since most geological materials experience yielding from the very beginning, it is necessary to define the yield function for the continuous yielding behavior leading towards the failure, peak, critical or ultimate condition. One of the major advances in the application of plasticity theory was made by Drucker et al. (1957). They were concerned

with the limitations of perfect plasticity when applied to a frictional material with the Mohr-Coulomb failure criterion. The limitation came about because the failure envelope was treated as a yield envelope, and the normality condition implied an unacceptably large rate of dilation at failure. Moreover, the implication was that this rate was always applied, which was in conflict with the experimental evidence that in some cases soils reduce in volume during yield. To overcome these deficiencies, they proposed the idea of using a “cap” type yield function to define the continuous yielding of soils.

There are two important consequences for soil models in the contribution of Drucker et al. (1957). The first is that the usual consolidation curve is but a case of work-hardening stress-strain relationship, and can be associated with successive yield envelopes. The second follows from the first one in that when a soil is isotropically normally consolidated, an increase in mean effective stress would cause yield. The introduction of this work-hardening plasticity into soil mechanics contributed in large measure to the development of Critical State Soil Mechanics at Cambridge.

The additional feature which has been an integral part of all Cambridge models has been the concept of critical state (Roscoe et al., 1958). Extensive research at Cambridge University had shown that soil and other granular materials, if continuously distorted until they flow as a frictional fluid, will come into a well-defined critical state (Roscoe and Schofield, 1963; Schofield and Wroth, 1968). The locus of the critical state points from drained and undrained tests lie on a unique line on a three dimensional space ( $q$ - $p$ - $v$ ), called the critical state line (CSL). Its projection on  $q$ -  $p$  space and  $v$ - $\ln p$  space are given as:

$$q = Mp \quad (2-1)$$

and

$$\Gamma = v + \lambda \ln p \quad (2-2)$$

respectively, where  $p = \frac{\sigma_1 + \sigma_2 + \sigma_3}{3}$  and  $q = |\sigma_1 - \sigma_3|$ . The associated volumetric and shear strains are described by  $\dot{\epsilon}_v = \dot{\epsilon}_1 + \dot{\epsilon}_2 + \dot{\epsilon}_3$  and  $\dot{\epsilon}_q = \frac{2}{3}|\dot{\epsilon}_1 - \dot{\epsilon}_3|$ .  $M$  is the slope of critical state line in the  $p$ -  $q$  space and  $\Gamma$  and  $\lambda$  are the intercept at  $p = 1$  kPa and slope of the critical state line in the  $v$ - $\ln p$ , and  $v$  is the specific volume, respectively. Once the CSL is reached, soils undergo unlimited distortion without any change in the state parameters. This is process is stated mathematically as:

$$\frac{\dot{p}}{\dot{\epsilon}_q} = \frac{\dot{q}}{\dot{\epsilon}_q} = \frac{\dot{\epsilon}_v}{\dot{\epsilon}_q} = 0 \quad (2-3)$$

The first term,  $\frac{\dot{p}}{\dot{\epsilon}_q}$ , implies that at critical state, no further changes occur in the mean effective stress upon further straining the soil once the soil reaches the critical state. The second term,  $\frac{\dot{q}}{\dot{\epsilon}_q}$  states that no further changes in strength can occur once the soil has reached the critical state. Lastly, the term  $\frac{\dot{\epsilon}_v}{\dot{\epsilon}_q}$  represents a condition of zero dilatancy

upon reaching the critical state. Zero dilatancy in drained conditions amounts to  $\frac{\dot{\varepsilon}_v}{\dot{\varepsilon}_q} = 0$ ,

and in undrained conditions,  $\frac{\dot{u}}{\dot{\varepsilon}_q} = 0$  where  $u$  is the pore water pressure.

## 2.6 Granular Dilatancy

The correct description of volume changes due to imposed stress is fundamental to the modeling of the stress-strain behavior of soils. The remarkable phenomenon of the coupling between *volume and shape changes* observed qualitatively and termed granular *dilatancy* by Osborne Reynolds (Reynolds, 1885) has influenced many a concept in granular media and soil mechanics. Reynolds (1902) demonstrated the granular dilatancy with two rubber balloons, each full of colored water that his audience saw standing in a tube above each balloon in turn (Schofield, 2005). One balloon contained only water. The other contained a fully saturated dense aggregate. When he squeezed each balloon in turn, the water level rose in the tube from the water-filled balloon whereas the water level lowered down in the other tube. He explained this surprise result by using the dilatancy phenomenon that when the dense sand is sheared it tends to dilate and enlarge its voids. If there is a water supply at the moment, the enlarging voids draw the water from the supply, leading to the fall in water level. Since then much importance has been attached to the Reynolds' concept in the literature on granular media and soil mechanics. Whilst various attempts have been made to incorporate dilatancy into constitutive models little regard is made to its mechanical origins. Many of the models have either failed to recognize the "Reynolds' Effect" as an *internal kinematical constraint* or otherwise have

not followed its full mathematical consequences. This constraint has been discussed in the past by Kanatani (1982), Goddard and Bashir (1990), Houlsby (1993) and Collins and Muhunthan, (2003), and is reviewed in more detail later in this study.

One of the earliest attempts to account for the increased shear strength due to dilatancy in dense sand was by D.W.Taylor (1948). Taylor used the term *interlocking* to describe the effects of dilatancy. He calculated the power at *peak* strength for some direct shear-box data and found that the energy input is partly dissipated by a critical state friction component and partly by the work needed to increase the volume.

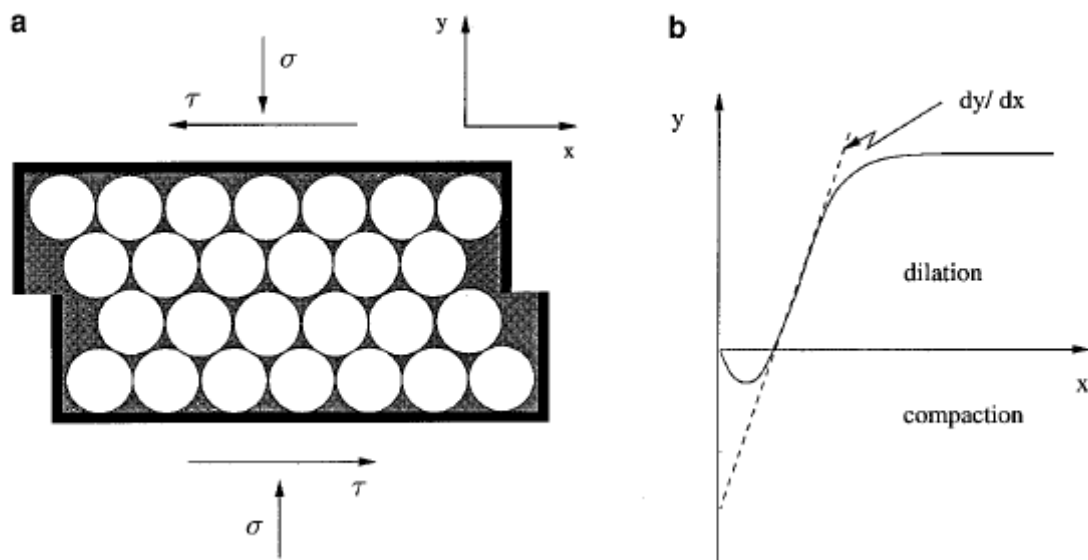


Figure 2-7: Taylor's shear box analogy (Deshpande and Cebon, 1999)

Fig. 2-7 shows the schematic diagram of direct shear box;  $\sigma$  is the applied normal stress,  $\tau$  is the applied shear stress,  $dx$  is the horizontal displacement and  $dy$  the vertical displacement. Energy input to the system is  $\tau dx$ ; the work needed to lift  $\sigma$  through

distance  $dy$  is  $\sigma dy$ ; and the energy dissipated by friction is  $\mu\sigma dy$ . Considering energy balance, one will obtain:

$$\tau dx = \mu\sigma dx + \sigma dy ; \tau dx - \sigma dy = \mu\sigma dx \quad (2-4)$$

Eq.2-4 can be rearranged as

$$\frac{\tau}{\sigma} = \mu + \frac{dy}{dx} \quad (2-5)$$

This shows that the peak strength of the dense granular material under a normal stress is drawn from internal friction and interlocking (dilatancy). Taylor also saw that an increase in the effective stress reduces the interlocking, so that above a critical effective pressure there will not be an increase of volume but a reduction.

As part of his research thesis at Cambridge, Thurairajah (1961) performed a number of triaxial shear tests and calculated the proportion of work that went into Taylor's dilation and the proportion that went into the change of elastic energy in an effectively stressed soil. His work with both drained and undrained tests on kaolin clays and sand led to some remarkable observations. He found that the rate of work dissipated in plastic deformation is equal to the product of the effective mean normal stress, with  $M$ , and the magnitude of the plastic shear strain rate. Moreover, he found that this result applied not only when paths reached critical states but *at all stages* of the test paths. These important results have recently been reviewed by Schofield (2000) and Muhunthan and Olcott (2002). This phenomenon has been recently termed as Thurairajah's Dissipation Function by Schofield (2005). Adopting the standard notation for triaxial tests, Thurairajah's dissipation function can be cast in the form:

$$\hat{\Phi} = Mp|\dot{\epsilon}_q^p| \quad (2-6)$$

Equating the plastic work done on the system to the dissipation function:

$$\dot{W}^p = p\dot{\epsilon}_v^p + q\dot{\epsilon}_q^p = Mp|\dot{\epsilon}_q^p| \quad (2-7)$$

where  $\dot{\epsilon}_v^p$  and  $\dot{\epsilon}_q^p$  denote the volumetric and shear components of the plastic strain rate tensor respectively (these rates can be interpreted as increments for rate independent materials).

Based on minimum rate of internal work assumption, Rowe (1962) related dilatancy to the principal stress ratio as:

$$\frac{\sigma_1}{\sigma_3} = K_\mu \left( 1 - \frac{\dot{\epsilon}_v}{\dot{\epsilon}_1} \right) \quad (2-8)$$

where  $K_\mu$  is a parameter that depends on friction angle. The above relationship was termed the *stress-dilatancy* relation. It has been used as a flow rule in a number of soil plasticity models.

Using the critical state soil mechanics invariants, Eq. (2-8) can be rewritten as:

$$d = \frac{\dot{\epsilon}_v^p}{\dot{\epsilon}_q^p} = \frac{9(M - \eta)}{9 + 3M - 2M\eta} \quad (2-9)$$

where  $\eta = \frac{q}{p}$  is the stress ratio.

Influenced by Rowe's study, many of the critical state constitutive models for soils interpret (2-7) and similar forms as a stress-dilatancy relationship. For example, (2-7) can be rewritten as:

$$d = M - \eta \quad \text{or} \quad \eta = M - d \quad (2-10)$$

Burland (1965) and Roscoe and Burland (1968) proposed a modification to Thurairajah's dissipation function  $\hat{\Phi}$  and replaced (2-7) by:

$$p\dot{\epsilon}_v^p + q\dot{\epsilon}_q^p = \hat{\Phi} = p\sqrt{\dot{\epsilon}_v^{p^2} + M^2\dot{\epsilon}_q^{p^2}} \quad (2-11)$$

where now the volumetric plastic strain rates also contribute to the dissipation. Eq. 2-11 is also sometimes rewritten as a stress-dilatancy relation:

$$d = \frac{M^2 - \eta^2}{2\eta} \quad (2-12)$$

However, it will be shown later that the above interpretations of granular dilatancy as a function of stress precludes consideration of other sources.

## 2.7 Cam Clay models

At the core of Critical State Soil Mechanics was the creation of the constitutive models called original and modified Cam Clay based on the theory of plasticity and the prediction of the successive ductile yielding states of specimens on the wet side of critical. In the family of critical state based models (Schofield and Wroth, 1968, Roscoe and Burland, 1968), the stress-dilatancy relationship was interpreted as an equation for the plastic potential. Invoking Drucker's stability postulate (Drucker et al., 1957), the integrated form of the stress-dilatancy relationship was used to generate the yield curves and to develop plastic stress-strain models. Many of the extant, plasticity-based models in geomechanics do, in one form or another, incorporate these ideas.

The stress-dilatancy relation (Eq. 2-10) was used as the basis for the original Cam Clay (OCC) model of Schofield and Worth (1968), who realized that it could be interpreted as an equation for the plastic potential  $g(p,q)$ , as it can be rewritten:

$$\frac{q}{p} = -\frac{\partial g / \partial p}{\partial g / \partial q} + M \equiv \frac{dq}{dp} + M \quad (2-13)$$

which integrates to give

$$q = Mp \ln \left( \frac{p_c}{p} \right) \quad (2-14)$$

so that invoking Drucker's stability postulate, which requires a normal flow rule, Eq. (2-14) could also be used as that of the yield surface, with  $p_c$  being interpreted as the normal consolidation pressure.

Proceeding as above, Eq.2-12 can be integrated to give the modified Cam Clay (MCC) (Wood, 1990):

$$q^2 - M^2 p(p_c - p) = 0 \quad (2-15)$$

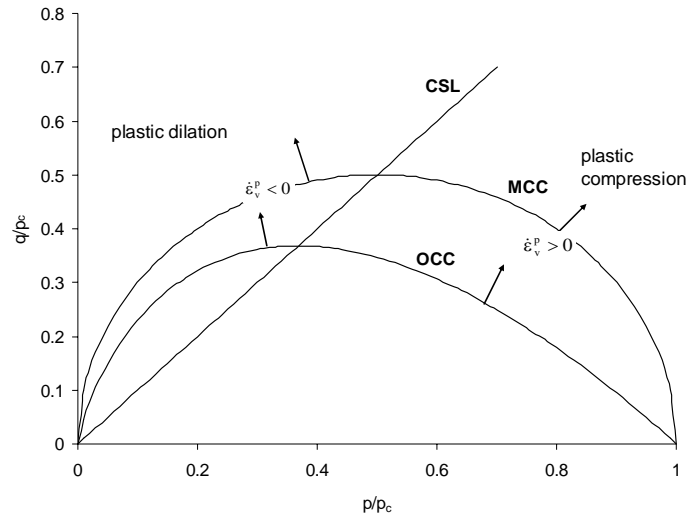


Figure 2-8: Normalized OCC and MCC yield curves

Fig.2-8 shows the yield curves of OCC and MCC models in normalized space. The shape of the OCC model looks like a bullet whereas the MCC is an ellipse. As can be seen in the Fig.2-8, the OCC is not continuous and has a corner at  $q = 0$ . This results in unacceptable volumetric deformation around the corner and also causes numerical problems in implementing it into numerical codes. The MCC model does not suffer from this shortcoming and is therefore widely used in numerical codes and practical applications. The normally consolidated pressure depends on plastic volumetric strain, and thus the hardening rule for the family of Cam Clay models is given as:

$$\dot{p}_c = p_c \frac{(1+e)\dot{\epsilon}_v^p}{\lambda - \kappa} \quad (2-16)$$

## **2.8 Critical state based sand models**

Although application of Cam Clay models to normally consolidated clays have been quite successful, they suffer from limitations when used to model sands: (a) for states of stress below the critical state line, these models predict only compressive volumetric strains whereas sands exhibit dilation before the critical state is reached (prepeak dilation). For example, as shown in Fig.2-2, relatively dense sand changes its behavior from contractive to dilative before it reaches the critical state line. However, the critical state dilatancy relationships (Eqs. 2-10 & 2-12) predict that a change in contractive to dilative behavior can only occur when the stress ratio  $\eta$  exceeds the critical state stress ratio  $M$ . Thus the models cannot capture such behavior; (b) the yield surface of these models is circular in the principal stress space; thus it cannot predict different strengths for compression and extension loading conditions (c) the hardening or yielding is defined through total volumetric plastic strains (or void ratio), thus the definition of hardening does not include the effect of deviatoric plastic strains.

It is generally agreed that non-associated flow rules, some form of shear hardening, induced anisotropy, and the improved modeling of dilatancy, must be added to the basic structure of critical state soil mechanics in order to obtain an acceptable degree of realism in these models for sands.

### **2.8.1 Improved stress-dilatancy rules**

Many sand models make use of the “state parameter” concept proposed by Been and Jefferies (1985). In these models the voids ratio  $e$  is replaced by a “state parameter” as the fundamental variable, which determines the size of the yield surface and the flow

rule. The state parameter is defined to be the displacement of the current point from the critical state line in the  $(e, \ln p)$  plane. It can be expressed either as the difference between the current and critical state voids ratio evaluated at constant pressure, or as  $\ln(p/p_{csl})$ , or simply as  $p/p_{csl}$ , where  $p_{csl}$  is the critical state pressure evaluated at constant voids ratio, (Leroueil, 1997 and Wang et al., 2002). Key to these models is the assumption that the critical state line in  $e$ - $\ln p$  space is *unique*. A major difficulty in determining critical state for dense sands is the frequent occurrence of shear band localization, at or just after the peak stress is achieved. Experimental issues in determining the critical state and investigating its uniqueness have been discussed by Chu (1995), Chu and Lo (1994), Mooney et al. (1998), Vaid et al. (1999), Santamarina and Cho (2001), Klotz and Coop (2002), and Papadimitriou et al. (2005).

Stress-dilatancy relationships of Rowe and Cam Clay models are only a function of  $\eta$ . Rowe (1962) did suggest that the stress-dilatancy relationship for granular soils must include a variable depending on the sample density and the stress history. As the state parameter represents the sample density and confining pressure, Li and Dafalias (2000, 2002), Manzari and Dafalias (1997) proposed an improved state dependent dilatancy relationship as:

$$d = \frac{d_0}{M} (M_f - \eta) \quad (2-17)$$

where  $M_f$  is now evolving with state parameter ( $\psi$ ) that takes zero at critical state and negative and positive values when the states are on loose and dense side of critical state line, respectively. In accord with critical state concepts the evolution of  $M_f$  was proposed

as  $M_f = M + m\psi$  by Manzari and Dafalias (1997) and as  $M_f = M \exp(m\psi)$  by Li and Dafalias (2000, 2002). At the critical state,  $\psi = 0$  gives  $M_f = M$ ; thus the dilatancy rule becomes that of original Cam Clay. For dense sand the state parameter takes negative value i.e.  $\psi < 0$ ,  $M_f < M$  hence the dilatancy could also become zero for  $\eta < M$ . Therefore, the above relations can predict phase transition and ultimate state with the variation of state parameter.

These stress-dilatancy relationships have been used with the bounding surface framework for the prediction of granular soil behavior. The peak stress ratio or slope of ultimate state line ( $M_b$ ), which serves as the bounding surface is also assumed to be a function of the state parameter. Manzari and Dafalias (1997) used a linear relationship  $M_b = M - n\psi$  which similar to the one used for  $M_f$ . Li and Dafalias (2000, 2002) used  $M_b = M \exp(-n\psi)$ . It is noted that for dense sand  $M_b > M$  because  $\psi < 0$ . This idea of having a peak stress ratio varying with state parameter in order to address the issue of peak stress and subsequent softening of dense sand in drained conditions was proposed by Wood et al. (1994). There is hierarchy of similar kinds of models in the literature. All of them are based on critical state framework, but they differ only in defining the  $M_f$  and  $M_b$ . For example, Wang et al. (2002) proposed slightly different relations as,  $M_f = M_0 + (M - M_0)I_p$ ,  $M_b = M + \beta(I_p^{-0.5} - 1)$  where  $M_0$  is a material constant and  $I_p$  is the state pressure index which is also a measure of state of the material from critical state line. In fact,  $I_p$  is related to  $\psi$  as,  $\psi = \lambda \ln(I_p)$ . In the proposal of Severn-Trent sand,

Gajo and Wood (1999) also made use of the state parameter in the definition of  $M_f$  and  $M_b$ .

Nova (1982) proposed a minor modification to the original Cam Clay stress-dilatancy relation as:

$$(1 - N)d = M - \eta \quad (2-18)$$

where  $N$  is a density-independent material property. He assumed  $N$  to be a constant based on the test data of Stroud (1971). If  $N = 0$  then Eq. (2-18) becomes the Cam Clay flow rule. This model was further discussed by Jefferies (1997), who demonstrated that the extra term introduced by  $N$  represented stored rather than dissipated energy.

Jefferies (1993) used Nova's relationship to develop the "Nor-Sand" model for granular materials within the framework of critical state soil mechanics. He postulated that an infinity of isotropic Normally Consolidate Lines exist for sands, which prevents the direct coupling of yield surface size to void ratio. When the normality condition is used for the flow rule, the Cam Clay yield surfaces produce unrealistic dilation rates for dense sand. On the other hand, despite using the normality condition, Nor-Sand predicts realistic dilation rates by defining limiting hardening loci proportional to the state parameter at the image stress. Hence, the maximum dilatancy rate is controlled by the state parameter; this in turn controls the peak stress ratio.

Jefferies and Shuttle (2002) modified Nova's flow rule (Eq.2-18) by replacing  $M$  with  $M_f$ , where  $M_f = M - |\psi_i|$ .  $\psi_i$  is related to state parameter as,  $\psi_i = \psi - \lambda(1 - \eta/M)$ . Recently, Rouse et al. (2006) have gone one step further and combined Nova's flow rule

with state-based dilatancy, and allowing for particle shape, to get  $M_f = M - |N\chi\psi|$ , where the parameter  $\chi$  represents the particle shape.

It is a well-known fact that both the geometrical packing of grains (fabric) and the contact forces between them strongly control the mechanical behavior of particulate systems, such as sands. A micro mechanics based parameter is often introduced into the stress-dilatancy relation to capture the effects of fabric. Oda (1975) and Mehrabadi and Nemat-Nasser (1983) used the second invariant of the deviatoric part of the fabric tensor in their stress-dilatancy equation as their fabric measure. Wan and Guo (2001, 2004) have also proposed a stress-dilatancy model that depends on a measure of the fabric tensor.

### **2.8.2 Shear hardening**

Classical critical state soil mechanics models only involve volumetric hardening (Eq.2-16). As is shown in Fig. 2-8, for  $\eta < M$ , contractive behavior (i.e.  $\dot{\epsilon}_v^p > 0$ ) is predicted. According to Eq.2-16 the increment rate of normally consolidated pressure ( $\dot{p}_c > 0$ ) is positive, therefore the yield surface expands (hardening) during shear deformation in the region of  $\eta < M$ . For  $\eta > M$ , dilation occurs ( $\dot{\epsilon}_v^p < 0$ ); therefore the rate of increment of normally consolidated pressure is negative ( $\dot{p}_c < 0$ ) which makes the yield surface shrink (softening). At critical state  $\eta = M$ , this gives  $\dot{\epsilon}_v^p = 0$  and  $\dot{p}_c = 0$ , therefore no change in yield surface size. However, there will be continuous shear deformation without any change in states. Hence, a volumetric hardening rule would not simulate the prepeak dilation behavior that dense sands exhibit in the region of  $\eta < M$ .

Models incorporating shear hardening have been proposed to overcome this by Nova and Wood (1979), Mroz and Norris (1982), Boukpeti and Drescher (2000), and Collins and Kelly (2002). In these models the rate of increment of the normally consolidated pressure is expressed in terms of total work done by the volumetric and shear strains as:

$$\dot{p}_c = p_c \frac{(1 + e)(\dot{\epsilon}_v^p + \beta \dot{\epsilon}_q^p)}{\lambda - \kappa} \quad (2-20)$$

where  $\beta$  is model parameter. According to the Eq. 2-20,  $\dot{p}_c$  remains positive even though  $\dot{\epsilon}_v^p$  could become negative. For example, at or above critical state  $\eta \geq M$  and  $\dot{\epsilon}_v^p \leq 0$ ; but  $\dot{p}_c > 0$  because of the contribution of shear hardening (Eq. 2-20). So, the yield surface continues to expand despite the fact that sample is dilating. This modification in hardening rule enables the prediction of prepeak dilation behavior of dense sand.

### 2.8.3 Non-associative flow rule

It is usually assumed in classical plasticity theory that the plastic potential function and the yield function are the same, i.e. the associated flow rule is assumed, for example in Cam Clay (Schofield and Wroth, 1968). Poorooshasb et al. (1967) and Tatsuoka and Ishihara (1974) performed a series of triaxial tests at different stress paths involving loading, unloading, and reloading to determine the yield condition experimentally for different sands. They concluded that the yield loci suggested by Cam Clay does not appear to duplicate real behavior. In addition, it has been found that use of the associated flow rule leads to large volumetric dilation. Therefore, the non-associated flow rule is employed to overcome this shortcoming.

Lade and Duncan (1975) developed a non-associative elastoplastic model, based on experimental studies (Lade and Duncan, 1973). The failure criterion is expressed in terms of stress invariants as  $f = I_1^3 - \kappa_1 I_3$  and the plastic potential function takes the same form as  $\psi = I_1^3 - \kappa_2 I_3$  but with a different shape in the stress space. In the same line, Zienkiewicz and Mroz (1984) introduced “generalized plasticity” which does not need yield surfaces and plastic potentials to be defined. Instead of a yield surface and plastic potential, fields of unit vectors are defined for both loading and unloading processes. This enables successful simulation of both monotonic and cyclic loading of sands (Pastor et al., 1985, 1990)

#### **2.8.4 Double hardening models**

Based on the concept of multiple yield mechanisms (Koiter, 1953), Prevost and Hoeg (1975) employed two separate yield mechanisms to describe the behavior of soils. This concept, referred to as “double hardening”, was later adopted by a number of researchers (Lade, 1977; Vermeer, 1978; Ohmaki, 1979; Sribalaskandarajah, 1996). Vermeer (1978) used a functional form for the shear yield surface to get the first component of plastic strain. The yield surface closely matched the experimental shear yield surface by Stroud (1971) and Tatsuoka and Ishihara (1974) and a non-associated flow rule that is based upon Rowe’s stress-dilatancy relation. The second component of plastic strain is purely volumetric and a volumetric yield locus is used. Molenkamp (1981) has produced a far more sophisticated version of Vermeer’s model, with full 3D capability and consistent derivations, known as MONOT. Ghaboussi and Momen (1979,

1982) also used the double hardening principles to construct an elastoplastic constitutive model for sands which can be used for monotonic as well as cyclic loading conditions.

### **2.8.5 Stored plastic work**

Recently, applications of the thermomechanics framework to geomechanics problems (Collins and Houlsby, 1997, Collins and Kelly, 2002 and Collins and Muhunthan, 2003) have had a fair amount of success. It has been shown that the soil models based on thermomechanics functions, such as the Helmholtz free energy, dissipation function, do not violate thermodynamic laws as opposed to the plasticity models derived based on extant procedures. It has been shown that the well-known original Cam Clay violates thermodynamic laws (Collins and Hilder, 2002; Collins and Kelly, 2002; Collins and Muhunthan, 2003). The concept of stored plastic work or frozen energy is the most important aspect of these models. Critical state based soil models often assume that the energy input to the system is entirely dissipated in frictional work. Nevertheless, some part of the input energy could be stored within plastically stressed force chains because of the highly heterogeneous nature of the stress and deformation fields at the micro level (Collins 2005, Collins and Kelly 2002, Collins and Muhunthan, 2003). The stored energy is represented by the free energy function; the dissipation function gives the frictional work loss in the system. Once these functions have been specified, by using a systematic approach, the flow rule, yield condition can be deduced from them (Collins and Kelly, 2002).

Collins and Houslby (1997) demonstrated that a non-associated flow rule is a necessary property of a frictional material, in which the plastic deformations are

governed by stress ratios rather than by the magnitudes of certain yield stresses as in metal plasticity. Collins (2005) clarified that there are two causes of dilatation in a soil, one due to Reynolds dilatancy, the other due to the recovery of the frozen energy. Collins et al. (2006) have further extended this work and modeled the Reynolds dilatancy in the framework of thermomechanics.

The original critical state concepts were developed mainly based on the behavior of reconstituted, essentially isotropic, materials. The behavior of sands, particularly the angular sands commonly encountered in the field have a better defined granular structure. These materials possess a significant degree of fabric anisotropy leading to the difficulties faced by the original critical state models to sands. Yet, none of the sand models discussed above directly accounted for this phenomenon. As a result while ad hoc improvements have been made in the predictions by these models, some of the parameters used by them have little physical meaning.

This study makes use of the fabric based plasticity model for anisotropic behavior of clays developed by Muhunthan and his colleagues (Muhunthan et al., 1996; Masad et al., 1998) to develop a physically based model for sands as shown in the next chapter.

## *Chapter 3*

### **THE NEW ANISOTROPIC SAND MODEL**

#### **3.1 General**

There have been two major trends in describing the soil behavior. The first one is motivated by plasticity in which a soil medium is treated as a homogeneous continuum. It provides for a viable means of modeling the behavior of the soil mass (Schofield and Wroth, 1968). Many useful theories including the critical state soil mechanics framework have been developed based on this idealization (Roscoe et al, 1963; Roscoe and Burland, 1965).

The second approach is based on micromechanics in which soils are treated as assemblies of discrete particles. The early stages of this approach treated a soil medium as an assembly of regular and irregular arrays of rigid frictional particles and derived analytical solutions to describe their collective behavior (Mindlin, 1949; Rowe, 1962). The contact distribution of particles in the basic models was subsequently modified with a probabilistic distribution function to reflect their anisotropic nature (Horne, 1965; Oda, 1972; Matsuoka, 1974). The advances in computational power enabled the simulation of contact deformation of spheres under loads using Newtonian laws of motion and led to the development of Discrete Element Method (Cundall and Strack 1978). It has since become a tool simulate the behavior of an assembly of spherical particles in a computer

and has been used to identify a number of problems in granular mechanics including dilatancy and the development of shear bands (Suiker and Fleck, 2004, Barthust and Rothenburg, 1990).

The continuum plasticity models often do not account directly for the micromechanics of granular irreversible deformation whereas the detailed study of the particulate nature of soil material is mathematically complicated and its applicability to field problems and design is limited (Scott, 1987).

Therefore, a new approach in which the plasticity theory is improved with the proper choice of additional parameters based on micromechanics has been used by a number of researchers. This approach takes advantage of the continuum theory as a powerful technique for practical applications; however, it recognizes the particulate nature of soils and incorporates into plasticity theory the features of the spatial arrangement of solid particles and associated voids, termed granular fabric.

### **3.2 Fabric measure based on void space**

The mechanical behavior of granular materials is strongly influenced by its microstructure. In triaxial compression tests on sands, Oda (1972b) observed that the strength of granular soils is different depending on the direction of compression with respect to the horizontal. Moreover, he observed that non-spherical particles tend to be rotated perpendicular to the direction of a maximum compression. Void ratio or the porosity is often used to characterize the state of packing in granular materials. These scalar measures, however, are insufficient to characterize the directional behavior of granular

materials. Higher order micro-structural variables known as “fabric tensors” have been used to describe the distribution and orientation of grains and voids (Oda et al., 1982, 1985; Mehrabadi et al., 1982; Tobita, 1989; Pietruszczak and Krucinski, 1989a; Bathurst and Rothenburg, 1990; Muhunthan et al., 1996). Models incorporating fabric measures are also extant in the literature (Wan and Guo, 2004, Tsutsumi and Hashiguchi, 2005; and Zhu et al., 2006).

This study makes use of the void fabric tensor measure to characterize fabric effects in granular media (Muhunthan et al, 1996; Masad and Muhunthan, 2000). Void fabric tensor is developed based on the concept of a representative elemental volume (REV) which consists of sufficient number of particles to make the statistical treatment valid. The REV can be generally of any shape such as cubical, spherical, etc. In this study, an idealized spherical REV with voids shaded as shown in Fig. 3-1 is chosen. Using averaging techniques the distribution of void ratio within the REV can be approximated by a directional function  $e_c(\mathbf{l})$  of the form (Muhunthan et al., 1996; Masad et al. 1998):

$$e_c(\mathbf{l}) = e(1 + \Omega_{ij}l_i l_j) \quad (3-1)$$

where  $e_c(\mathbf{l})$  is the magnitude of the void ratio vector in the direction of the unit vector  $\mathbf{l}$ ,  $e$  is the isotropic void ratio of the soil, the components of the unit vector  $\mathbf{l}$  are given by  $l_1 = \sin\theta\sin\phi$ ,  $l_2 = \cos\theta$  and  $l_3 = \sin\theta\cos\phi$  (Fig. 3-1), and  $\Omega_{ij}$  is termed the void fabric tensor. If the voids are isotropically distributed, the components of the void fabric tensor become zero and Eq. (3-1) reduces to the isotropic average value,  $e$ , of the void ratio. Thus, the components of the void fabric tensor represent deviations from the isotropic distribution of

voids. The components of  $\Omega_{ij}$  can be obtained from microscopic observations within a representative elemental volume (REV). Details of the experimental procedure and the complete derivation of Eq. (3-1) are given in Muhunthan et al. (1996).

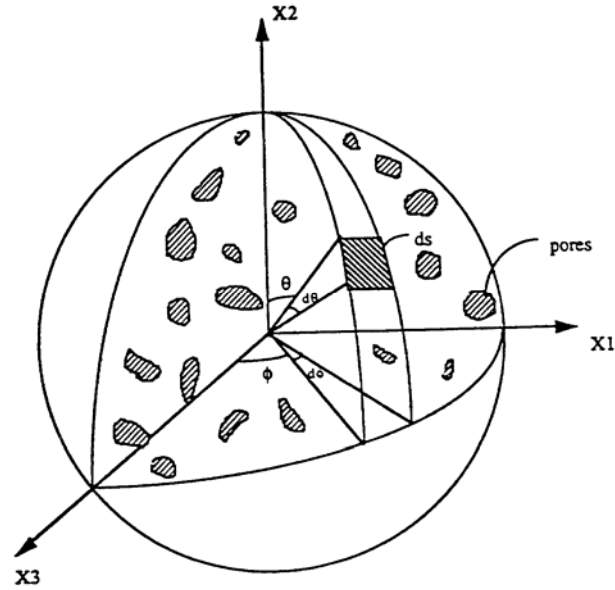


Figure 3-1: The coordinate system used in the void fabric tensor analysis

The specific volume  $v = 1+e$  has often been used in the development of concise critical state based stress-strain models for soils. The magnitude of the directional specific volume in  $\mathbf{l}$ -direction,  $v_c(\mathbf{l})$ , follows from the directional void ratio as:

$$v_c(\mathbf{l}) = v + \varphi v - \varphi \quad (3-2)$$

where  $\varphi = \Omega_{ij}l_i l_j$  and  $v$  is the isotropic specific volume.

### 3.3 Fabric change due to deformation

The changes in material points in granular materials induced by deformation are registered by the evolution of its fabric. Past investigators have explored the relationship between fabric and strain originating with the seminal contribution by Philofsky and Finn (1967) who introduced the idea of measuring strain by stereological principles. Kanatani (1984) extended this work and developed relationships between strain and different fabric tensors. Satake (1989) developed the average strain in granular materials as a function of the relative displacement between particles and the branch vector which connects the centroids of pairs of particles. This is utilized by Iai (1993) to develop a concept of effective strain in granular materials and re-interpret the stress dilatancy relation in the Cam Clay model (Iai, 1994). In what follows, we explore a simpler relationship between volumetric strain and changes in void fabric tensor (see also Muhunthan et al. 1996).

The rate of change of volume in granular materials equals the rate of change in volume of voids, thus the rate of change in void ratio. Differentiating Eq.(3-1):

$$\dot{e}_c(\mathbf{1}) = \dot{e}(\mathbf{1} + \Omega_{ij}l_i l_j) + e\dot{\Omega}_{ij}l_i l_j \quad (3-3)$$

Summation of the directional rate of volume change over all directions leads to:

$$\dot{e}_c = \dot{e} + e\dot{\Omega}_{ij}l_i l_j \quad (3-4)$$

Denoting  $\dot{\mathcal{Q}} = \dot{\Omega}_{ij}l_i l_j$ , Eq. (3-4) can be simplified to:

$$\dot{e}_c = \dot{e} + e\dot{\mathcal{Q}} \quad (3-5)$$

The above relationship shows that the rate of change of directional volume consists of two components; the standard macroscopic component and one that is dependent on the rate of change of fabric. The decomposition of the rate of volume change is shown schematically as in Fig. 3-2. In extant granular models, rate of volume change is assumed to occur entirely within the void skeleton due to contraction/dilation of voids (Fig. 3-2(b)). The derivation here shows that the evolution of anisotropic granular fabric contributes an additional contribution to the rate of volume change (Fig. 3-2c). This additional rate of volume change that occurs within the sample must, therefore, be incorporated in plasticity models to reflect its contribution.

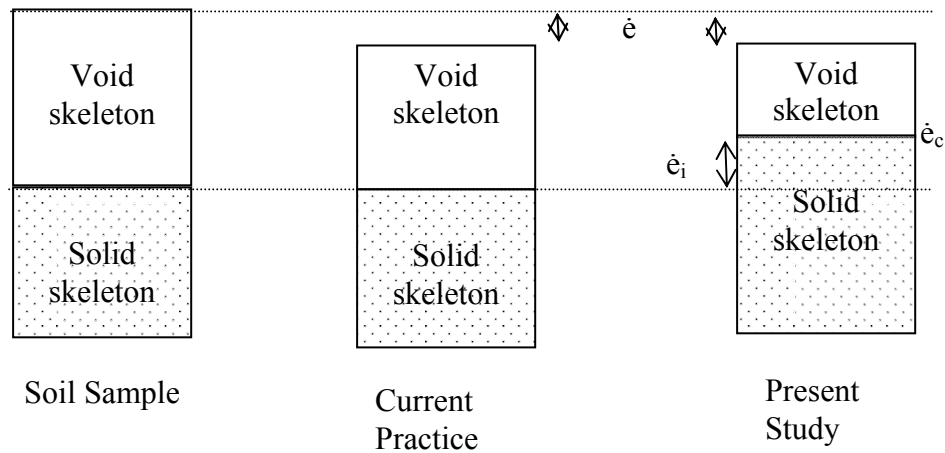


Figure 3-2: Schematic description of volume changes in void and solid skeleton

For small strains, the rate of volumetric strain in granular materials is equal to the rate of change of the volume divided by the current total volume (total volume =  $1+e$ ).

Dividing Eq. (3-5) by the total volume:

$$\frac{\dot{e}_c}{1+e} = \frac{\dot{e}}{1+e} + \frac{e\dot{g}}{1+e} \quad (3-6)$$

Defining  $\dot{\epsilon}_{vc} = \frac{\dot{\epsilon}_c}{1+e}$  and  $\dot{\epsilon}_v = \frac{\dot{\epsilon}}{1+e}$ , Eq. (3-6) can be re-written as;

$$\dot{\epsilon}_v = \dot{\epsilon}_{vc} - \frac{e}{1+e} \dot{\vartheta} \quad (3-7)$$

$\dot{\epsilon}_v$  can be recognized as the standard macroscopic volumetric strain rate measured by experiments..

Since the fabric tensor  $\Omega_{ij}$  is deviatoric, it is possible to relate its change to the deviatoric or shear strain change,  $\dot{\epsilon}_{ij}$  through the use of an isotropic tensor valued functional representation (Boehler, 1987):

$$\dot{\Omega}_{ij} = \dot{\Omega}_{ij}(\Omega_{kl}, \dot{\epsilon}_{kl}, e) \quad (3-8)$$

The functional form is generally complex. However, if the principal axes of  $\dot{\epsilon}_{ij}$  and  $\dot{\Omega}_{ij}$  are assumed to be coincident, the relation can be modeled as (Muhunthan et al., 1996):

$$\dot{\Omega}_{ij} = \beta \dot{\epsilon}_{ij} \quad (3-9)$$

with:

$$\beta = a_1(1-1/e) + a_2(1-1/e)\Omega_{ik}\Omega_{ki} \quad (3-10)$$

where  $a_1$  and  $a_2$  are scalar functions of the isotropic void ratio. It is noted in passing that the detailed relationship between fabric and the strain deviator tensor has been studied by Kanatani (1985). Denoting  $\dot{\epsilon}_{ij}l_i l_j = \dot{\epsilon}_q$  for triaxial condition, and multiplying Eq. (3-9) by  $l_i$  and  $l_j$  one will get:

$$\dot{\vartheta} = \beta \dot{\epsilon}_q \quad (3-11)$$

where  $l$  is chosen at any convenient direction to study fabric changes with deformation.

Substituting Eq. (3-11) in Eq. (3-7) results in:

$$\dot{\epsilon}_v = \dot{\epsilon}_{vc} - \frac{e}{1+e} \beta \dot{\epsilon}_q \quad (3-12)$$

The last expression shows that the rate of volumetric strain in is coupled with the rate of shear strain in anisotropic soils. The relationship Eq. (3-12) can be simplified with the use of a coupling parameter,  $\alpha$  as (see also Muhunthan et al. 1996):

$$\dot{\epsilon}_{vc} = \dot{\epsilon}_v + \alpha \dot{\epsilon}_q \quad (3-13)$$

where  $\alpha = \frac{e}{1+e} \beta$

It is evident from the above discussion that the relationship between volumetric strain and shear strain is purely kinematic and is induced by fabric anisotropy.

### 3.4 Decomposition of plastic strain

Most plasticity models of granular media consider the plastic volumetric strain to be solely contributed by changes in stress. This precludes contributions from other mechanisms to plastic volumetric strain. The kinematic relationship between volumetric strain and fabric relationship developed here enables us to put forward a proposal for an additional source of plastic strain that arises purely as a result of changes in fabric. Accordingly, the plastic volumetric strain  $\dot{\epsilon}_v^p$  is considered to be:

$$\dot{\epsilon}_v^p = \dot{\epsilon}_{vc}^p - \alpha \dot{\epsilon}_q^p \quad (3-14)$$

Re arranging Eq. (3-14) and denoting  $\dot{\epsilon}_{vi}^p = -\alpha \dot{\epsilon}_q^p$

$$\dot{\epsilon}_v^p = \dot{\epsilon}_{vc}^p + \dot{\epsilon}_{vi}^p \quad (3-15)$$

where  $\dot{\epsilon}_{vc}^p$  is that part that is caused by changes in stress and  $\dot{\epsilon}_{vi}^p$  is that part that arises as a result of changes fabric anisotropy.

The above formulation suggests that the overall plastic volumetric strain rate in granular materials is contributed by two sources.  $\dot{\epsilon}_{vi}^p$  is that part that arises as a result of changes fabric anisotropy and thus termed “*fabric induced volumetric strain*”. Since  $\dot{\epsilon}_{vi}^p = -\alpha\dot{\epsilon}_q^p$ , it always remains dilative during loading. This part of plastic volumetric strain is predominant in granular materials as their aggregate arrangements are highly anisotropic. The coupling between *volume and shape changes* observed qualitatively and termed granular *dilatancy* by Osborne Reynolds (Reynolds, 1885) has influenced many a concept in the modeling of the stress-strain behavior of soils. However, whilst various attempts have been made to incorporate dilatancy into constitutive models, little regard is made to its mechanical origins. Goddard and Bashir (1990) have shown that Reynold’s dilatancy is essentially a kinematical constraint. Further, Kanatani (1982), Goddard & Bashir (1990) and Houlsby (1993) have argued that such an internal kinematic constraint does not contribute to plastic energy dissipation. Since  $\dot{\epsilon}_{vi}^p$  is a kinematic constraint and is always dilative, it is assumed here  $\dot{\epsilon}_{vi}^p$  is that due to Reynolds effect.

Micro-mechanical studies have shown that when a granular material is subjected to loading, the load is carried by a combination of strong and weak networks ((Radjai *et al*). These studies also show that no plastic strains occur in the force chains and all the

plastic deformation occurs in the weak frail network. Thus, all plastic energy dissipation will occur in the weak networks and therefore corresponding strains must be used in the description of the dissipation function as well as in hardening rules. Based on this analogy,  $\dot{\epsilon}_{vc}^p$ , the effective plastic volumetric strain is considered to be occurring inside the weak networks and therefore must be included in both dissipation and hardening rules.

Division of volumetric strain as in Eq. (3-15) has been explored in the past by Shamoto et al. (1998) and Zhang et al. (1999) for modeling the behavior of sands under cyclic loading. A rather different division of the plastic volume strain has been proposed by Chandler (1985) and Nixon and Chandler (1999). The shear induced plastic strain  $\dot{\epsilon}_{vi}^p$  is that part of the volume strain which is recovered after a loading cycle; whilst the stress induced part is the “settlement or accumulated plastic strain” which remains after a loading cycle is completed. The two volume strains  $\dot{\epsilon}_{vi}^p$  and  $\dot{\epsilon}_{vc}^p$  can hence be thought of as the “reversible” and “irreversible” plastic volume strains in this context.

According to the proposed division of volumetric strains, both dilative and contractive volumetric strains are present right from the beginning of loading contrary to extant constitutive models. The new separation of volume changes in granular media is incorporated into the plasticity theory to develop a new anisotropic sand model.

### 3.5 Yield loci of anisotropic sand

The proposed division of plastic volumetric strain by the two sources; fabric induced kinematic  $\dot{\epsilon}_{vi}^p$ , and stress induced  $\dot{\epsilon}_{vc}^p$  enables us to revise the plastic dissipation function (Eq (9)) proposed by Burland (1965) that was used to develop the modified Cam Clay model. Kanatani (1982), Goddard & Bashir (1990) and Houlsby (1993) have argued that since the fabric induced volumetric strain,  $\dot{\epsilon}_{vi}^p$  is the manifestation of internal kinematic constraints, it does not contribute to plastic dissipation (see also Collins and Muhunthan 2003; Collins et al. 2006). Thus, we revise Eq. (2-11) as:

$$\hat{\Phi} = p\sqrt{\dot{\epsilon}_{vc}^p{}^2 + M^2\dot{\epsilon}_q^p{}^2} \quad (3-16)$$

Note that only  $\dot{\epsilon}_{vc}^p$  enters into the above dissipation function. We also note that the choice of the modified Cam Clay dissipation function for revision was motivated by experimental observations, since,  $\dot{\epsilon}_{vc}^p$  is the compressive “accumulated strain increment” induced by cyclic loading under drained conditions as discussed in the previous section. These increments have been found to be approximately normal to a modified Cam Clay type surface by Chang and Whitman (1988) and Nieuemunis et al. (2005). Following the family of critical state models, equating the revised dissipation function to the plastic work done results in:

$$p\dot{\epsilon}_v^p + q\dot{\epsilon}_q^p = p\sqrt{(\dot{\epsilon}_v^p + \alpha\dot{\epsilon}_q^p)^2 + M^2\dot{\epsilon}_q^p{}^2} \quad (3-17)$$

The above equation can be simplified to give the ratio of plastic strains as:

$$\frac{\dot{\epsilon}_v^p}{\dot{\epsilon}_q^p} = \frac{M^2 + \alpha^2 - \eta^2}{2(\eta - \alpha)} \quad (3-18)$$

Eq. 3-18 can be interpreted as a stress-dilatancy rule, which contains an additional parameter, the fabric anisotropy  $\alpha$ .

Recognizing the plastic strain ratio above as the associated flow rule of the theory of plasticity, (3-18) can be integrated to give the yield locus for the anisotropic sand model as (Wood, 1990):

$$\frac{p}{p_c} = \left[ \frac{M^2}{M^2 + (\eta - \alpha)^2} \right] \quad (3-19)$$

where  $p_c$  is the value of  $p$  when  $\eta = \alpha$ . The yield loci for different values of the fabric anisotropy parameter  $\alpha$  are as shown in Fig. 3-3. It is evident that non zero values of  $\alpha$  result in rotated and distorted elliptical yield loci. They reduce to the ellipse that is centered along the  $p$  axis as in modified Cam Clay when  $\alpha$  is zero.

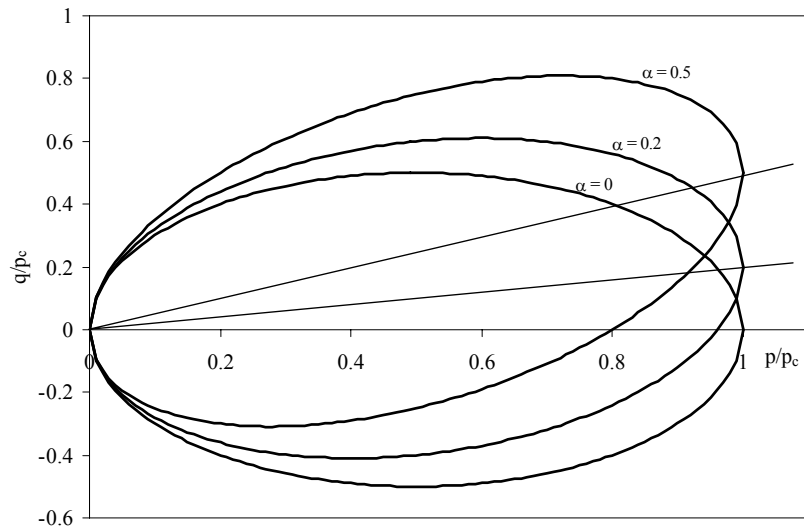


Figure 3-3: Yield locus of new anisotropic sand model with different  $\alpha$  values

Oda (1993) has also produced yield loci which are distorted ellipses with rotation when he included the fabric tensor as measure of induced anisotropy for granular materials. He demonstrated that the yield locus of the shape of the distorted ellipse with rotation fits very well with the experimentally determined yield locus (Yasufuku, 1990) for anisotropically consolidated sands.

### 3.6 Datum states of dilatancy

The inclusion of the fabric anisotropy parameter  $\alpha$  in the dissipation function and consequently in the yield curve results in three important datum states as shown in Fig. 3-4. Firstly, when subjected to isotropic strains,  $\dot{\epsilon}_q^p = 0$  the resulting stress state is *not* isotropic but lies upon the “kinematic normal consolidation line” KNCL, with slope  $\alpha$ .

In most critical state based models, relationships of the form (3-19) are often characterized as a form of stress-dilatancy relationship. However, as discussed earlier granular dilatancy consists of kinematic (Reynolds type) as well as stress-induced components. Thus the use of stress-dilatancy in relationships of the form (3-19) is not appropriate for anisotropic soils. It is just a flow rule as used here (see also Collins and Muhunthan 2003).

There is a second datum state at which the volumetric strain  $\dot{\epsilon}_v^p = 0$  and where it changes its sign from positive to negative. The line on which this occurs is often termed the phase transformation line (PTL) encountered in undrained tests (Ishihara 1978),

though Mroz (1998) suggested the term “Zero dilatancy line” since the plastic volumetric strain rate is zero on this line. From (19), the slope of the PTL can be determined to be

$$\eta = \sqrt{M^2 + \alpha^2} .$$

The third datum line corresponds to the state defined by  $\dot{\epsilon}_{vc}^p = 0$ . An expression for  $\dot{\epsilon}_{vc}^p$  can be derived from Eq. (3-19) using the decomposition of the volumetric plastic strains (Eq. (3-13)) as:

$$\frac{\dot{\epsilon}_{vc}^p}{\dot{\epsilon}_q^p} = \frac{M^2 - (\eta - \alpha)^2}{2(\eta - \alpha)} \quad (3-20)$$

When  $\dot{\epsilon}_{vc}^p = 0$ :

$$\eta = M + \alpha ; \quad \frac{\dot{\epsilon}_v^p}{\dot{\epsilon}_q^p} = -\alpha \quad (3-21)$$

This is the classic Taylor (1948) stress-dilatancy relation. Notice, however, that  $\dot{\epsilon}_{vi}^p$  is non-zero at this state; therefore, dilation is now entirely due to the Reynolds effect. Even though the sand is dilating, the dissipation is entirely due to shear as at this state the dissipation function (3-17) reduces to:

$$\hat{\Phi}_T = Mp \left| \dot{\epsilon}_q^p \right| \quad (3-22)$$

which is the classical Thurairajah (1961) dissipation function that was used in the original Cam Clay model (Roscoe et al. 1963). Some further properties of this line were discussed by Collins and Muhunthan (2003) and Collins (2005), who termed it as the “Reynolds-Taylor Line” (RTL). As the undrained stress path of dense sands becomes asymptotic to

this line, it was also termed as the asymptotic line by Gudehus et al. (1976) or the “ultimate line” by Poorooshab (1989) in the literature.

In general,  $\alpha$  evolves with shear and the three datum state lines, KNCL, PTL and RTL rotate as the deformation proceeds. It should be noted when  $\alpha = 0$ , the yield curve reduces to an ellipse centered along the  $p$  axis as in modified Cam Clay, RTL and PTL coincide and become the standard critical state, and KNCL becomes the isotropic consolidation line (ICL).

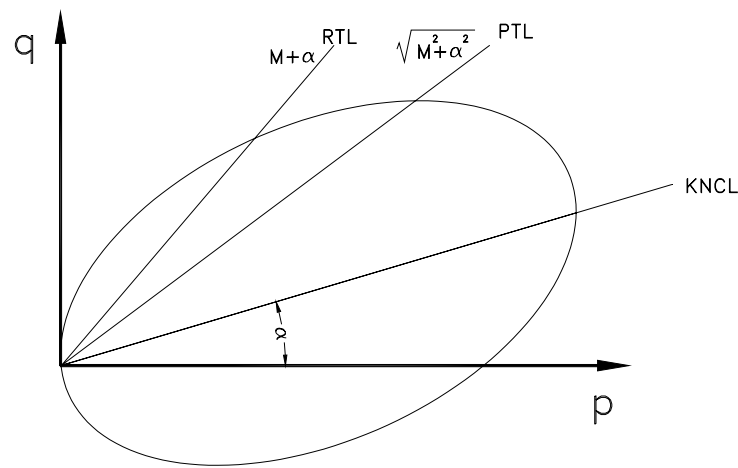


Figure 3-4: Features of new anisotropic sand model

In compression tests, these datum rotate counter-clockwise (Fig. 3-5), therefore RTL moves inside the PTL in the extension side. In the extension region, where  $\dot{\epsilon}_q^p$  is negative, the resultant volumetric strain rate due to fabric anisotropy,  $\dot{\epsilon}_{vi}^p$  is compressive, and would result in overall volume decrease. Thus, if a specimen is unloaded from a

given dilatational state, at constant pressure, and then sheared in the opposite direction, the specimen starts to contract plastically, and reach the RTL first with no possibility of attaining PTL. This would be the case for sands with a collapsible structure for which  $\alpha$  would be negative to begin with.

Usually the shearing in the extensive side develops anisotropy in that direction destroying the anisotropy that developed in the compressive side. In other words, the value of the fabric anisotropy parameter goes from positive to negative according to the sign of plastic shear strain. Upon further deformation the evolution of  $\alpha$  and accordingly the locations of RTL and PTL would essentially follow the pattern as in the case of normal sands. This has been observed in the past by several experiments on ultra loose sands (e.g. Alarcon et al. 1988). As one would expect in such a kinematic hardening, anisotropic model, the material is exhibiting a Bauschinger effect. This is also a feature of the model of Houlsby (1993), who notes that this is entirely consistent with the ‘sawtooth’ analogy, where there is a definite preferred orientation needed to produce dilation.

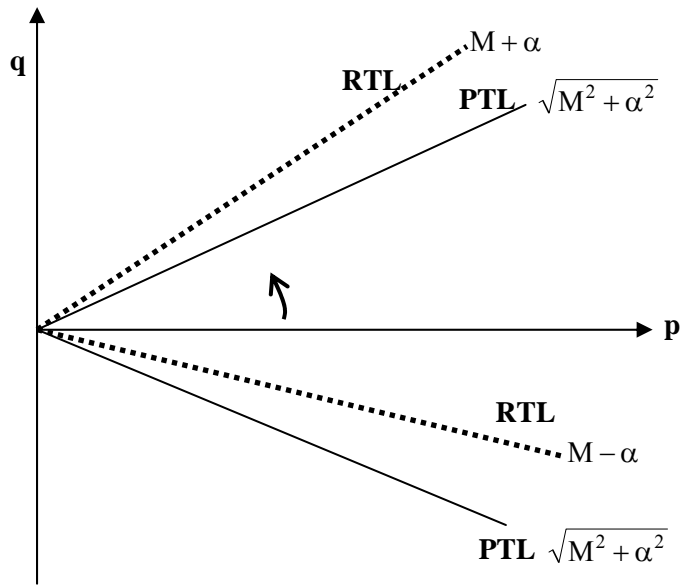


Figure 3-5: Dilatancy datum in compressive and extensive sides

The insights gained from the granular dilatancy model and its implications on plastic dissipation and the yield surface discussed above are utilized in the following sections to model monotonic and cyclic behavior of sands within the context of bounding surface elasto-plasticity.

## *Chapter 4*

### **MODEL PARAMETERS**

This chapter presents a discussion of the various parameters of the model and their determination using laboratory test.

#### **4.1 Experimental observations**

A series of drained and undrained triaxial compression tests were conducted by Olcott (2001) on Ottawa sand, manufactured by U.S. Silica from Ottawa Illinois. Specimens were prepared using water sedimentation. The sand is a silica sand consisting of mostly rounded grains with a specific gravity of 2.65. The grain size distribution is given in Figure 4-1. Soil index properties include a coefficient of uniformity of 1.51, coefficient of curvature of 0.97, and a mean grain size of 0.44mm. According to USCS, the sand is classified as poorly graded (SP). The maximum void ratio was determined in accordance with ASTM D4254-91 Method C. The minimum void ratio was determined using a slight variation of ASTM D4253-93 (Olcott, 2001). The ASTM maximum and minimum void ratios for Ottawa F-35 sand were determined to be 0.76 and 0.56 respectively.

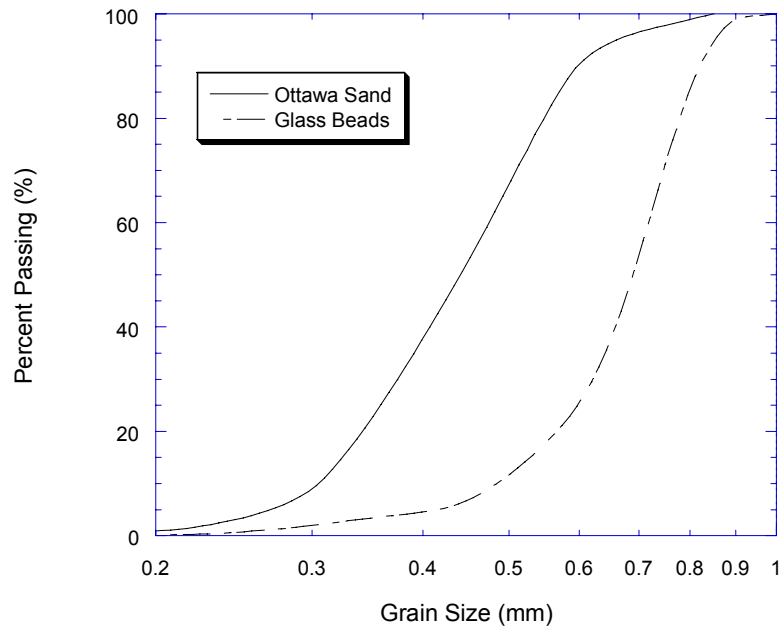


Figure 4-1: Grain Size Distribution for Ottawa F-35 Sand and Glass Beads

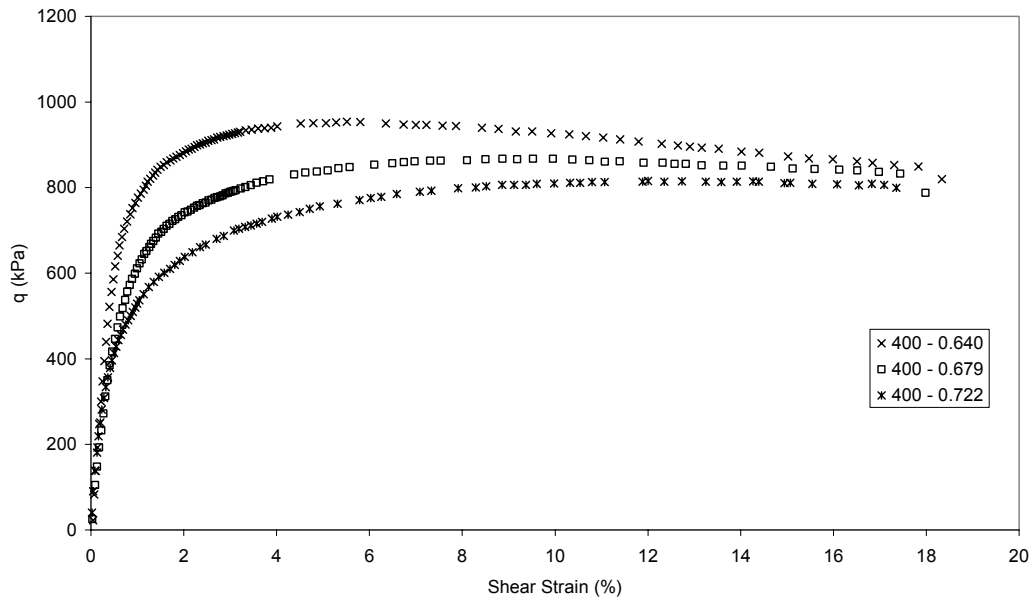
A Brainard-Kilman Model S-600 triaxial loading frame manufactured by GEO Store from Stone Mountain, Georgia was used to conduct all triaxial compression tests. Allowable deformation rates range from 0.0025mm/min to 5.0 mm/min. The maximum allowable cell pressure for this load frame is 1200 kPa, but limitations such as supply pressure, maximum line pressures, and regulators limited the maximum allowable cell pressure to 800 kPa.

Typical measured stress, strain and volume change characteristics of sands with differing void ratio but consolidated to the same initial confining stress are as shown in Figure 4-2. It can be seen that the critical state condition is not achieved in any of these specimens even after 18% of shear strain.

The measured shear stress strain and volumetric values are used to calculate the plastic dissipation rate,  $\zeta_m = \frac{\hat{\Phi}}{p|\dot{\epsilon}_q^p|}$  using necessary energy corrections (Muhunthan and Olcott, 2002; Muhunthan et al. 2004) and plot its variation with strain as shown in Fig. 4-3. It can be seen that after an initial scatter  $\zeta_m$  values attain a constant value around 3 to 4 % strain and remains constant beyond. Similar data for simple shear tests have been given by Stroud – see Muir Wood (1990). As emphasized by Muhunthan *et al* (2004) this result enables the slope of the final critical state line in q-p space, to be determined from data obtained at low strain levels, and so avoiding the difficulties caused by the development of inhomogeneous deformations, which occur at strains greater than 20%.

Furthermore, the constant value  $\zeta_m$  is found to be equal to M independent of the initial consolidated conditions thus reducing the plastic dissipation  $\hat{\Phi}$  to Thurairajah's dissipation function  $\hat{\Phi}_T$  (Eq. 2-11). Consequently,  $\dot{\epsilon}_{vc}^p$  must necessarily be zero. Thus, in accord with the proposed theory, the Reynolds Taylor Line (RTL) is attained at this stage (Eq. 3-20) and sand state continues to remain in this state. Since  $\dot{\epsilon}_{vc}^p = 0$  in this state, the rate of change of volumetric strain is entirely due to Reynolds dilatancy, given by  $\dot{\epsilon}_{vi}^p = -\alpha\dot{\epsilon}_q^p$  (see Eq. 3-14). This is evident from the near linear volumetric response in the post RTL region for the strains considered here (Fig. 4-2).

Note that there is scatter in the  $\zeta_m$  values at the initial stages due to the fact that the realization of M to its ultimate value is not instantaneous but gradual as the granular assembly becomes fully mobilized. This was also recognized and discussed by



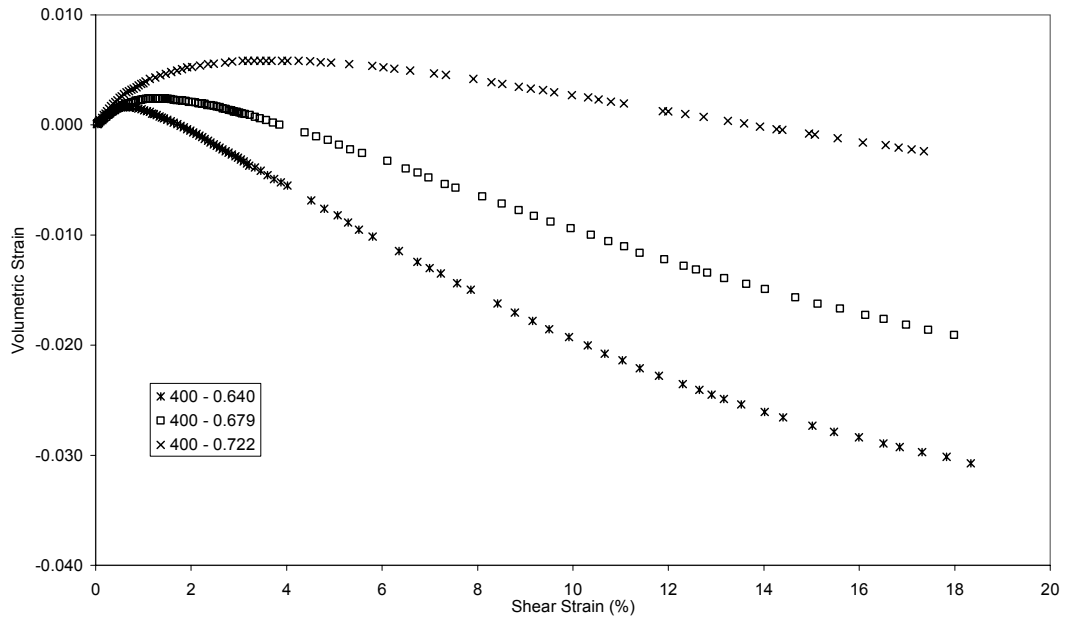


Figure 4-2: Typical drained test results on Ottawa sand

Kabilamany and Ishihara (1990). Following their proposal, the variation of  $M$  is modeled by an inverse tangent relation between  $M$  and the plastic shear strain:

$$M = M_0 + \frac{2}{\pi}(M_f - M_0) \arctan(\varepsilon_q^P / S) \quad (4-1)$$

where  $M_0$  is the initial value (estimated to be 0.9), and  $M_f$  is the final value of  $M$  (Fig.4-2). The value of  $M_f$  is 1.14 for Ottawa sand, whilst  $S$  is taken to be 0.012.

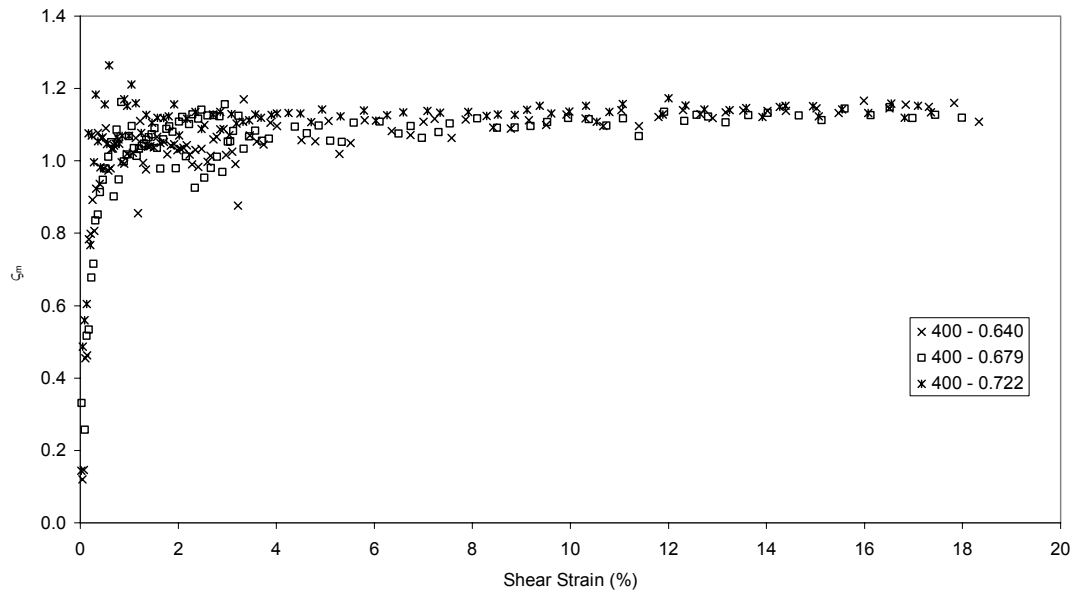


Figure 4-3: Variation of  $\zeta_m$  with shear strain

## 4.2 Critical state line

The uniqueness of the critical state line in the three dimensional space ( $q$ ,  $p$ ,  $e$ ) is central to current critical state based soil models and practical approaches in determining the residual shear strength characteristics. The original critical state concepts were developed mainly based on the behavior of reconstituted, essentially isotropic, materials. As further experimental information has been obtained, it has become evident that although in some cases a unique critical state line is found, this by no means is universal. For example, Riemer and Seed (1997) and Mooney et al. (1997) and (1998), show dependence of the CSL in the void ratio  $e$  – mean effective pressure  $p$  space on the loading direction and manner, while Yoshimine and Ishihara (1998) show the same for

the ultimate steady state line. The behavior of sands, particularly the angular sands commonly encountered in the field, appears to deviate significantly from the original premises of critical state in the sense of a non-unique critical state line. Such deviation has been attributed to the microstructure or fabric of naturally deposited granular medium, and sand models accounting for fabric anisotropy have introduced the possibility of a critical state line in the  $e - p$  space which is not unique, but dependent on the fabric, inherent and/or evolving, with considerable success in simulation of data (Li and Dafalias, 2002, Dafalias et al., 2004).

Li and Dafalias (2002) and Dafalias et al. (2004) proposed that the dependence can be introduced through the value of the critical void ratio  $e_0$  at  $p = 0$  as:

$$e_0 = e_A \exp(-A) \quad (4-2)$$

where  $A$  is the fabric parameter. The results of this dependence are shown in Fig. 4-4, where the parallel “translation” of the CSL resulting from such dependence may be observed. For  $A = 0$  (isotropic fabric) the  $e_0 = e_A$ . Note that  $e_A \equiv \Gamma$  (Eq. 2-2). Since the state parameter  $\psi$  is now measured from the “translating” CSL, the peak stress ratio  $M_b$  and stress-dilatancy relations are indirectly dependent on the fabric parameter (Sec.2.8.1).

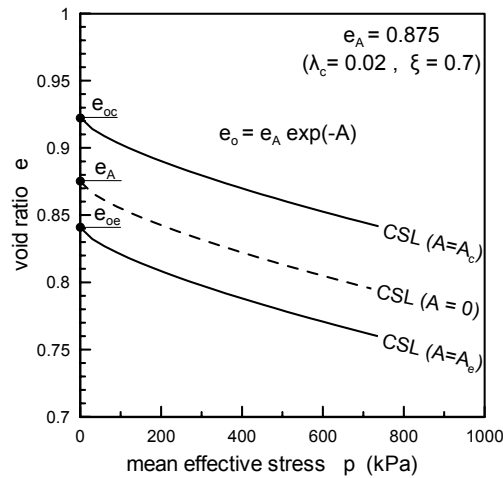


Figure 4-4: The relocation of the CSL as a function of the anisotropy parameter A

This feature is automatically captured by the current theory because here the RTL, which is equivalent to the CSL in critical state theory, rotates and translates in  $q - p$  space and  $e - \ln p$  space, respectively, with the fabric anisotropy parameter,  $\alpha$ . Therefore, the concept of RTL can be useful in determining the state parameter  $\psi$ . Moreover, no assumption is made about the existence or uniqueness of a critical state line. However, if a homogenous, drained test can be sustained until the dilation ceases, without the occurrence of significant crushing, then the sand would reach a final, critical state line.

### 4.3 Evolution of fabric anisotropic parameter

As explained in the section 4.1, beyond shear strain of 3 – 4 % the plastic dilation is purely kinematic and equal to the fabric anisotropic parameter,  $\alpha$ . However, it is evident that the fabric anisotropic parameter is not a constant, as samples at different packing have entirely different slopes of volumetric strain vs. shear strain curves (Fig.4-

2). Desai (1995) has suggested that under a combination of shear and hydrostatic stresses, anisotropy of geologic materials first increases. But upon further loading, it must necessarily decrease as the relative magnitude of the hydrostatic stress increases. Thus, as the loading is increased, the material will self-adjust and tend toward the isotropic state; which represents an amorphous condition (Drucker, 1991). Horne (1965) had surmised that during the initial stages of deformation grains tend to align with the major principal stress direction resulting in the development of anisotropy in that direction. But after some deformation, when the sliding between particles is no longer confined to specific directions, the degree of anisotropy decreases, causing a decrease in the stress ratio as well as the rate of dilation. These proposals suggest that  $\alpha$  must vary with shear strain, beginning at zero, since the material is assumed initially isotropic, here growing to a maximum level of anisotropy and thereafter reducing progressively. Accordingly, the following set of equations is proposed to capture the evolution of  $\alpha$ :

$$\dot{\alpha} = A \dot{\epsilon}_q^p \left( \alpha_f - \alpha \frac{\dot{\epsilon}_q^p}{|\dot{\epsilon}_q^p|} \right) \quad (4-3)$$

$$\alpha_f = \alpha_m \{ \exp(-d_2 \langle v_k - v_{k0} \rangle) \} \quad (4-4)$$

where  $d_2$  is material constant,  $\alpha_m$  is the maximum anisotropy that the sample could develop and  $v_k = e + \lambda \ln p$ ;  $v_{k0} = e_0 + \lambda \ln p_c$  ( $e_0$  is initial void ratio). The Macauley brackets  $\langle \rangle$  define the operation  $\langle Z \rangle = \bar{h}(Z)Z$ , where  $\bar{h}$  being the Heaviside step function, which takes zero or one if the argument is less or greater than zero, respectively. The

incremental rate of fabric anisotropy parameter has been proposed following Houlsby (1993).

The rate of dilation with shear strain after attainment of the Reynolds Taylor state is given by the tangential slope of the volumetric curve (Fig. 4-2 (b), Eq. 3-21). The peak slope of this curve would correspond to the maximum level of anisotropy,  $\alpha_m$ , attained. Using the curves in Fig 4-2(b) and other similar data at various combinations of initial void ratios and confining pressures (Olcott, 2001), the maximum level of anisotropy  $\alpha_m$  can be calculated and plotted as a function of  $v_{k0}$  as shown in Fig. 4-5. Based on this,  $\alpha_m$  is assumed to vary as:

$$\alpha_m = B \exp(-bv_{k0}) \quad (4-5)$$

where  $B$  and  $b$  are material constants. For Ottawa sand  $B = 30405$ ,  $b = 16.44$ , respectively.

The following table summarizes the model parameters, the material constants used in them, and corresponding equations.

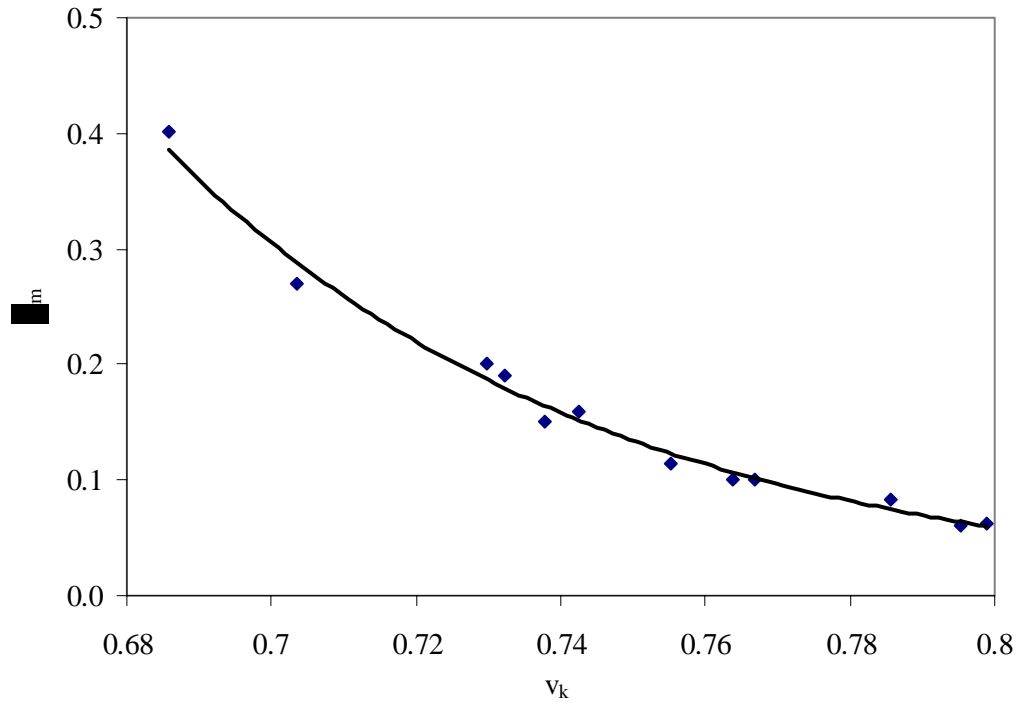


Figure 4-5: variation of maximum anisotropy with  $v_k$

Table 4-1: Summary of model parameters

Model parameter	Material constants
fabric anisotropic parameter, $\alpha$ (Eq. 4-3, 4-4 & 4-5)	$A, \alpha_m, d_2, B, b$
slope of critical state line in q-p space, $M$ (Eq.4-1)	$M_0, M_f=M_c, S$
slope of critical state line in v-lnp space	$\lambda, \kappa, N$
elastic moduli (Eq. 5-27, 5-28)	$G_0, p_a, \nu$
plastic moduli (Eq. 5-21)	$H_0$

## *Chapter 5*

### **BOUNDING SURFACE SAND MODEL**

#### **5.1 General**

The anisotropic sand model developed under triaxial loading in the previous chapter is extended here to general 3 – D conditions using the bounding surface theory of plasticity (Dafalias and Popov, 1975). In the early days, the load-deformation problems in geotechnical analysis were solved by employing the simplest linear elastic or rigid-plastic material models. However, soil is a multi-phase material that consists of solids, water, and air; hence its mechanical response is highly nonlinear, inelastic, rate dependent, and anisotropic. Therefore, in order to describe nonlinear mechanical behavior of soils, several nonlinear models have been proposed. Nonlinear soil models based on the Mohr-Coulomb and the hyperbolic stress-strain formulation (Duncan and Chang, 1970) have been used successfully to model embankments under monotonic loading. Since the dependence of the stress-strain relationship on stress path and stress history is ignored in these models the unloading path would trace back the initial loading path unless a different modulus (unloading-reloading modulus) is used. Masing's laws (Masing, 1926) are often used to capture the hysteresis effects of soil response under cyclic loadings.

It is virtually impossible to model path dependence and dilatant characteristics of soils by elastic models. For example, if a clockwise shear stress produced dilation then

conversely an anticlockwise shear stress would have to produce compression (Schofield, 1980). Moreover, granular materials exhibit permanent volumetric deformation during drained cyclic loading. This permanent volumetric deformation is the primary reason for the progressive build up of excess pore pressure during undrained cyclic loading that leads to liquefaction. Several empirical formulations have been proposed to compute the volumetric strains due to shear strain changes. Martin et al. (1975) proposed an empirical relationship that relates the incremental volumetric strain,  $\Delta\varepsilon_{vd}$ , to the cyclic shear strain amplitude,  $\gamma$ , where  $\gamma$  is presumed to be the “engineering” shear strain and the current accumulated volumetric strain,  $\varepsilon_{vd}$  :

$$\Delta\varepsilon_{vd} = c_1(\gamma - c_2\varepsilon_{vd}) + \frac{c_3\varepsilon_{vd}^2}{\gamma + c_4\varepsilon_{vd}} \quad (5-1)$$

where  $c_1$ ,  $c_2$ ,  $c_3$ , and  $c_4$  are constants. It can be noted that the above equation enables the volumetric strain increment to decrease with accumulation of strains.

An alternative and simpler formula is proposed by Byrne (1991):

$$\frac{\Delta\varepsilon_{vd}}{\gamma} = c_1 \exp(-c_2 \frac{\varepsilon_{vd}}{\gamma}) \quad (5-2)$$

where  $c_1$  and  $c_2$  are constants which can be related to the relative density,  $D_r$  (Byrne, 1991).

Constitutive models that are derived based on plastic theory avoid such empirical relations because the irrecoverable volume strain is naturally coupled with the shear strain, and is given by the stress-dilatancy relation. History of the previous loadings can be tracked by the proper use of plastic internal variables. As strain increment directions

are given by the plastic potential function as opposed to the linear elastic theory where strain increment directions are coaxial to the stress increments, dilative behavior can be modeled in the theory of plasticity; i.e. both clockwise and anti-clockwise shear would produce dilation. Thus, the theory of plasticity is central to the advanced developments of constitutive modeling for liquefaction analysis.

## 5.2 Classical plasticity

When using the concepts of the theory of classical plasticity, one has to formulate: (a) the yield condition defining elastic and inelastic deformation domains (b) the flow rule relating the increments or rates of stress and irreversible strain, and (c) the hardening rule specifying the evolution of the yield surface in the course of plastic deformation and the evolution of hardening parameters defining the state of the material. In stress space, the surface is represented by:

$$F(\sigma'_{ij}, q_n) = 0 \quad (5-3)$$

Since constitutive relations refer to the deformation of the soil skeleton, the state of the material and yield condition are defined in terms of the effective stress  $\sigma'_{ij}$  and plastic internal variables  $q_n$  accounting for the past loading history. The internal variables are usually scalar or second-order tensor quantities such as the plastic work, the plastic strains, etc.

If small strain theory is assumed, and  $\varepsilon_{ij}$ ,  $\varepsilon_{ij}^e$ , and  $\varepsilon_{ij}^p$  are total, elastic, and plastic strains, respectively, the total strain rate is decomposed into:

$$\dot{\epsilon}_{ij} = \dot{\epsilon}_{ij}^e + \dot{\epsilon}_{ij}^p \quad (5-4)$$

The elastic incremental constitutive relations are given by

$$\dot{\epsilon}_{ij}^e = C_{ijkl} \dot{\sigma}'_{ij} \quad \text{or} \quad \dot{\sigma}'_{ij} = E_{ijkl} \dot{\epsilon}_{ij}^e \quad (5-5)$$

where  $C_{ijkl}$ ,  $E_{ijkl}$  are the elastic compliance and moduli matrices, respectively.

The plastic constitutive relations require the definition of the direction (or vector) of plastic loading (flow rule)  $L_{ij}$  and the plastic modulus, both functions of the state, which in turn determine the loading function  $L$  as:

$$L = \frac{1}{K_p} L_{ij} \dot{\sigma}'_{ij} \quad (5-6)$$

where  $K_p$  is plastic modulus. Plastic loading, unloading, and neutral loading occur when  $L > 0$ ,  $L < 0$ , and  $L = 0$ , respectively. The inclusion of  $K_p$  in  $L$  allows for the description of unstable behavior (softening) when both scalar quantities  $L_{ij} \dot{\sigma}'_{ij}$  and  $K_p$  are negative but  $L > 0$  (Dafalias, 1982 & 1986). The plastic strain increment and increment in internal variables are given in terms of  $L$  as:

$$\dot{\epsilon}_{ij}^p = \langle L \rangle R_{ij} \quad (5-7)$$

$$\dot{q}_n = \langle L \rangle r_n \quad (5-8)$$

where the brackets  $\langle \rangle$  define the operation  $\langle z \rangle = z \bar{h}(z)$ ,  $\bar{h}$  being the Heaviside step function, and  $R_{ij}$ ,  $r_n$  are functions of the state. In classical plasticity,  $L_{ij}$  and  $R_{ij}$  are defined as the gradient of a plastic potential,  $G = 0$ , and gradient of a yield locus,  $F = 0$ ;

both are equal to each other if the associated flow rule is assumed, i.e.  $G \equiv F$ .  $r_n$  is the direction of the internal variable increment.

The plastic modulus  $K_p$  is obtained by the consistency condition:

$$\dot{F} = \frac{\partial F}{\partial \sigma_{ij}} \dot{\sigma}_{ij} + \frac{\partial F}{\partial q_n} \dot{q}_n = 0 \quad (5-9)$$

Substituting Eq. 5-8 into 5-9 gives:

$$K_p = - \frac{\partial F}{\partial q_n} r_n \quad (5-10)$$

In Cam Clay models, the yield surface is assumed to undergo isotropic and kinematic hardening along the hydrostatic axis, described by one single scalar  $q_n$ , which measures the plastic volumetric strain. If  $e$  is the total void ratio, the plastic volumetric strain is expressed as

$$\dot{\varepsilon}_{ii}^p = \frac{\dot{e}^p}{(1 + e_0)} \quad (5-11)$$

where  $\dot{\varepsilon}_{ii}^p$  is the trace of the plastic volumetric strain rate tensor,  $e_0$  is the initial void ratio, and  $\dot{e}^p$  is increment in plastic void ratio. Following the critical state framework, the plastic void ratio increment,  $\dot{e}^p$  is expressed as:

$$\dot{e}^p = (\lambda - \kappa) \frac{\dot{p}_c}{p_c} \quad (5-12)$$

Combining (5-11) & (5-12),

$$\dot{\epsilon}_{ii}^p = \frac{(\lambda - \kappa) \dot{p}_c}{(1 + e_0) p_c} \quad (5-13)$$

Thus,  $K_p$  is given by:

$$K_p = -\frac{\partial F}{\partial p_c} (1 + e_0) \frac{p_c}{\lambda - \kappa} \quad (5-14)$$

Combining (5-4), (5-5), and (5-6), the stress and strain increment for elastoplastic deformation is expressed as (Dafalias, 1986):

$$\dot{\sigma}_{ij} = D_{ijkl} \dot{\epsilon}_{kl} \quad (5-15)$$

where  $D_{ijkl}$ , elastoplastic modulus:

$$D_{ijkl} = E_{ijkl} - \bar{h}(L) B^{-1} P_{ij} Q_{kl} \quad (5-16)$$

$$Q_{kl} = E_{klrs} L_{rs}; \quad P_{ij} = E_{ijab} R_{ab} \quad (5-17)$$

$$B = K_p + L_{ab} E_{abcd} R_{cd} \quad (5-18)$$

### 5.3 Kinematic hardening models

Many of the typical foundation problems encountered by geotechnical engineers involve stress reversals, rotation of principal stresses and anisotropic behavior. Earthquake and offshore structures introduce the additional complication of cyclic loading and degradation.

In the classical theory of plasticity, the region enclosed by the yield surface is assumed to be purely elastic and plastic deformation is predicted when the stress state lies on the yield surface and the stress probe is acting outward, i.e.  $L > 0$ . Therefore, a loading that originates from a point inside the yield surface produces elastic deformation until it

reaches the yield surface. Thereafter, both plastic and elastic deformations occur during loading, i.e.  $L > 0$ , only elastic deformation is predicted for unloading, i.e.  $L < 0$ . On the contrary, most geological materials such as clay, rock, and sand do not exhibit purely elastic behavior during unloading and the yield surface, when defined by a small offset value, usually encloses an elastic domain lying in the vicinity of the loading point. Indeed, in some cases the yield surface may not exist at all, i.e., most geological materials experience yield from the very beginning. Moreover, they also show significant hysteretic behavior during unloading – reloading cycles. Therefore, the isotropic hardening model cannot reproduce realistic soil behavior as the yield surface expands uniformly with plastic deformation, so that the size of the elastic region, controlled by the maximum stresses that have been applied, becomes very large. This feature does not allow the classical plasticity models to predict strain accumulation in drained and progressive pore water pressure build up for undrained cyclic deviatoric loading within a stress domain which has been defined as elastic. Therefore, kinematic hardening models were proposed to better describe cyclic loading phenomena in soils.

### **5.3.1 Multi – surface plasticity models**

Prager (1955, 1956) was first to introduce the kinematic hardening rule in plasticity, in which he assumed that yield surface translates without rotation in the stress space in the direction of the strain increment. Ziegler (1959) modified Prager's hardening rule and assumed the rate of translation to take place in the direction of the reduced-stress vector. In kinematic hardening models, the size of yield surfaces remained unchanged

during translation. However, it is argued that mixed hardening rules (Isotropic and Kinematic hardening) where the yield surface is allowed to translate and expand should be used for the realistic representation of soil behavior under cyclic loading condition (Hashiguchi, 1986; Chen and Huang, 1994). Iwan (1967), starting from a one-dimensional model, generalized for multi-dimensional cases in the stress space by assuming a collection of yield surfaces arranged in a series-parallel combination instead of the usual single surface. Each one of the yield surfaces is assumed to obey a linear work-hardening law of the Prager type, but the combined effect gives rise to a non-linear hardening law and can effectively model the Bauschinger effect. Independently, Mroz (1967, 1969) proposed a similar model introducing the concept of the field of work hardening moduli. This field is defined by a configuration of surfaces of constant work hardening moduli in the stress space. To do so, he postulated that the response of a material is governed by a collection of nested yield surfaces, with each surface obeying a linear kinematic hardening law. He also proposed a new kinematic hardening rule that controls the movements of the yield surfaces.

As this framework requires many memory surfaces to keep track of previous loading histories, it is widely called “multi-surface” plasticity. The multisurface framework has been used by several researchers for both clays and sands under monotonic as well as cyclic loading conditions (Prevost, 1977, 1985, Elgamal et al., 2003). Although there are definite advantages in using a multi-surface framework for modeling soil behavior, it does not have a smooth transition from an elastic to fully plastic state for reversed loading, which is observed experimentally on most materials.

Moreover, in a multi-surface formulation, the plastic modulus varies in piecewise fashion and this requires large storage capacity in numerical modeling to keep track of the combined information of many surfaces.

On the contrary, the bounding surface theory of plasticity, originally introduced by Dafalias and Popov (1976) using the plastic internal variables concept and independently by Krieg (1975) in conjunction with an enclosed yield surface, uses only two surfaces; a bounding surface and a loading surface to define a continuous variation of the plastic modulus between them. Therefore, the bounding surface plasticity formulation is used in this study. Subloading surface models (Hashiguchi, 1989, 1998) are sub sets of bounding surface plasticity, as they have the similar structures.

#### **5.4 Bounding surface plasticity**

Bounding surface plasticity has been one of the advanced plasticity theories, which has been applied to numerous problems in geotechnical engineering with a fair amount of success. The theory assumes that all states of soil behavior are enclosed by a surface, which was given different names such as limiting (Krieg, 1975), consolidation (Mroz et al., 1979; Mroz and Norris, 1982), failure (Fardis et al., 1983), or memory surface (Tseng and Lee, 1983). Dafalias (1986) called this surface the bounding surface, and in modeling soil behavior, the normal consolidation surface is considered to be the bounding surface (Dafalias and Hermann 1982; 1986). In spite of the different names, the role of the enclosed surface is essentially the same, as follows: for any given stress state within or on the bounding surface, a proper mapping rule associates it to a corresponding

“image” stress point on the surface. A measure of the distance between the actual and image stress points is used in order to specify the plastic modulus at the actual stress state in terms of a bounding plastic modulus at the “image” stress state (Dafalias, 1986).

Initially the bounding surface theory was applied to clays (Dafalias and Herrmann, 1986). Bardet (1984, 1986) extended its application to sands using a single elliptic surface with variable aspect ratio. Crouch et al. (1994) made further advancement to the bounding surface plasticity for two-dimensional stress space and Crouch and Wolf (1994 a, b) for three-dimensional stress space. The bounding surface concepts have become integral to many soil models, especially for the prediction of their cyclic behavior (Dafalias and Manzari, 1997; Noorzad, 1998; Wang et al., 2002; Li and Dafalias, 2000, 2002). Although the approach is geometric in nature and makes no appeal to physical reasoning of the problem, it lends itself to a number of general and versatile formulations in removing the inherent restrictions in the conventional theory of plasticity.

The loading surface or yield surface is assumed to be of the same shape as the bounding surface (Fig. 4-1). This enables the latter not to intersect but translate and deform with the bounding surface. The bounding surface and loading surface are defined by:

$$F(\bar{\sigma}_{ij}, \bar{q}_n) = 0 \text{ and } f(\sigma_{ij}, q_n) = 0 \quad (5-19)$$

respectively, where  $\bar{q}_n$  and  $q_n$  are internal variables for the bounding and loading surfaces, respectively.  $\bar{\sigma}_{ij}$  is the image point on the bounding surface for the stress point  $\sigma_{ij}$  on the loading surface (Fig.5-1). The image point is found in a way such that the

gradient at the stress point and image point are the same. The plastic modulus on the loading surface is found using linear interpolation with the distance  $\delta$  between the image and stress points. The distance  $\delta$  is expressed in terms of the coordinates as:

$$\delta = [(\bar{\sigma}_{ij} - \sigma_{ij})(\bar{\sigma}_{ij} - \sigma_{ij})]^{1/2} \quad (5-20)$$

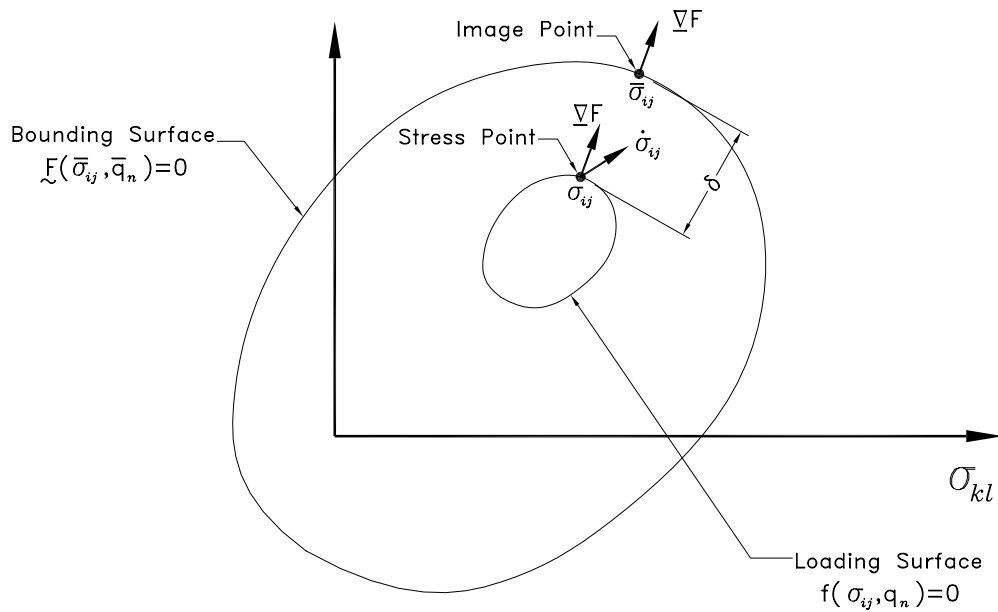


Figure 5-1: Schematic illustration of the bounding surface in a general stress space

The plastic modulus at image point  $K_p$  is found using the consistency condition  $\dot{F} = 0$  (Eq. 4-9), and the plastic modulus at the image point,  $K$  is given as:

$$K = K_p + H_0(\sigma_{ij}, \epsilon_{ij}^p) \left( \frac{\delta}{\delta_0} \right)^{0.5} \frac{M_{RTL} - \eta}{\eta} \quad (5-21)$$

where  $\delta_0$  is the maximum possible distance  $\delta$  could take,  $H$  is a model constant that depends both on the current stress and accumulated plastic strains, and  $M_{RTL}$  is the slope the RTL. When  $\delta \rightarrow 0$ ,  $K \rightarrow K_p$ ; the loading surface touches the bounding surface and the standard classical plasticity formulation holds. Inclusion of  $\eta$  into the plastic modulus allows one to simulate strain softening and control the dilatancy in dense sand. A similar approach is used by Bardet (1986) and Khalili et al. (2005).

### 5.5 New sand model in $q - p$ space

The bounding surface version of the new sand model is first formulated in a triaxial  $q - p$  space as there is a vast amount of experimental data available to verify it. It is then generalized to 3 - D conditions. The bounding surface of the new sand model is obtained from (Eq. 3-19) as:

$$F = (\bar{q} - \alpha\bar{p})^2 - M^2\bar{p}(p_c - \bar{p}) = 0 \quad (5-22)$$

The loading function  $L$  (Eq. 4-6) becomes:

$$L = \frac{1}{K}(n_p\dot{p} + n_q\dot{q}) \quad (5-23)$$

where

$$n_p = \frac{\partial F / \partial \bar{p}}{G_F}, \quad n_q = \frac{\partial F / \partial \bar{q}}{G_F} \quad (5-24)$$

$$G_F = \left[ \left( \frac{\partial F}{\partial \bar{p}} \right)^2 + \left( \frac{\partial F}{\partial \bar{q}} \right)^2 \right]^{1/2} \quad (5-25)$$

$$\frac{\partial F}{\partial \bar{p}} = -2(\bar{q} - \alpha \bar{p})\alpha - M^2(p_c - 2\bar{p}) \quad (5-26)$$

Substituting for  $p_c$  using equation (Eq. 5-22),

$$\frac{\partial F}{\partial \bar{p}} = -2(\eta - \alpha)\alpha \bar{p} + (M^2 - (\eta - \alpha)^2)\bar{p} \quad (5-25)$$

$$\frac{\partial F}{\partial \bar{q}} = 2(\eta - \alpha)\bar{p} \quad (5-26)$$

### 5.5.1 Elastic strains

The shear modulus is assumed to be a function of the mean effective pressure,  $p$  and current void ratio  $e$  (Richart et al., 1970; Anandarajah, 1994):

$$G_s = G_0 p_a \frac{(2.97 - e)^2}{1 + e} \left( \frac{p}{p_a} \right)^{1/2} \quad (5-27)$$

The bulk modulus is related to  $G_s$  in terms of the Poisson's ratio as:

$$K_s = \frac{2G(1 + \nu)}{3(1 - 2\nu)} \quad (5-28)$$

where  $p_a$  is atmospheric pressure,  $G_0$  is the model parameter.

The rate of elastic strains follow as:

$$\dot{\epsilon}_v^e = \frac{\dot{p}}{K_s}; \quad \dot{\epsilon}_q^e = \frac{\dot{q}}{3G_s} \quad (5-29)$$

### 5.5.2 Plastic strains

The bounding surface of the new sand model is as shown in Fig. 5-2. The loading surface is shrunk to a point (Dafalias and Herrmann 1986). Thus, the image point is now found using a “radial” mapping and the plastic strains are formulated from (5-7) as:

$$\dot{\epsilon}_v^p = \frac{1}{K} (n_p \dot{p} + n_q \dot{q}) n_p \quad (5-30)$$

$$\dot{\epsilon}_q^p = \frac{1}{K} (n_p \dot{p} + n_q \dot{q}) n_q \quad (5-31)$$

The parameter K is found using the interpolation relation in Eq.5-21. The distance between current stress point and image point is given by:

$$\delta = [(\bar{p} - p)(\bar{q} - q)]^{1/2} \quad (5-32)$$

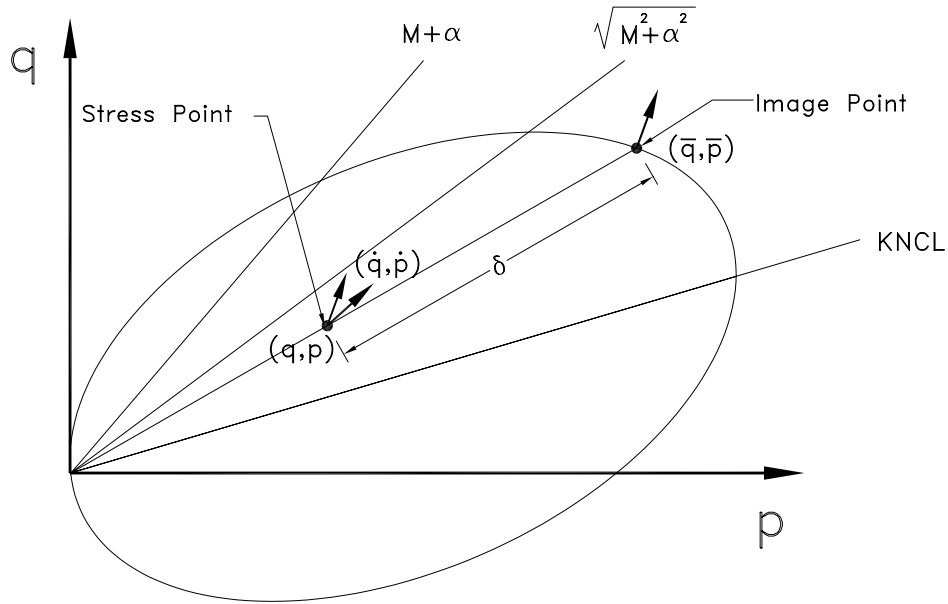


Figure 5-2: Bounding surface illustration in q-p space for the new sand model

Use of the  $\alpha$  parameter in the volumetric hardening rules used in the family of critical state leads to the anisotropic hardening law for the model from which  $K_p$  can be found as follows:

$$\dot{p}_c = p_c \frac{(\dot{\varepsilon}_v^p + \alpha \dot{\varepsilon}_q^p)}{\lambda - \kappa} = p_c \frac{\dot{\varepsilon}_{vc}^p}{\lambda - \kappa} \quad (5-33)$$

$$K_p = -\frac{\partial F}{\partial p_c} \frac{\partial p_c}{\partial \varepsilon_{vc}^p} n_{pc} \quad (5-34)$$

$$n_{pc} = n_p + \alpha n_q \quad (5-35)$$

$$K_p = M^2 \bar{p} \frac{p_c}{\lambda - \kappa} \frac{[M^2 - (\eta - \alpha)^2]}{G_F} \bar{p} \quad (5-36)$$

### 5.5.3 Formulation of incremental stress-strain relations

The total volumetric and deviatoric shear strain increments are given as:

$$\dot{\varepsilon}_v = \dot{\varepsilon}_v^e + \dot{\varepsilon}_v^p \quad (5-37)$$

$$\dot{\varepsilon}_q = \dot{\varepsilon}_q^e + \dot{\varepsilon}_q^p \quad (5-38)$$

Substituting Eq. (5-29), (5-30) and (5-31) into Eq. (5-37) and (5-38), the incremental stress-strain relation for the triaxial loading condition can be obtained as:

$$\begin{pmatrix} \dot{\varepsilon}_v \\ \dot{\varepsilon}_q \end{pmatrix} = \begin{bmatrix} A & B \\ B & C \end{bmatrix} \begin{pmatrix} \dot{p} \\ \dot{q} \end{pmatrix} \quad (5-39)$$

where

$$A = \frac{1}{K_s} + \frac{1}{K} n_p n_p \quad (5-40)$$

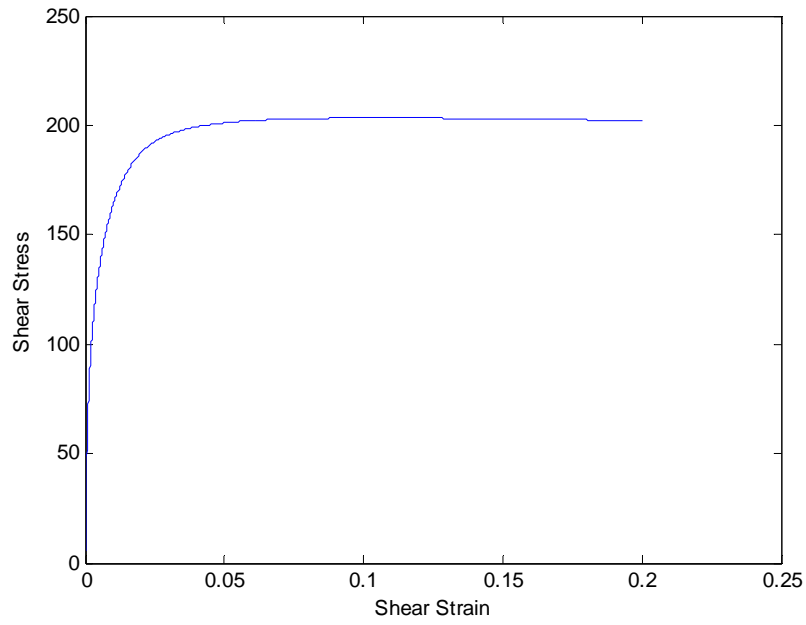
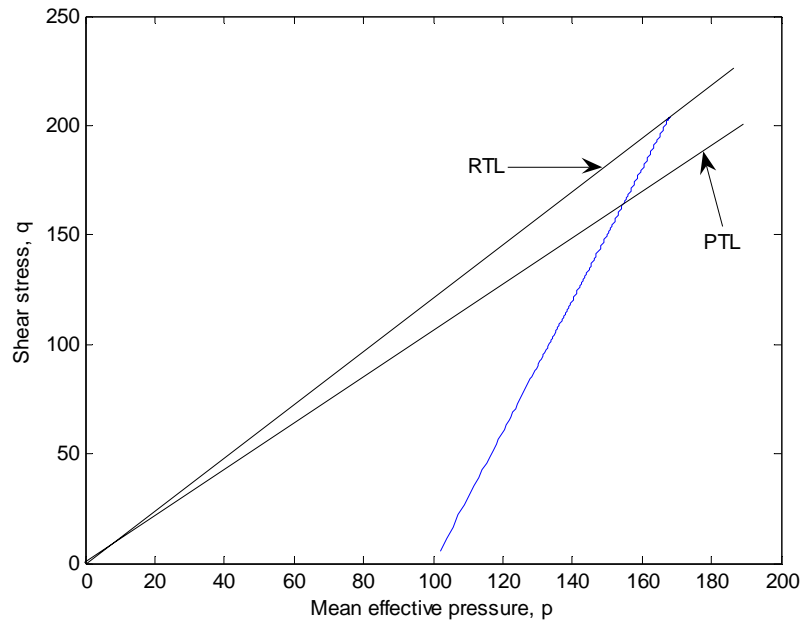
$$B = \frac{1}{K} n_p n_q \quad (5-41)$$

$$C = \frac{1}{3G_s} + \frac{1}{K} n_q n_q \quad (5-42)$$

For undrained loading, the condition of the total volumetric strain increment is zero,  $\dot{\epsilon}_v = 0$ .

#### 5.5.4 Model prediction

The above formulation was coded into MATLAB and some simple simulations were performed to ensure that the new sand model captures the behavior of sand. Typical predictions of drained and undrained tests by the model are shown in Fig. 5-3 and 5-4. Both tests start from mean effective pressure of 100 kPa, with the void ratio of 0.72. In the drained test, the sample initially contracts for stress states below PTL. Once the stress path crosses the PTL, the behavior changes from contraction to dilation. The sample continues to dilate at RTL as shown in Fig.5-3 (a) & (c). Similarly, in the undrained test, positive pore water pressure builds up initially below PTL. Once the stress path crosses the PTL, it begins to dilate, and negative pore water pressure builds up. In this case also, the sample continues to dilate at RTL as shown in Fig.5-4 (a). Therefore, the model predicts the sand behavior satisfactorily in  $q - p$  space.



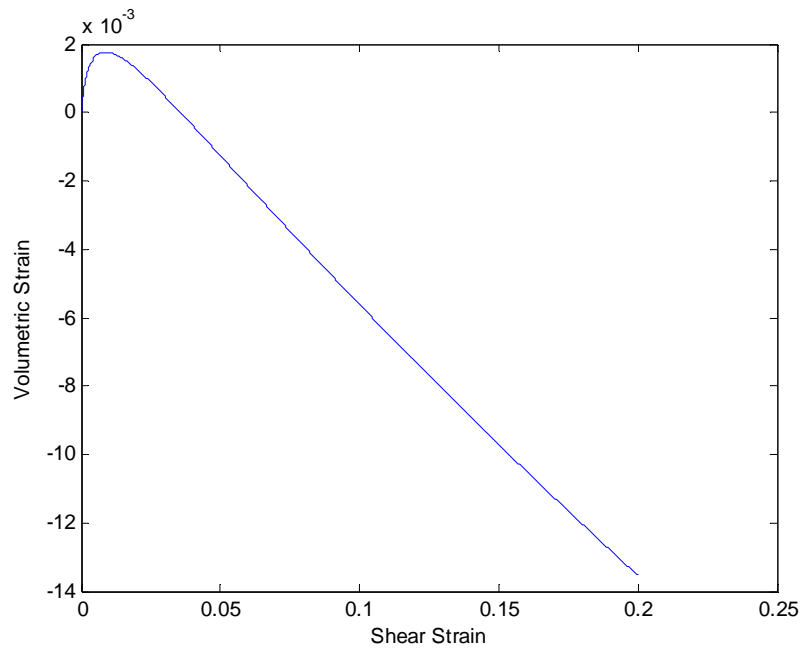


Figure 5-3: Simulation of drained triaxial test (a) stress path in  $q - p$  space (b) shear stress vs. shear strain (c) volumetric strain vs. shear strain

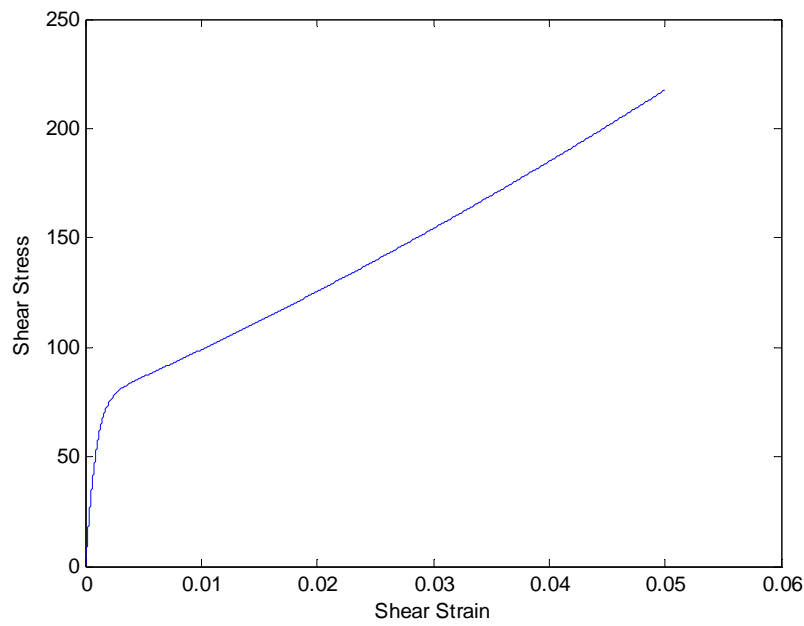
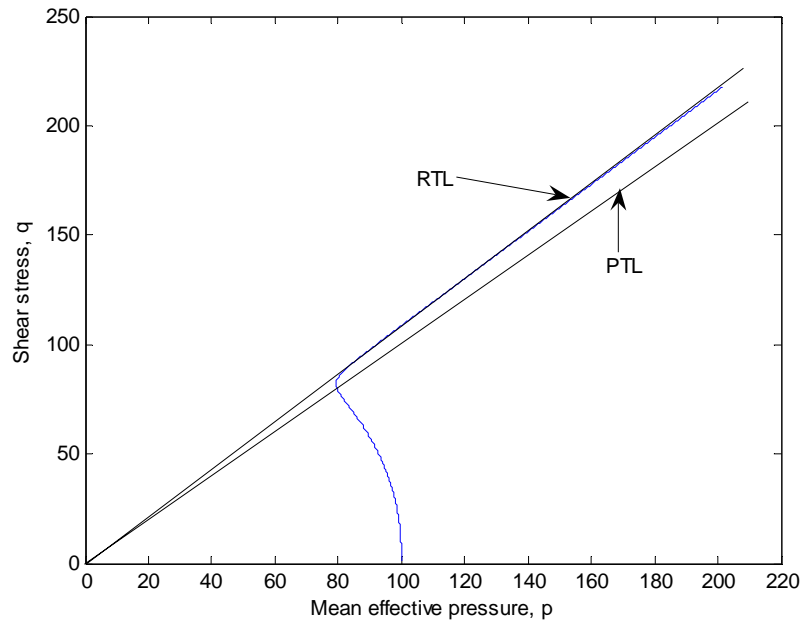


Figure 5-4: Simulation of undrained triaxial test (a) stress path in  $q - p$  space (b) shear stress vs. shear strain

However, it is evident from Fig. 5-5 that the incremental formulation does not capture the actual behavior of sand during unloading. This has also been the case with past investigations (Dafalias and Manzari, 2004). Dafalias and Manzari (2004) chose to modify their stress-dilatancy relation (Eq.12 ) with an ad hoc term to represent the “effect of fabric” to capture this behavior. We present a new mechanism based on the plastic volumetric strain decomposition to rectify this defect. It is conceived that the dilatational volumetric strains are held up by the applied stress ratio and these are “reversible” during unloading. Subsequently, during unloading as the stress ratio decreases, the dilatational volumetric strain is recovered. Thus, the reversible plastic volumetric strain takes the form:

$$\varepsilon_v^p = c[1 - e^{-\beta\eta}] \quad (5-39)$$

where  $c$ ,  $\beta$  are constants, and  $\varepsilon_v^p$  is the dilatational volumetric strain during the unloading. Constant  $c$  can be found equating with the conditions at the point of load reversal.

Eq. (5-39) can be rewritten in rate form by taking derivatives,

$$\dot{\varepsilon}_v^p = c\beta e^{-\beta\eta}\dot{\eta} \quad (5-40)$$

The prediction of the proposed mechanism is shown in Fig. 5-5 and it can be seen that it agrees well with the experimental data.

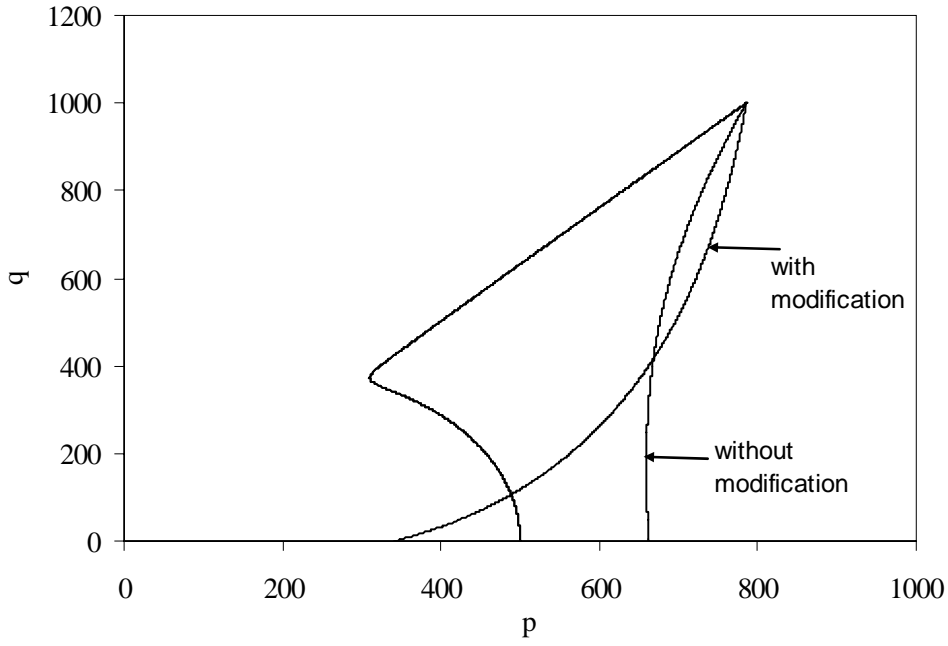


Fig.5-5: Typical loading-unloading stress path

### 5.6 Generalization of new sand model

The new anisotropic sand model is now generalized into six dimensional spaces using invariants in order to implement it into numerical code such as FLAC3D. The stress invariants and their gradients are defined by (Dafalias and Herrmann, 1986):

$$I = \sigma_{ii} \quad ; \quad \frac{\partial I}{\partial \sigma_{ij}} = \delta_{ij} \quad (5-43)$$

$$J = \left( \frac{1}{2} s_{ij} s_{ij} \right)^{1/2} \quad ; \quad \frac{\partial J}{\partial \sigma_{ij}} = \frac{s_{ij}}{2J} \quad (5-44)$$

$$S = \left( \frac{1}{3} s_{ik} s_{kj} s_{ji} \right)^{1/3} \quad ; \quad \theta = \frac{1}{3} \sin^{-1} \left[ \frac{3\sqrt{3}}{2} \left( \frac{S}{J} \right)^3 \right] \quad (5-45)$$

$$\frac{\partial \theta}{\partial \sigma_{ij}} = \frac{\sqrt{3}}{2J \cos 3\theta} \left[ \frac{s_{ik}s_{kj}}{J^2} - 3 \left( \frac{S}{J} \right)^3 \frac{s_{ij}}{2J} - \frac{2}{3} \delta_{ij} \right] \quad (5-46)$$

where  $\delta_{ij}$  is the Kronecker delta;  $\theta$  is the Lode angle which takes the values of  $\pm \pi/6$  for the loading conditions of triaxial compression and extension. The deviatoric tensors  $s_{ij}$ , shear stress  $q$ , and the mean effective stress  $p$  are defined as:

$$s_{ij} = \sigma_{ij} - p\delta_{ij} ; p = \frac{I_1}{3} ; q = \pm\sqrt{3}J \quad (5-47)$$

Yield function can be written as:

$$F(I, J, \theta, \kappa) = 0 \quad (5-48)$$

Gradient of the yield function  $L_{ij}$  is given as:

$$L_{ij} = F_{,I} \delta_{ij} + \frac{F_{,J}}{2J} s_{ij} + \frac{\sqrt{3}}{2 \cos 3\theta} \frac{F_{,\theta}}{J} \left[ \frac{s_{ik}s_{kj}}{J^2} - 3 \left( \frac{S}{J} \right)^3 \frac{s_{ij}}{2J} - \frac{2}{3} \delta_{ij} \right] \quad (5-49)$$

The fabric anisotropy parameter  $\alpha$  is replaced with a second order dimensionless deviatoric tensor  $\alpha_{ij}$ , which is related to  $\alpha$  of triaxial space as:

$$\alpha = \left( \frac{3}{2} \alpha_{ij} \alpha_{ji} \right)^{\frac{1}{2}} \quad (5-50)$$

Rewriting the new sand model (Eq.3-19):

$$F = (s_{ij} - p\alpha_{ij}) : (s_{ij} - p\alpha_{ij}) - M^2 p(p_c - p) = 0 \quad (5-50)$$

The partial derivative of yield function  $F$  with respect to  $I$ ,  $J$ , and  $M$ :

$$F_{,I} = -\frac{2}{3} (s_{ij} - p\alpha_{ij}) : \alpha_{ij} - M^2 (p_c - 2p) / 3 \quad (5-51)$$

$$F_{,J} = 2(s_{ij} - p\alpha_{ij}) \frac{2J}{s_{ij}} \quad (5-52)$$

$$F_{,M} = -2M(pp_c - p^2) \quad (5-53)$$

The energy dissipation equations in the family of critical state models have been formulated as a function of the frictional constant  $M$ . However, sand possesses different critical state strength values for compression and extension. In the triaxial compression ( $q > 0$ ) and extension ( $q < 0$ ) regions, the energy dissipation must necessarily be governed by the triaxial compression ( $M_c$ ) and triaxial extension ( $M_e$ ) critical state parameters, respectively. The parameters  $M_c$  and  $M_e$  can be obtained from the friction angle using the Mohr-Coulomb failure criterion.

The critical state parameter  $M$  is therefore interpolated between  $M_c$  and  $M_e$  as:

$$M = M_c g(\theta, c) \quad (5-54)$$

where

$$g(\theta, c) = \frac{2c}{1 + c - (1 - c) \sin 3\theta}; \quad c = \frac{M_e}{M_c}$$

Partial derivative of  $M$  with respect to  $\theta$  is given as:

$$\frac{M_{,\theta}}{M} = \frac{3(1 - c) \cos 3\theta}{1 + c - (1 - c) \sin 3\theta} \quad (5-55)$$

The evolution law for  $\alpha$  (Eq.4-3 & 4-4) is generalized as:

$$\dot{\alpha}_{ij} = A \|\dot{\epsilon}'_{ij^p}\| \left( \alpha_{ij}^f - \alpha_{ij} \text{sign} \left( \frac{\dot{\epsilon}'_{ij^p}}{(\dot{\epsilon}'_{ij^p} : \dot{\epsilon}'_{ij^p})^{1/2}} \right) \right)$$

where  $\dot{\epsilon}'_{ij^p}$  is the deviatoric part of the plastic strain tensor.

$$\alpha_{ij}^f = \alpha_0 \{ \exp(-d_2 \langle v_k - v_{k0} \rangle) \} n_{ij}; \quad n_{ij} = \frac{L'_{ij}}{(L'_{ij} : L'_{ij})^{1/2}} \quad (5-56)$$

where  $L'_{ij}$  is the deviatoric part of the gradient  $L_{ij}$ .

## *Chapter 6*

### **MODEL IMPLEMENTATION**

#### **6.1 General**

The Fast Lagrangian Analysis of Continua in 3 Dimensions (FLAC3D) was developed by Itasca Consulting Group, Inc. as a general three-dimensional procedure for analysis of geotechnical/geological media subjected to static, dynamic, water flow, and thermal loading conditions (Itasca, 2002). FLAC3D uses a finite difference approach that incorporates the Lagrangian description capable of computing large deformations. It has gained wide acceptance among practicing engineers and researchers as a tool for the design and analysis of a range of engineering problems in rock mechanics, geomechanics, and soil mechanics. It has also been successfully used to numerically simulate a number of geotechnical problems. Besides many built-in nonlinear soil constitutive models such as Mohr-Coulomb, Cam Clay, etc., it provides a user interface to implement new constitutive models. FLAC3D is therefore selected for the current study.

#### **6.2 Dynamic analysis**

The dynamic analysis option in FLAC3D permits three-dimensional, fully dynamic analysis with FLAC3D. The calculation is based on the explicit finite difference scheme to solve the full equations of motion, using lumped grid point masses derived from the real density of surrounding zone as opposed to fictitious masses used for static

solution. FLAC3D also permits analysis of soil-interaction brought about by ground shaking by coupling the dynamic formulation with the structural element model. The dynamic option in FLAC3D is applicable to a wide range of problems in disciplines such as earthquake engineering, seismology, and mine rock burst.

Earthquake loading is basically a cyclic loading because of the shear wave transmission through the soil layers. “Equivalent-linear” and fully nonlinear methods are two commonly used in earthquake engineering for analyzing wave transmission and dynamic soil-structure interaction. In the equivalent-linear method (Seed and Idriss, 1969), a linear analysis is performed, with some initial values assumed for damping ratio and shear modulus in the various regions of the model. With the reference to laboratory-derived curves that relate damping ratio and secant modulus to amplitude of cyclic shear strain, an iterative procedure is performed until there are no further change in assumed and determined soil properties. In contrast, only one run is done with a fully nonlinear method, since nonlinearity in the stress-strain law is followed directly by each element as the solution marches on in time. If appropriate nonlinear laws are used, the dependence of damping and apparent modulus on strain level is automatically modeled.

Although the equivalent-linear method is conceptually simple and user-friendly, it takes drastic liberties with physics. On the other hand, the fully nonlinear method correctly represents the physics but demands more user involvement. If a comprehensive constitutive model is available, the fully nonlinear method can be used to reproduce some of the more-subtle dynamic phenomena. FLAC3D uses the latter procedure in solving dynamic problems. As the new anisotropic sand model captures the nonlinear behavior of

sands well, the new sand model is implemented into FLAC3D to simulate the liquefaction phenomena.

### **6.3 Modeling dynamic pore pressure generation**

Besides modeling the mechanical response of solid materials, FLAC3D also models the flow of fluid through a permeable solid, such as soils. The flow modeling may be done by itself, independent of the usual mechanical calculations of FLAC3D, or it may be done in parallel with the mechanical modeling in order to capture the effects of fluid/solid interaction (Coupled analysis). Fluid/solid interaction involves two mechanical effects. First, the fluid in a zone reacts to mechanical volume changes by a change in pore pressure. Second, changes in pore pressure cause changes in effective stress, which affects the response of the solids. In FLAC3D by default, the pore fluid simply responds to changes in pore volume caused the mechanical dynamic loading. The average pore pressure remains essentially constant in the analysis. However, if the permanent volumetric strain is accounted properly, FLAC3D generates excess pore pressure accordingly.

### **6.4 Explicit, Dynamic Solution (EDS) Scheme**

Numerical solution schemes face several difficulties when geomaterial models are implemented (Hart and Detournay, 2005). Three characteristics of geomaterials cause specific problems in implementing constitutive models.

1. Physical instability: Physical instability occurs in materials with softening behavior, such as rock, concrete and dense/over-consolidated soils. The softening behavior occurs when the material fails and parts of it accelerate and the stored energy is

released in the form of kinetic energy. Numerical solution schemes often have difficulties at this stage because the solution may fail to converge when a physical instability arises.

2. Path dependence of nonlinear materials: In most geo-mechanical systems, there are an infinite number of solutions that satisfy the equilibrium, compatibility and constitutive relations that describe the system. These solutions are corresponding to different stress paths, respectively. A correct solution needs to be identified for the actual stress path. For example, if an excavation is made suddenly (e.g., by explosion) then the solution may be influenced by inertial effects that introduce additional failure of the material. This may not be seen if the excavation is made gradually. The numerical solution scheme should be able to accommodate different loading paths in order to apply the constitutive model properly.
3. Nonlinearity of the stress-strain relation: This is referred to as the dependence of the elastoplastic stiffness matrix on the stress state. The numerical scheme needs to be able to accommodate the various forms of nonlinearity.

The above three characteristics of geo-materials, which cause difficulties in implementing the constitutive model, can all be addressed by using an *explicit, dynamic solution* (EDS) scheme, which is used by FLAC3D (Itasca, 2002) to implement elastoplastic constitutive models for soils and rocks. The scheme allows the numerical analysis to follow the evolution of a geologic system in a realistic manner, without concerns about numerical instability problems. In the explicit, dynamic solution scheme, the full dynamic equations of motion are included in the formulation, and the static equilibrium

state is reached by absorbing the energy in the system through inertial terms added in the formulation. During the ‘collapse’ failure process in softening materials, some of strain energy in the system is transferred into kinetic energy. The kinetic energy radiates from the source and dissipates through the inertial terms in the full dynamic formulations. Therefore, the numerical solution is always stable even when the system being modeled is unstable. On the contrary, schemes that do not include inertial terms must use some numerical procedure to treat physical instabilities. Even if the procedure is successful at preventing numerical instability, the stress path taken may not be a realistic one. However, the EDS scheme can follow the physical path and simulate the effect of the loading path on the constitutive response.

The EDS scheme also allows the implementation of strongly nonlinear constitutive models because the general calculation sequence allows the field quantities (velocities/displacements and forces/stresses) at each element in the model to be physically isolated from one another during one calculation step. This implementation in the general calculation sequence is described as follows.

The general calculation sequence for the EDS scheme is illustrated in Figure 6.1. The figure presents the calculation sequence of one loop calculation for one time step and for each tetrahedron element. In each sequence loop of the time step, the calculation solves two sets of equations: equilibrium of motion and constitutive relationships. The former is invoked to derive the new velocities and displacements from stresses and forces at each mass point. By application of the Gauss divergence theorem to the tetrahedron element, the derived velocities at each mass point are used to express the strain rates of

the tetrahedron element. Then, the constitutive equations are used to calculate new stress from strain rates. The key feature here is that each box in Fig. 6-1 updates all model variables from known values that remain fixed while control is within that box. For example, the lower box takes the set of velocities already calculated and, for each tetrahedron element, computes new stresses. The velocities and other variables are assumed to be frozen for the operation of the box, i.e., the newly calculated stresses do not affect the existing velocities. The assumption is valid provided the time step is so small that the calculated variables cannot propagate from one element to another during this time step. This EDS approach makes the implementation of the non-linear constitutive model possible. All inputs of strain rates and other variables in one tetrahedron element, during the time step, are fixed and not affected by the calculations in other elements. The stress increment calculation from strain rate is straightforward and there is no need to use any iteration process even if the constitutive law is highly nonlinear.

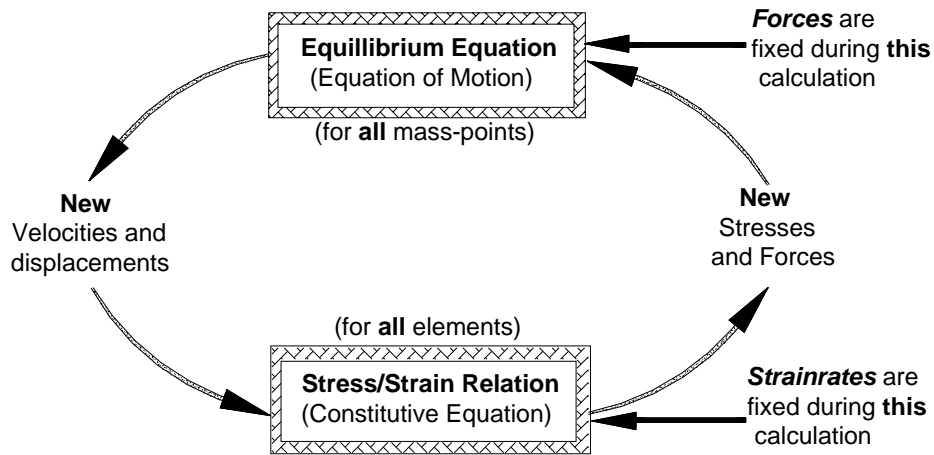


Figure 6-1: Calculation loop of EDS scheme in FLAC3D

## 6.5 Mechanical time step for numerical stability

The differential motion equations cannot provide valid answers unless the numerical scheme is stable. In FLAC, the idealized medium in the system is viewed as an assembly of point masses (located at the nodes) connected by linear springs. It was found from studying the oscillating mass-spring system with a finite difference scheme that a time step must be used that does not exceed a critical time step related to the minimum eigenperiod of the total system. Similarly, the EDS scheme in implementing non-linear constitutive models requires that the time step is so small that the calculated variables cannot propagate from one element to another during the time step. Hence, the stability criterion for the numerical scheme must provide an upper bound for the values of the time steps used in the finite difference scheme.

In FLAC3D, a characteristic of the numerical scheme is that a uniform unit time step  $\Delta t$  is adopted for the whole system. And, the nodal masses in the motion equations are taken as variables and adjusted to fulfill the local stability conditions.

The one-dimensional, one series mass-spring system governed by the differential equation is:

$$-kx = m \frac{d^2x}{dt^2} \quad (6-1)$$

where  $k$  is the stiffness of the spring, and  $m$  is the point mass. The critical time step corresponding to a second-order finite difference scheme for the equation is given by:

$$\Delta t = \sqrt{\frac{4m}{k}} \quad (6-2)$$

For an infinite series spring-mass case, the limit-stability criterion has the form

$$m = k(\Delta t)^2 \quad (6-3)$$

By selecting  $\Delta t = 1$ , the system will be stable if the magnitude of the point mass is greater than or equal to the spring stiffness. In FLAC3D, the validity of Equation (6-3) is extended to one tetrahedron by interpreting  $m$  as the nodal mass contribution  $m^l$  at local node  $l$  and  $k$  as the corresponding nodal stiffness contribution  $k^l$ . The nodal mass contribution as derived from the infinite series criterion provides an upper-bound value for the system under consideration. In order to obtain a stable numerical scheme, the nodal mass contribution should be given a value that is equal to or larger than the nodal stiffness contribution. By a simple diagonalization technique of the local stiffness matrix, the nodal stiffness contribution at local node  $l$  is given by

$$k_{qq} = \frac{\alpha_1}{9V} [n_q^1 S^1]^2 \quad (6-4)$$

where  $\alpha_1 = K + 4/3G$ ,  $K$  is the bulk modulus, and  $G$  is the shear modulus. No summation is implied on repeated index  $q$  of  $k_{qq}$ , which runs from 1 to 3. Then the upper-bound value for the nodal stiffness contribution can be expressed as:

$$k^l = \max(k_{11}, k_{22}, k_{33}) \quad (6-5)$$

which yields the expression for the tetrahedron mass contribution at node  $l$ :

$$m^l = \frac{\alpha_1}{9V} \max\left([n_i^{(l)} S^{(l)}]^2, i = 1,3\right) \quad (6-6)$$

to provide a numerically stable solution.

## 6.6 Mixed discretization

The EDS scheme in FLAC3D is set up on the basis of tetrahedron elements. The tetrahedron element is a constant strain-rate, three-dimensional element. However, these elements do not provide for enough modes of deformation when used in the framework of plasticity. For example, they cannot deform individually without change of volume as required by certain important constitutive laws and exhibit an over-stiff response as compared to that expected from the theory. To overcome this problem, a process of mixed discretization is applied in FLAC3D, as described in Marti and Cundall (1982).

For the mixed discretization technique, more volumetric flexibility is applied to an element by proper adjustment of the first invariant of the tetrahedral strain-rate tensor. A coarser discretization in zones is superposed on a finer tetrahedral discretization. Then,

the technique is accomplished by assigning the first strain-rate invariant and the first stress tensor invariant of any particular tetrahedron as the volumetric-average over all tetrahedral elements in a zone. As shown in Fig. 6-2, the individual tetrahedron will not keep constant volume when subjected to the pattern of deformation; however the total volume of the assembly of the tetrahedral elements (i.e. the zone) remains constant under that deformation pattern.

In FLAC3D, the discretization starts with zones. Then, each zone is internally discretized into tetrahedral elements. An eight-node zone, for instance, can be discretized into two different configurations of five tetrahedral elements (corresponding to overlay1 and overlay2 in Fig. 6-3). The calculation of nodal force can be carried out using one overlay or a combination of two overlays. The advantage of the two-overlay approach is to ensure symmetric response for symmetric loading.

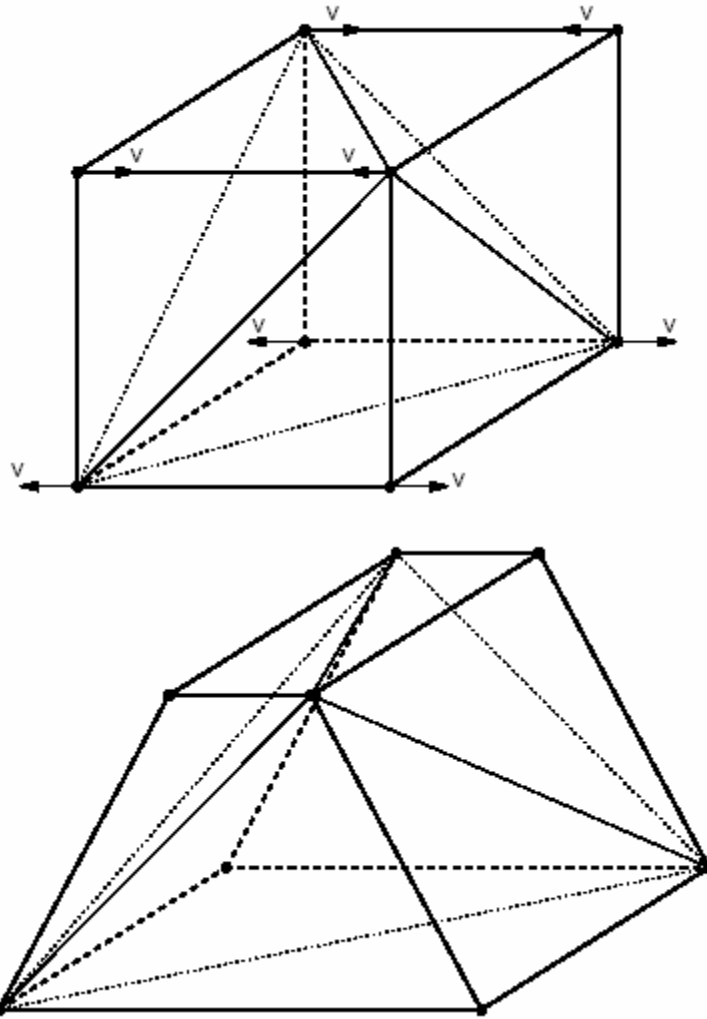


Figure 6-2: Deformation model for which mixed discretization would be most efficient

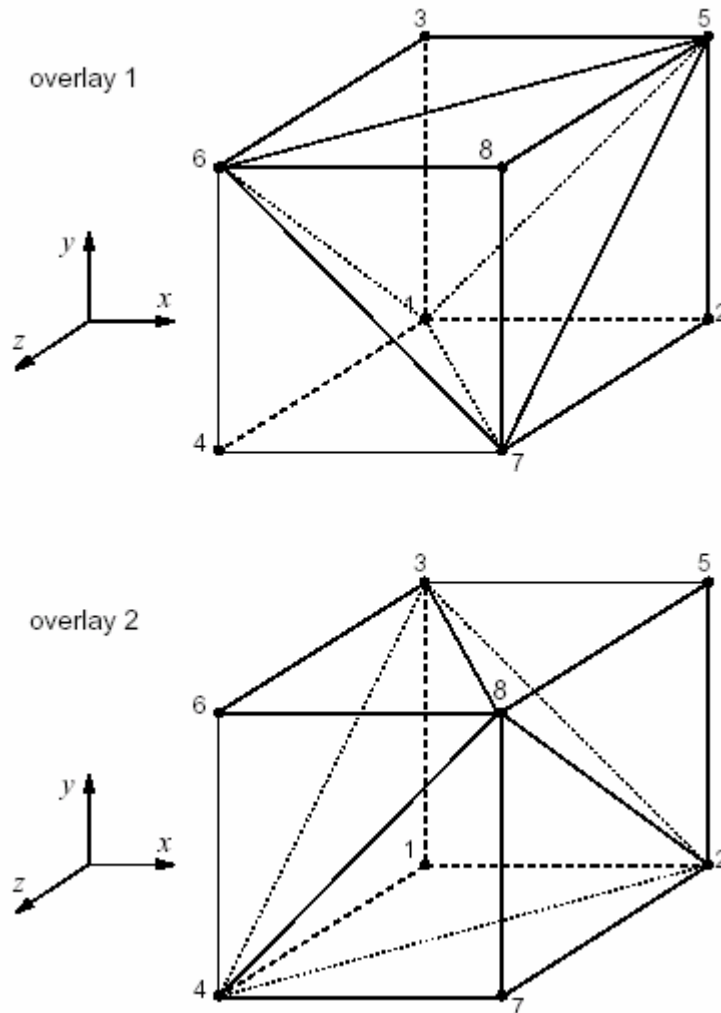


Figure 6-3: An 8-node zone with 2 overlays of 5 tetrahedra in each overlay

## 6.7 Model Implementation

User defined constitutive models can be written in C++ and compiled as DLL (dynamic link library) files that can be loaded whenever it is needed in FLAC3D simulation. The main function of the constitutive model is to return new stresses, given

strain increments. C++ is an object-oriented computer language using classes to represent objects. The data associated with an object are encapsulated by the object and are invisible outside the object. Communication with the object is by member functions that operate on the encapsulated data. In addition, there is strong support for a hierarchy of objects. New object types may be derived from a base object and the base-object's member functions may be superseded by similar functions provided by the derived objects. This arrangement confers a distinct benefit in terms of program modularity and the program can access the derived classes through the base objects.

The emphasis of the object-oriented approach of C++ is to provide a base class that includes a framework for implementing constitutive models, which are classes derived from the base class. The base class, called 'ConstitutiveModel', is termed an 'abstract' class because it declares a number of 'pure virtual' member functions. This means that no object of the base class can be created and that any derived-class object must supply real member functions to replace each of the pure virtual functions of the base class. The methodology of writing a constitutive model in C++ for operation in FLAC3D includes descriptions of the base class, member functions, registration of models, information passed between the model and FLAC3D, and the model state indicators. The implementation is achieved by supplying real member functions to replace each of the pure virtual functions of the base class.

A member function "const char \*Run(unsigned uDim, State \*ps)" as a main interface is called for each sub-zone (up to ten per zone for a two-overlay case ) at each cycle from within FLAC3D's zone scan. The model is coded within the member function

and updates the stress tensor from the strain increment tensor for each sub-zone at each cycle. The structure “ps” contains the current stress components and the computed strain increment components for the sub-zone being processed. For each sub-zone cycle, besides the updated stress tensor, the state parameters must also be returned.

As opposed to the implementation of constitutive models based on the conventional plasticity, the trial-and-correction approach, which is adopted by all built-in models implemented in the FLAC3D manual, is not used in the implementation of bounding surface constitutive model. This is because the yielding surface that defines the pure elastic deformation range doesn't occur in the bounding surface models. The main objective of the current model implementation is to calculate the elastoplastic stiffness matrix  $D_{ijkl}$  shown in Equation (3-26).

The flow chart for programming the anisotropic sand model is shown in Figure 6.4. This program is included in the member function “const char \*Run(unsigned uDim, State \*ps)”. Each tetrahedral element calls this member function for each cycle to update the stress state of the tetrahedron. After all tetrahedral elements in the zone are scanned, the state variables of the zone are modified according to the rule of the mixed discretization scheme. However, the modification of the stress state of the zone will be left for FLAC3D. The member function ConfineModulus(void) is used to return a value for its best estimate of the maximum confined modulus. This is used to determine the stable time step.

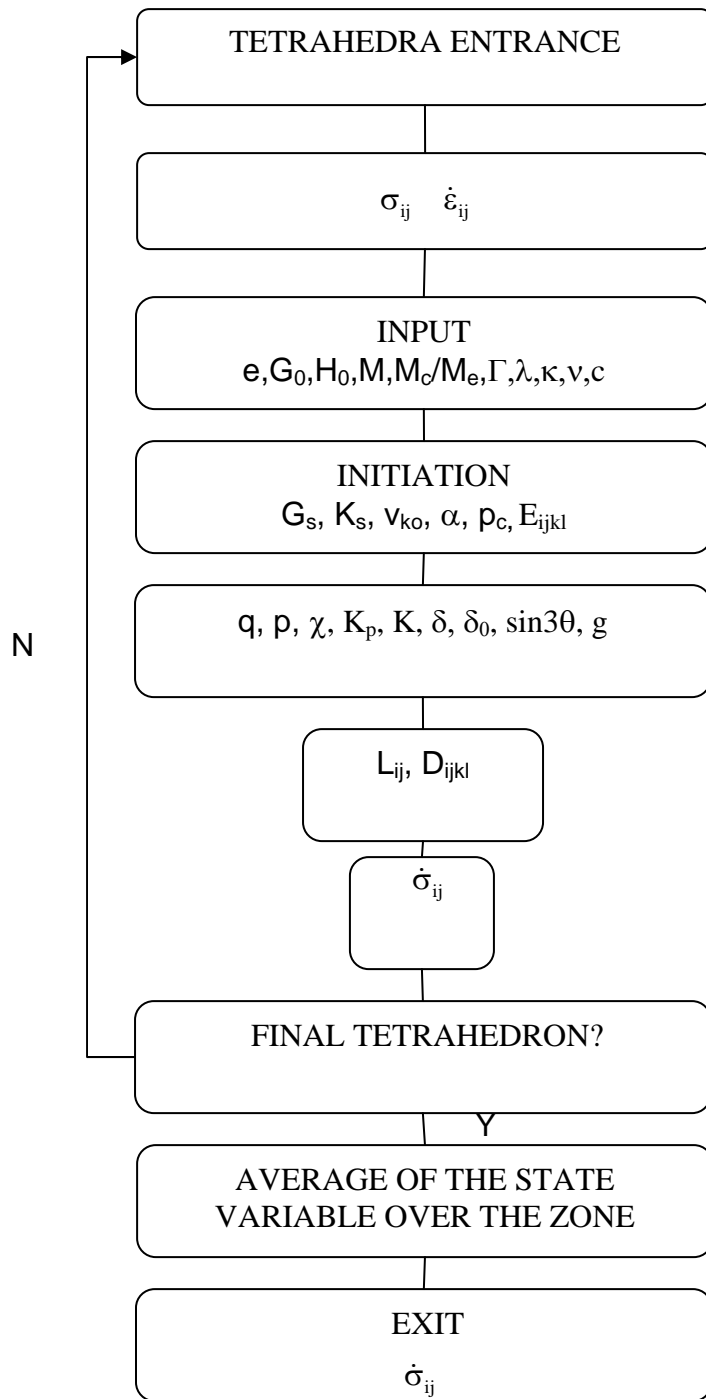


Figure 6-4: Flow chart for coding the constitutive model

## *Chapter 7*

### **FLAC3D ANALYSIS AND RESULTS**

The new sand model implemented in FLAC3D is verified using some available test data under monotonic and cyclic loading. Drained and undrained tests performed by Olcott (2001) are used for the verification of the new sand model under monotonic loading. Cyclic triaxial and centrifuge tests reported in “VELACS” project (Verification of Liquefaction Analysis by Centrifuge Studies, Arulanandan and Scott, 1993) are used to verify the prediction of cyclic loading.

#### **7.1 Monotonic laboratory triaxial test**

Triaxial tests are simulated numerically by using a single zone with unit dimensions. The grid is fixed in the z-direction and a prescribed velocity boundary condition applied at the top of the model (Fig 7-1). The material parameters used are summarized in Table 7-1. The desired initial consolidation pressure is applied by using the “initial” command of FLAC3D. The numerical prediction of triaxial behavior is verified against the tests performed by Olcott (2001) at different combinations of void ratio and consolidation pressure (Table 7-2).

Figs. 7-2 to 7-5 show shear stress vs. shear strain and volumetric strain vs. shear strain drained test prediction and experimental result for the consolidation pressure of 100, 200, 400, and 600 kPa. It can be seen that the model simulations closely match the

experimental results. Fig. 7-6 shows the prediction and experimental results for the undrained tests performed at the void ratio of 0.64 and mean effective pressures of 100, 400, and 750 kPa. Model predictions have again good agreement with experimental results.

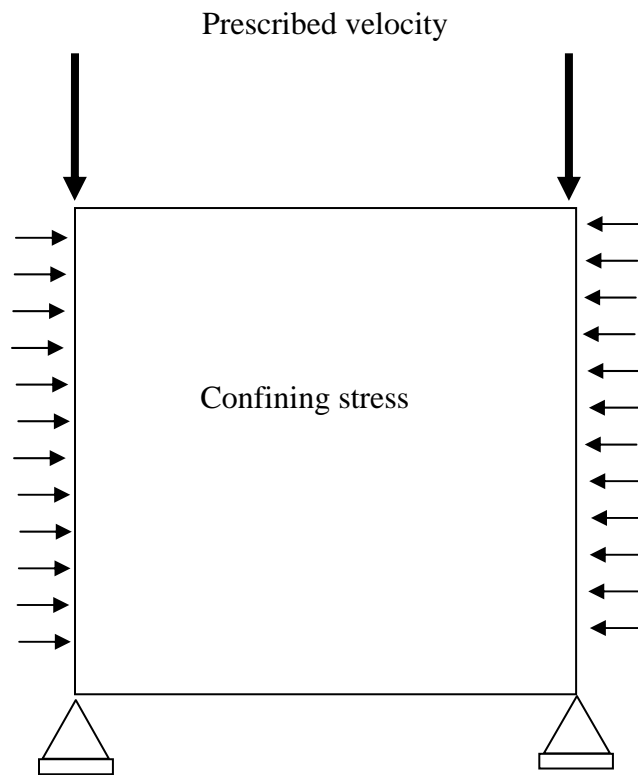


Figure 7-1: FLAC3D single zone; boundary conditions

Table 7-1: Material parameters of Ottawa sand

Material parameters	
$G_0$	125
$\nu$	0.3
$\lambda$	0.016
$\kappa$	0.005
$N$	2.74
$H_0$	10000
$M_c=M_f$	1.14
$M_e/M_c$	0.67
$c$	0.7
$B$	30405
$b$	-16.44
$M_0$	0.9
$S$	0.012
$A$	50
$d_2$	2

Table 7-2: Combinations of mean effective pressure and void ratio for the triaxial monotonic tests

Consolidation Pressure kPa	void ratio
100	0.637
100	0.681
100	0.715
200	0.676
200	0.699
200	0.739
400	0.640
400	0.679
400	0.722

600	0.670
600	0.699
600	0.731

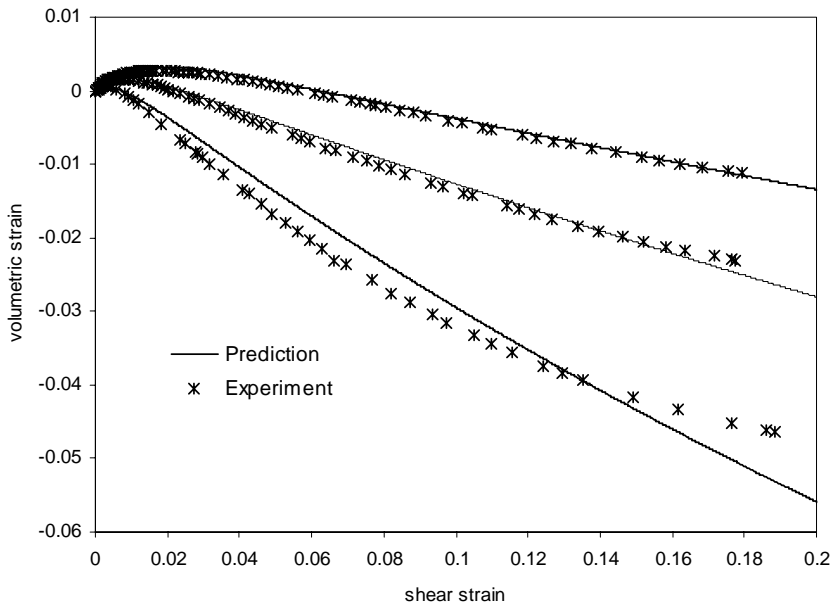
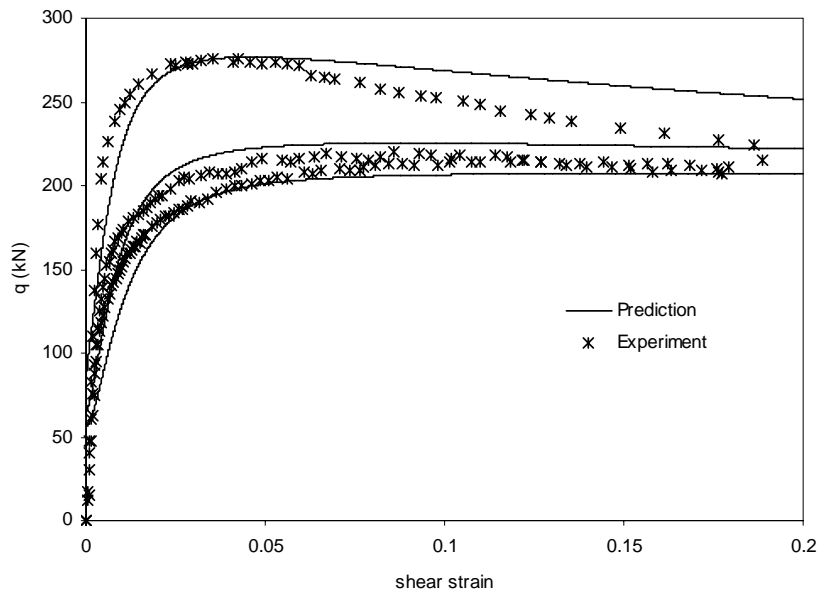


Figure 7-2: Measurements and prediction of drained tests at 100 kPa with different void ratios of 0.637, 0.681, 0.715 (a) shear stress vs. shear strain (b) volumetric strain-shear strain

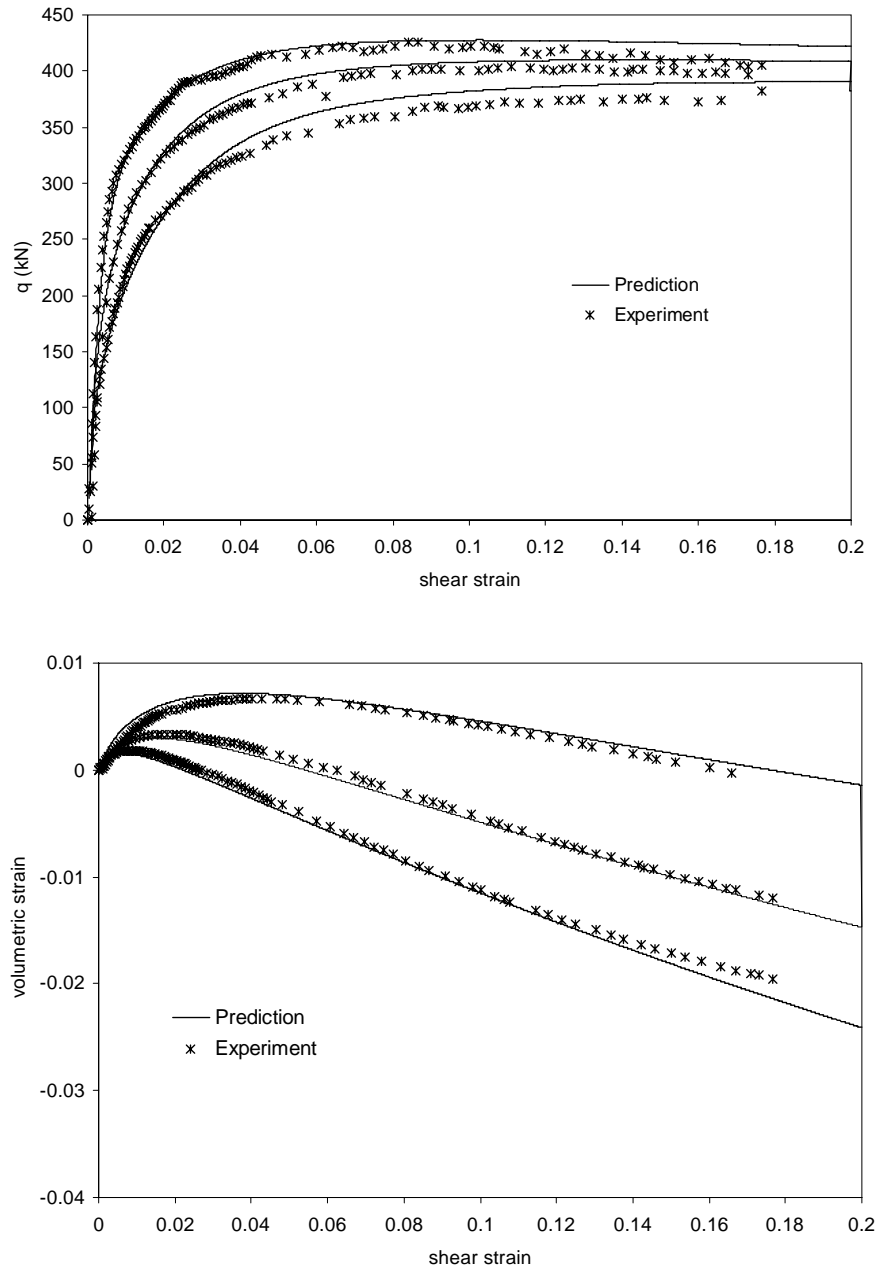


Fig. 7-3: Measurements and prediction of drained tests at 200 kPa with different void ratios of 0.676, 0.699, 0.739 (a) shear stress vs. shear strain (b) volumetric strain-shear strain

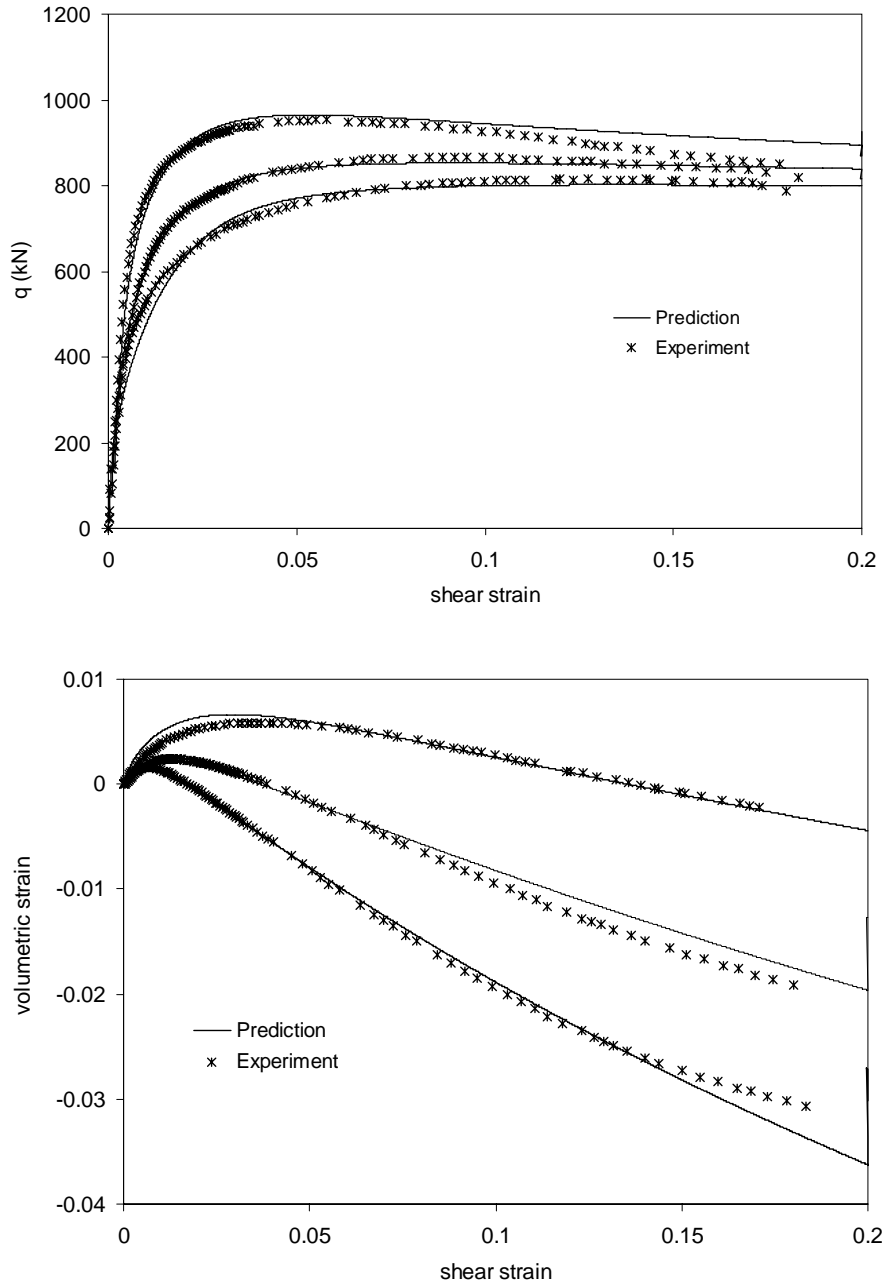


Figure 7-4: Measurements and prediction of drained tests at 400 kPa with different void ratios of 0.640, 0.679, 0.722 (a) shear stress vs. shear strain (b) volumetric strain-shear strain

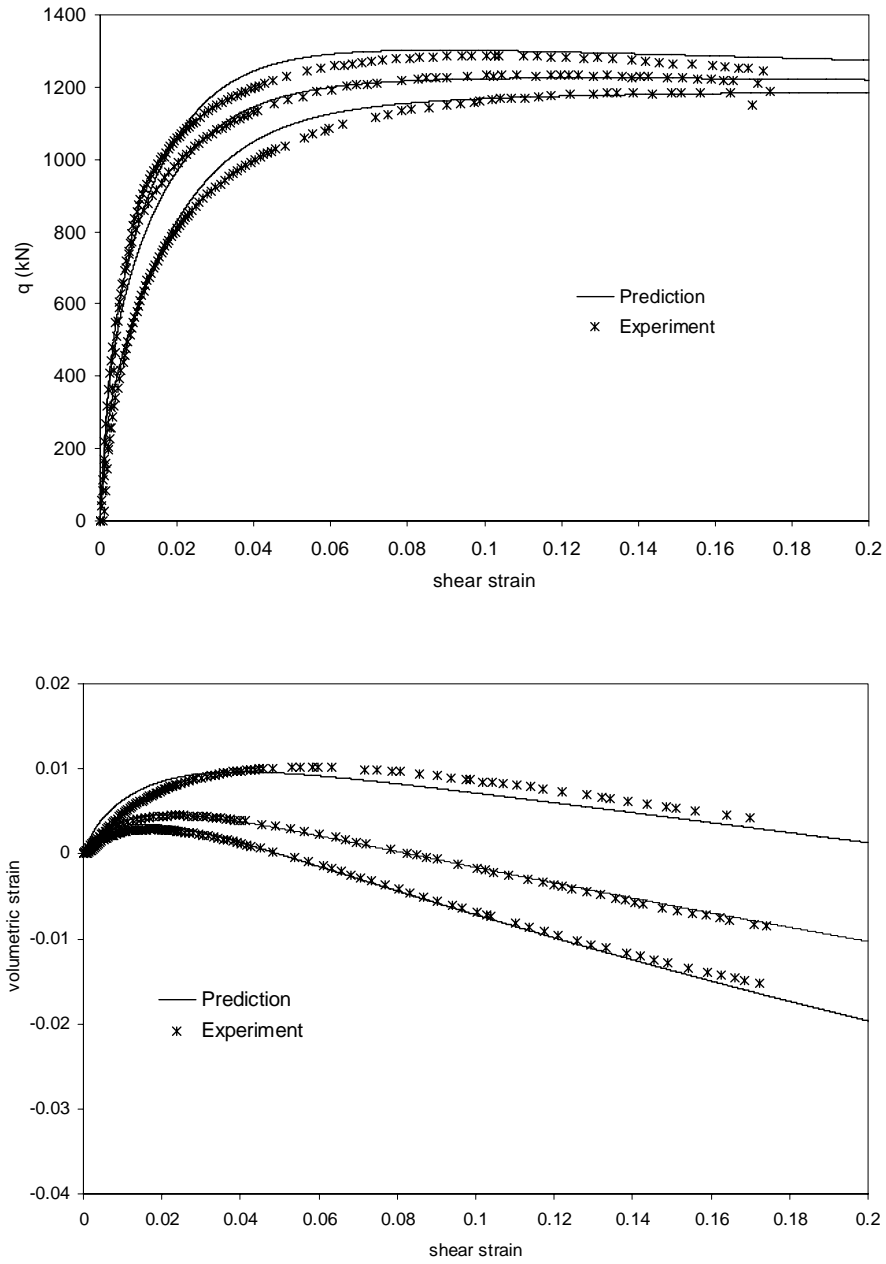


Figure 7-5: Measurements and prediction of drained tests at 600 kPa with different void ratios of 0.670, 0.699, 0.731 (a) shear stress vs. shear strain (b) volumetric strain-shear strain

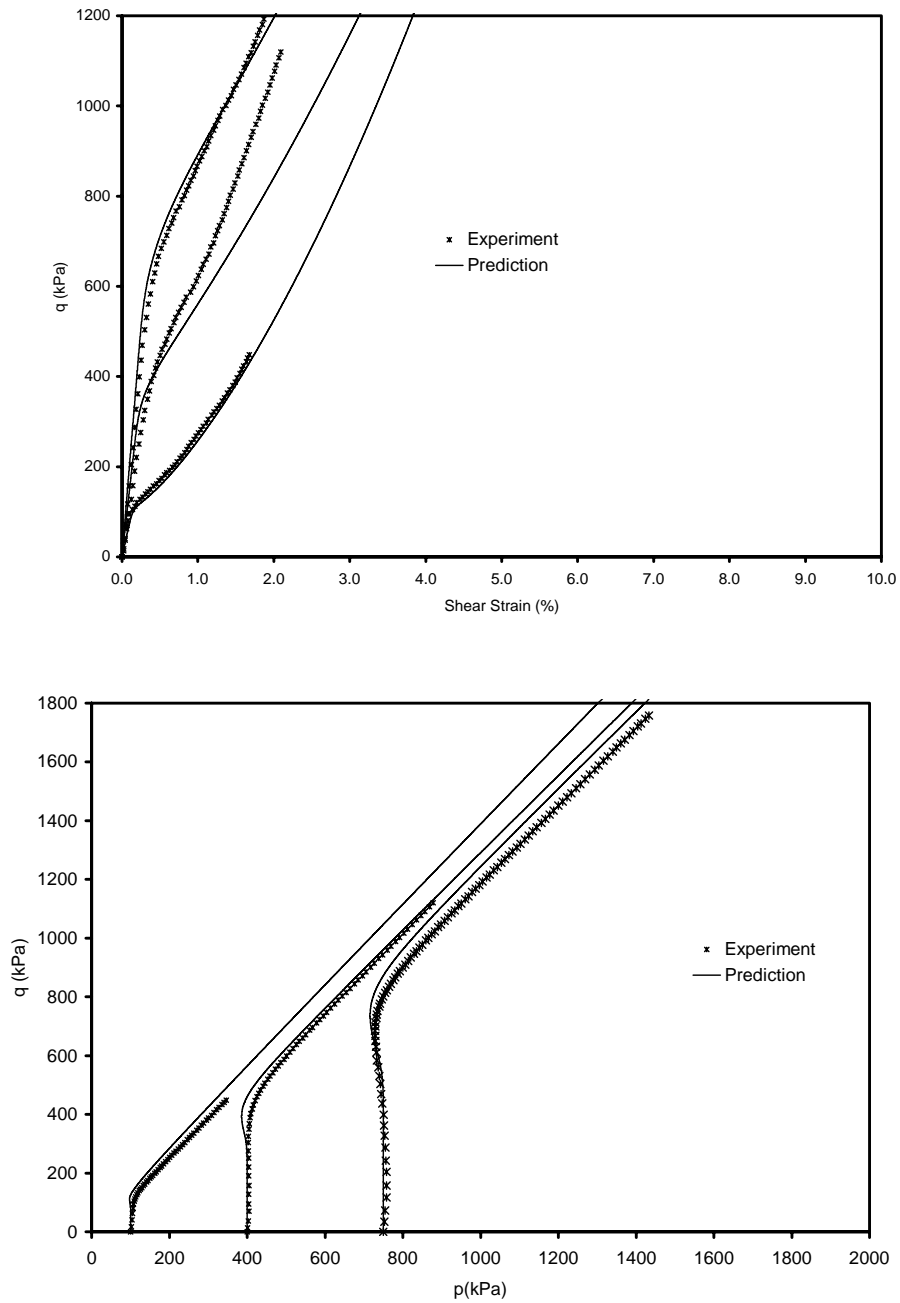


Figure 7-6: Measurements and prediction of drained tests at void ratio of 0.640 with different mean effective pressures of 100, 400, 750 kPa (a) shear stress vs. shear strain (b) shear stress vs. mean effective pressure

## 7.2 Cyclic laboratory triaxial test

Fig. 7-7 shows the stress path under an undrained cyclic triaxial test done on Nevada sand as a part of the VELACS project (Arulmoli et al., 1992). The sample was prepared at the void ratio of 0.65 with the air pluviation method. Fig. 7-8 shows the simulation of the new sand model. It can be seen that the simulation and experimental results agree well.

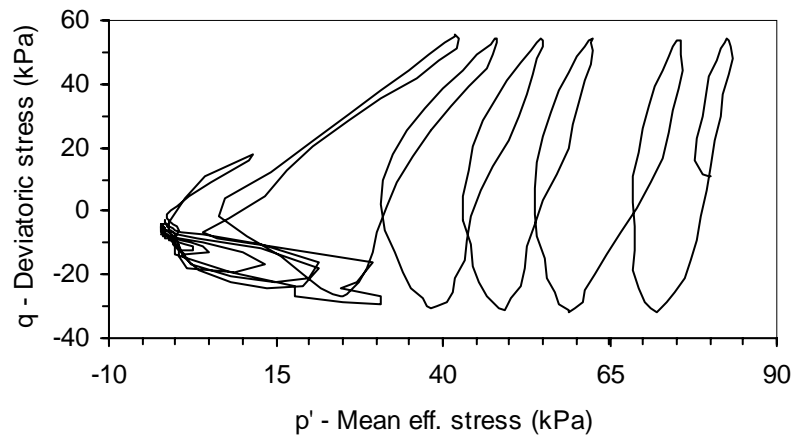


Figure 7-7: Measurement of cyclic triaxial test on Nevada sand consolidated at 80 kPa and void ratio of 0.65

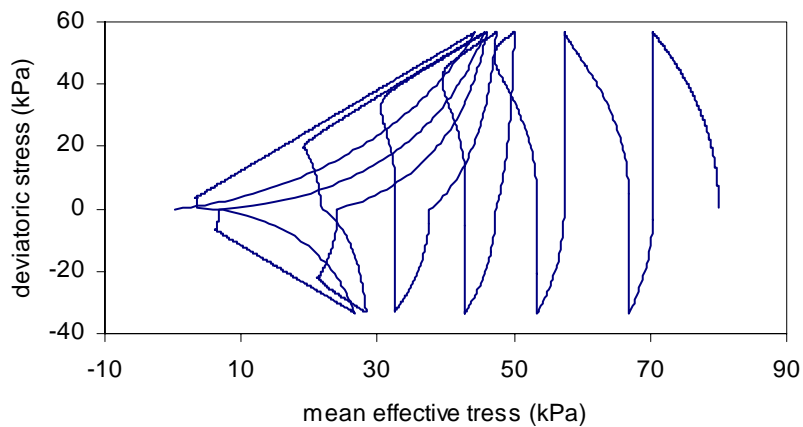


Figure 7-8: Prediction of cyclic triaxial test on Nevada sand consolidated at 80 kPa and void ratio of 0.65

### 7.3 Centrifuge testing

Centrifuge testing has been widely employed by geotechnical investigators in recent decades to study scale model problems in soils. The centrifuge offers the ability to simulate fairly realistic full-scale stress states together with uniform and measurable soil properties. Since centrifuge models replicate real field conditions, they are used to study the attenuation of acceleration, the generation and dissipation of pore pressure, and the rate and magnitude of settlement and lateral deformation during liquefaction. It has thus become a useful tool to study the mechanisms involved in liquefaction, remediation, as well as to validate numerical codes. One of the notable centrifuge studies on liquefaction was the VELACS Project (Arulanandan and Scott, 1993). Centrifuge test data are made available at: <http://gees.usc.edu/velacs/Centrifuge/cntdata.html> for use by researchers.

The centrifuge test results of “Model 1” (Arulanandan and Scott, 1993) are used here to verify the prediction of the new sand model. Fig. 7-9 shows the arrangement of the model of horizontally layered loose sand in a laminar box and placement of LVDT’s (Linear Variable Displacement Transducers), pore pressure transducers (PPT), and accelerometers to measure the vertical and horizontal response (AH & AV).

The laminar box consisted of a 20 cm high, horizontal layer of uniform Nevada No. 120 sand, placed at a relative density of 40 % by dry pluviation. It was fully saturated with water, spun at a centrifuge acceleration of 50g, and excited horizontally at the base. This combination was to simulate a 10 m soil layer in prototype. The input horizontal

acceleration time history at the base of the box consisted of 20 cycles of a 100 Hz sinusoidal input, with variable amplitude and maximum peak acceleration of 11.75 g. For the 50 g centrifuge acceleration of the test, this corresponds to a frequency of 2 Hz and peak acceleration of 0.235 g in the prototype. Some of the material parameters are extracted from Arulmoli et al. (1992) (Tab. 7-3) and the remainder are the same as that given in Tab. 7-1.

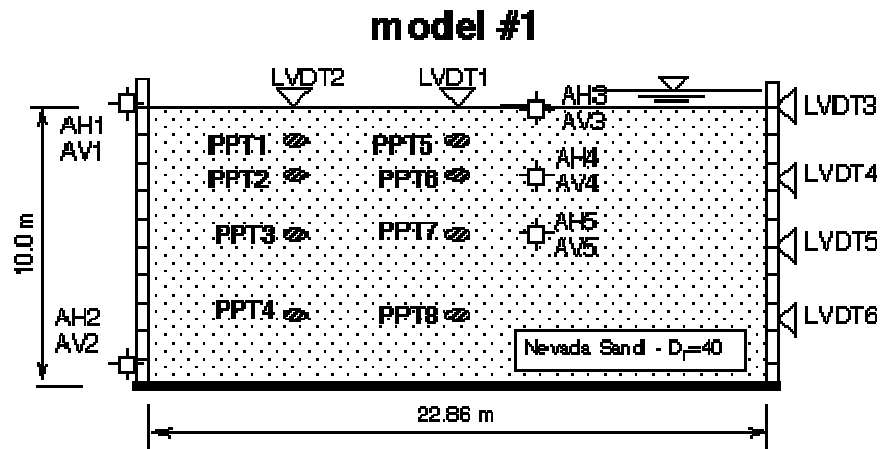


Figure 7-9: Centrifuge model arrangement

Table 7-3: Material parameters of Nevada sand

Material parameters	
$G_0$	250
$\nu$	0.3
$\lambda$	0.017
$\kappa$	0.003
$N$	2.74
$H_0$	10000
$M_c=M_f$	1.0
$M_c/M_e$	1.43

### **7.3.1 Numerical model of the centrifuge**

The finite difference mesh used for this model is given in Fig.7-10. When subjected to base shaking, the soil in the laminar box simulates approximately a semi-infinite layer. In order to reflect the semi-infinite condition in the numerical model, the grid points at the same horizontal level are tied-up together, i.e. grid points 1-2, 4-7, 9-11 etc. (Fig.7-10). In other words, the grid points at the same level are allowed to displace by the same amount. A static analysis was performed to determine the initial stress state and pore water pressure distribution of the model before applying dynamic excitation. Thereafter, the chosen acceleration time history was applied at the base of the model.

The recorded acceleration-time by the accelerometer, AH1 (Fig. 7-11) at the base is used as the input. Base line correction was performed to remove the noise present in the recorded acceleration time history. Base line corrected input along with the original history is presented in Fig.7-11.

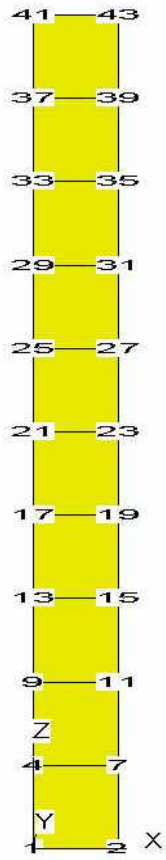


Figure 7-10: FLAC3D model of centrifuge testing

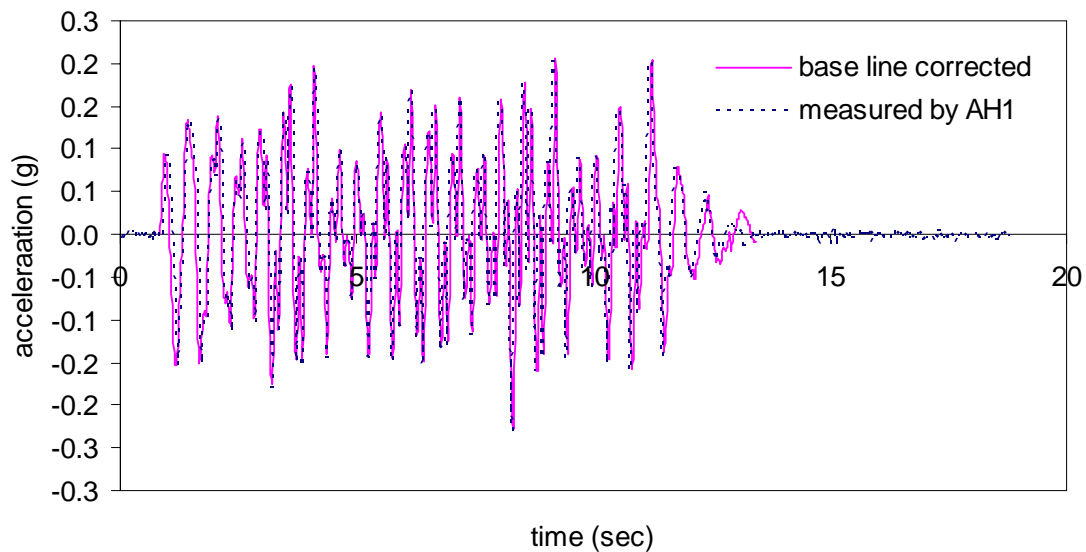


Figure 7-11: Acceleration input at the base

### 7.3.2 Results of numerical analysis

Fig. 7-12 shows the shear stress – mean effective pressure variation in zone 1. It can be seen that mean effective pressure reduces from initial value of about 95 kPa to all the way up to zero due to the generation of excess pore pressure in zone 1. As shown in Fig. 7-7 pore pressure transducers were placed at depths of 1.25 m (P1 & P5), 2.5 m (P2 & P6), 5.0 m (P3 & P7), and 7.5 m (p4 & P8). Fig. 7-13 to 7-16 show the measured and predicted excess pore pressure at these depths. It can be seen that the model predictions closely match with experimental measurements except at the depth of 7.5 m. The deviation is due to the fact that the undrained condition was assumed during the dynamic loading. However, in reality the pore pressure starts to dissipate after a few seconds

elapsed in sands as they have high permeability. Redistribution of pore water pressure is evident from the Figs. 7-13 to 7-16.

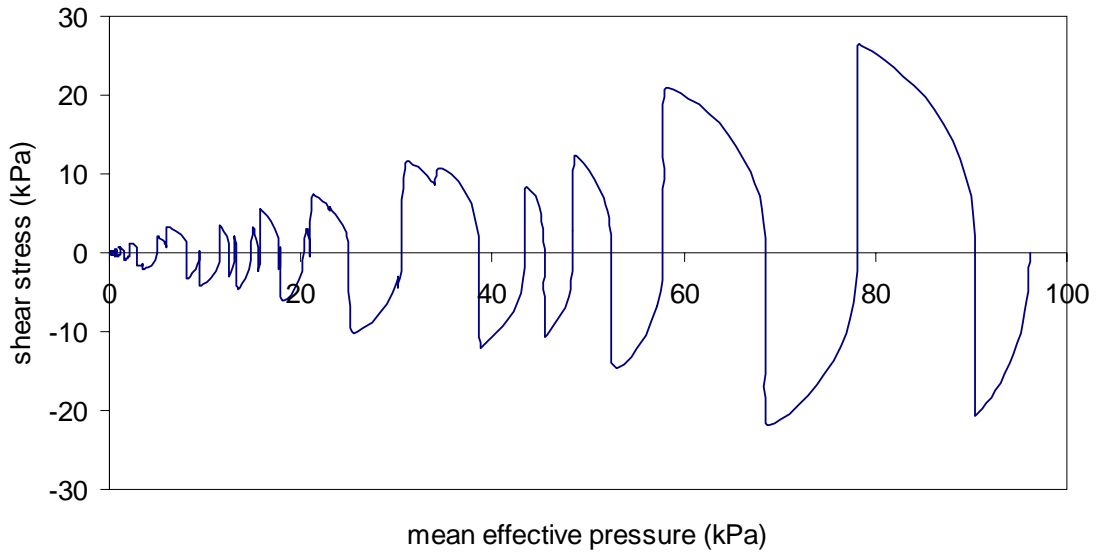


Figure 7-12: Shear stress – mean effective pressure variation in zone 1

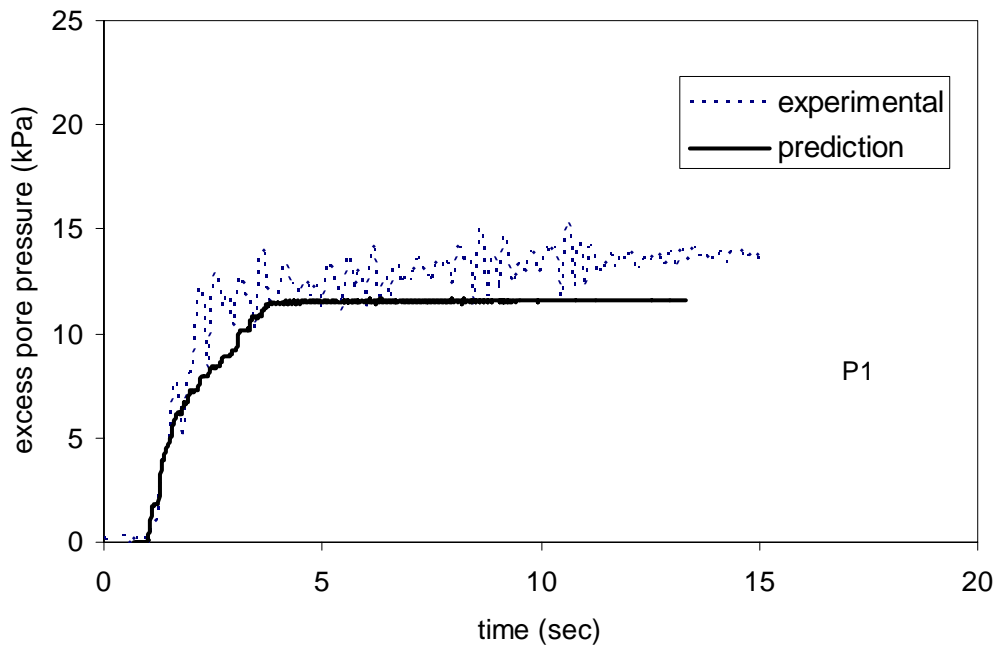


Figure 7-13: Experimental and prediction of pore pressure of transducer P1

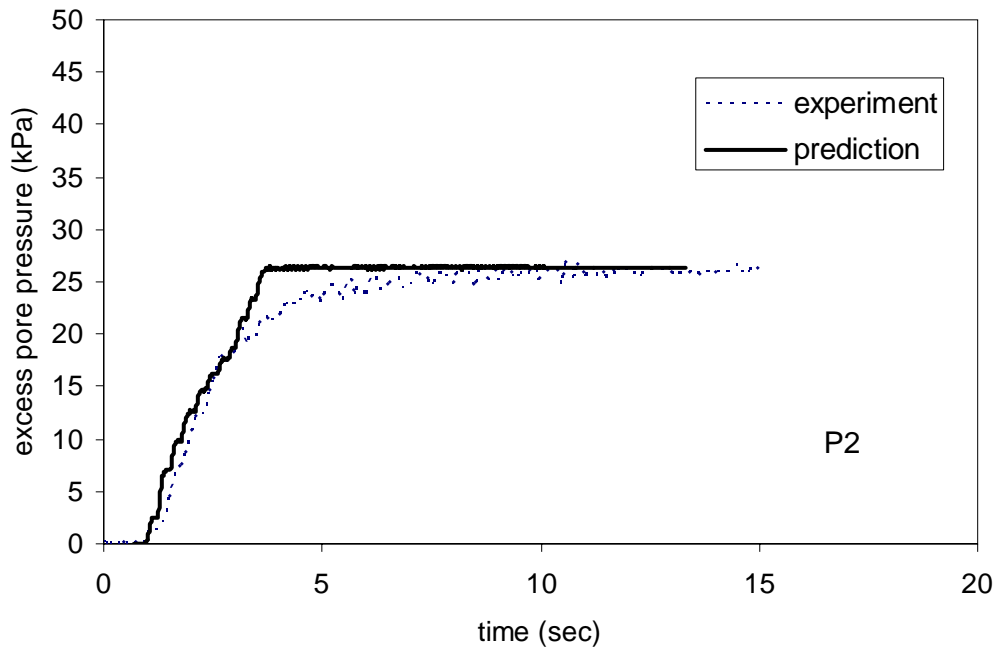


Figure 7-14: Experimental and prediction of pore pressure of transducer P2

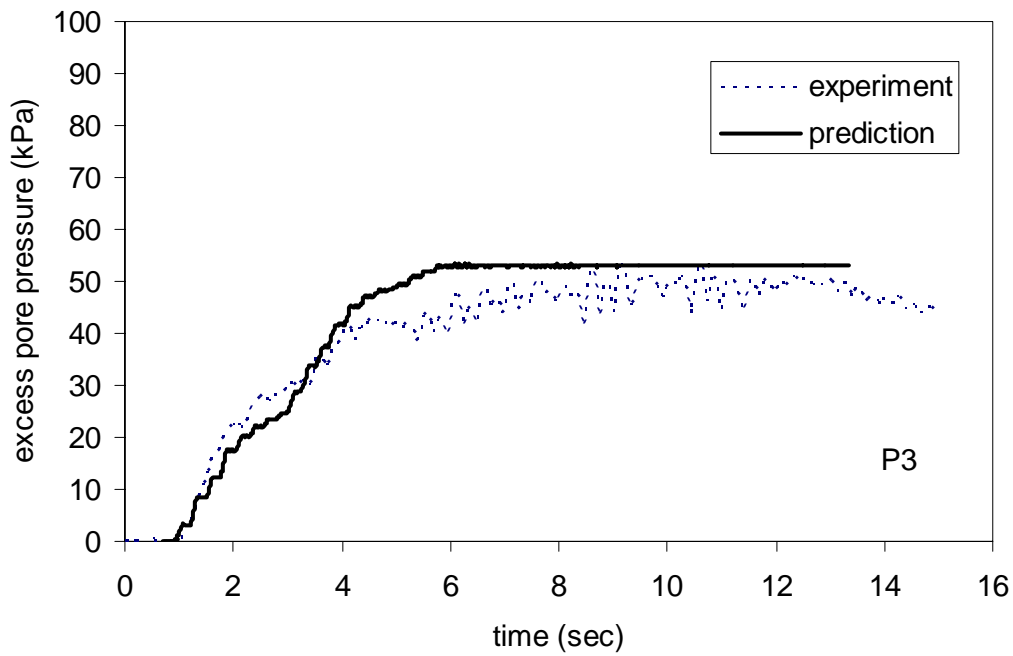


Figure 7-15: Experimental and prediction of pore pressure of transducer P3

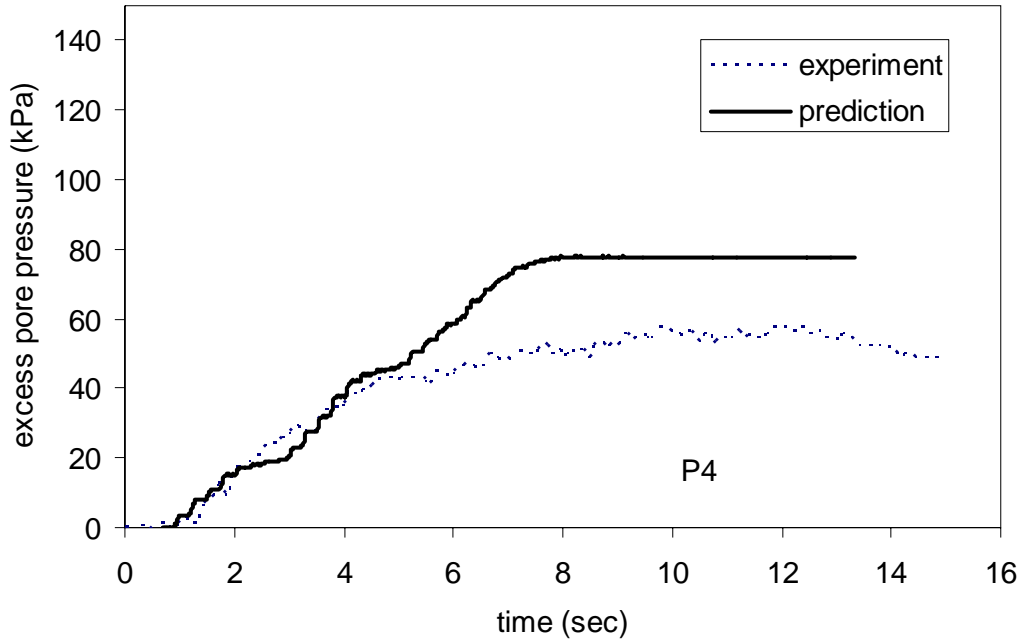


Figure 7-16: Experimental and prediction of pore pressure of transducer P4

Fig. 7-17 to 7-19 show the recorded and predicted acceleration at the depth of 0, 2.5, and 5 meters by the accelerometers AH3, AH4, and AH5 (Fig. 7-9). It is evident that the model predictions closely agree with recorded acceleration for about 5 seconds. Thereafter, the predicted accelerations attenuate very rapidly because the assumption of undrained condition makes the sand layer liquefy sooner than for the actual case. Therefore, refined analysis is needed to account for the pore pressure redistribution. This is described in the next section.

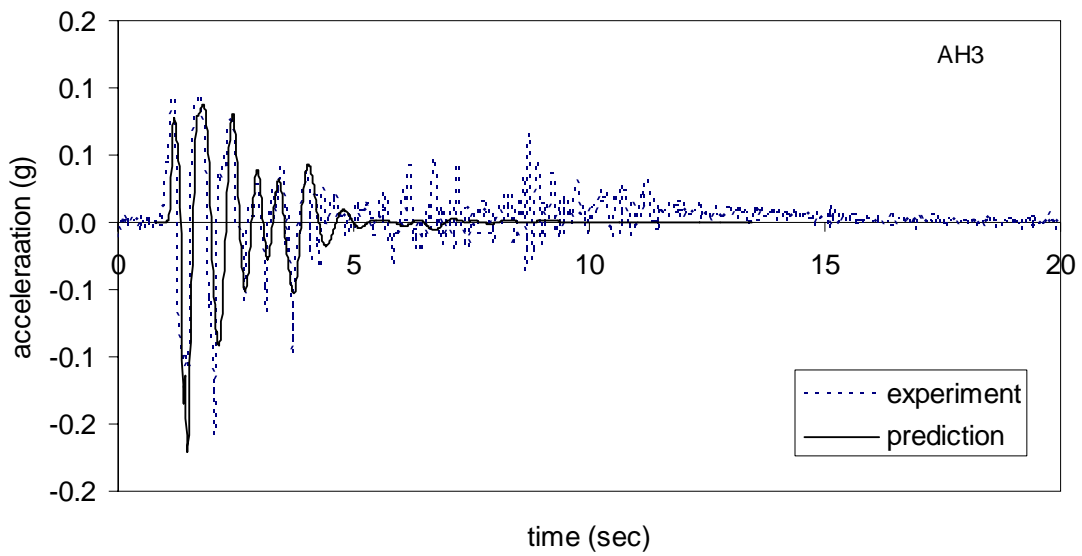


Figure 7-17: Experimental and prediction of acceleration of accelerometer AH3

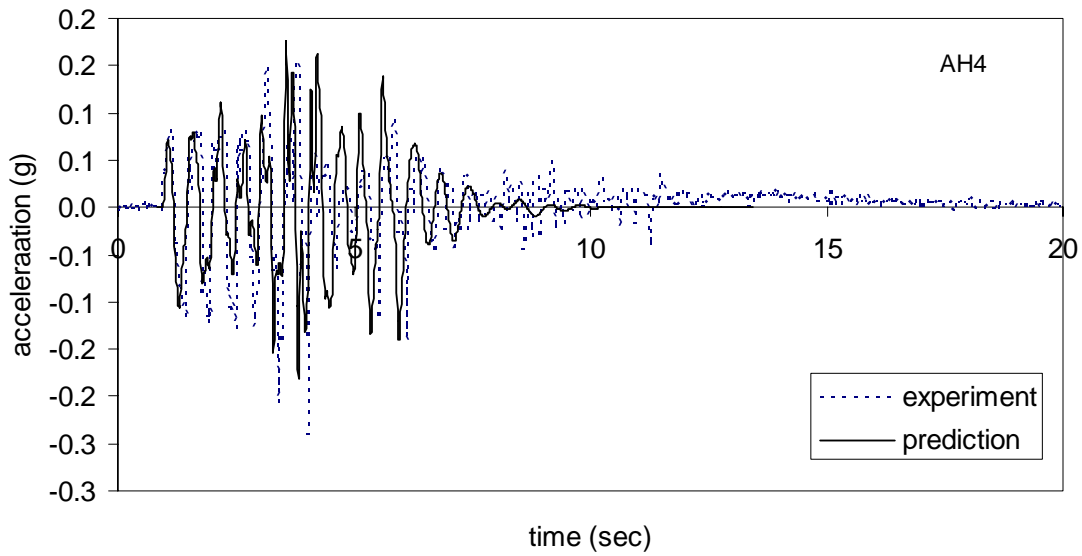


Figure 7-18: Experimental and prediction of acceleration of accelerometer AH4

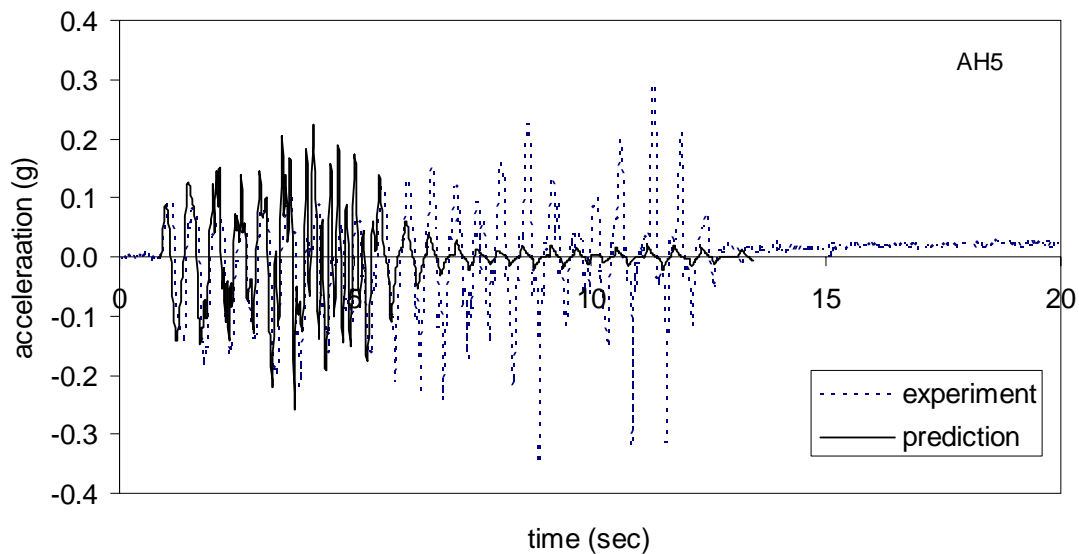


Figure 7-19: Experimental and prediction of acceleration of accelerometer AH5

#### 7.4 Coupled analysis

In order to take the pore pressure dissipation into account, a fully solid-fluid coupled analysis was performed. In this analysis, stresses and displacement in the solid matrix, pore pressure in the fluid phase, and mean fluid velocity are coupled by the Biot theory for the behavior of porous media with single phase and Darcy’s law for fluid transport. The coupled analysis in FLAC3D is done by turning on the option “fluid flow”.

The same finite different mesh (Fig.7-10) and boundary conditions were used. As flow of water was allowed to occur during shaking, pore pressure boundary conditions needed to be given. In FLAC3D all physical boundaries are assumed to be impermeable

by default. As the pore pressures at the surface remains zero always, the pore pressures at the top surface are made zero using the “initial” command. The remainder of the analysis is the same as the previous one. In addition to the material parameters used in the previous one, hydraulic conductivity of 0.0033 m/s is used (Arulmoli et al., 1992).

Fig. 7-20 shows the shear stress – mean effective pressure variation. It can be seen that, unlike in the undrained condition, zone 1 did not liquefy when the dissipation of pore pressure is allowed to occur. Fig. 7-21 to 7-24 show the prediction of pore pressure generation using coupled analysis. It can be seen that when dissipation is allowed to take place, the prediction matches well with the measurements. Fig.7-25 to 7-27 show the predicted acceleration time history. Close agreement with measured acceleration time history is also evident. Therefore, the non-liquefied zones are still stiff enough to pass the shear wave through them. This is evident from the acceleration time history (Fig.7-27).

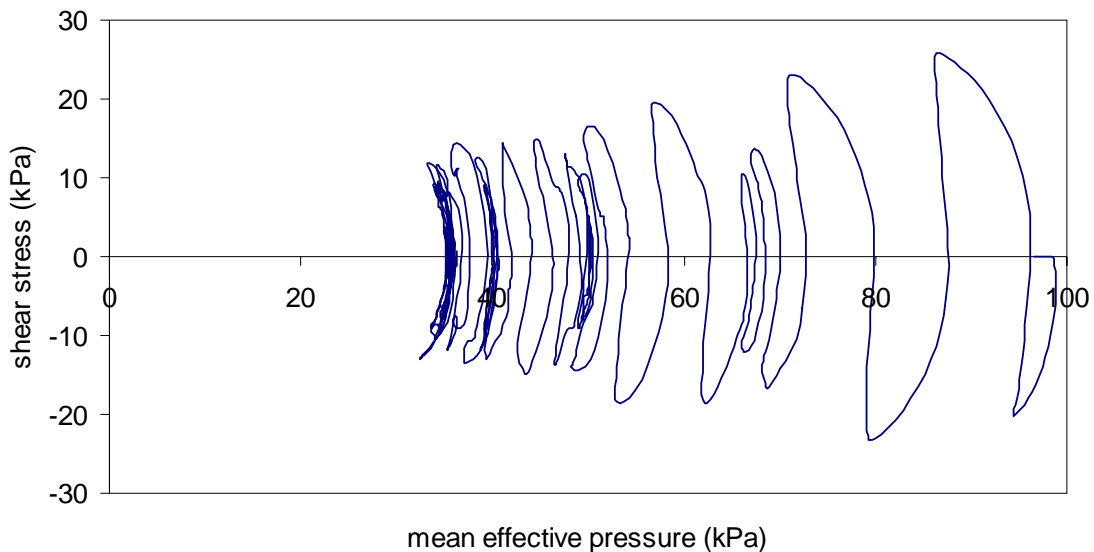


Figure 7-20: Shear stress – mean effective pressure variation in zone 1

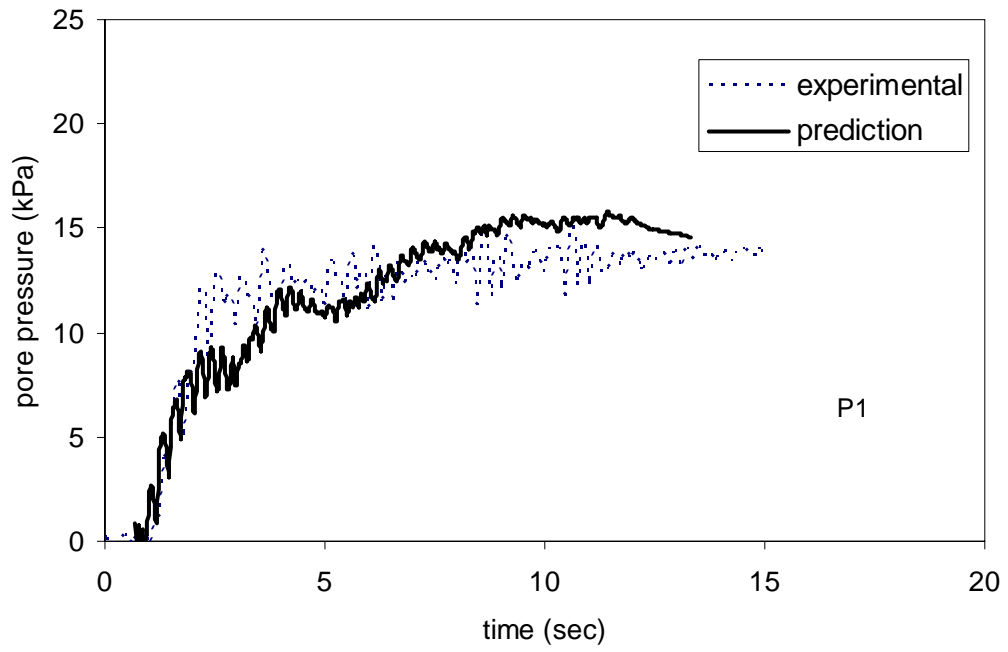


Figure 7-21: Experimental and prediction of pore pressure of transducer P1

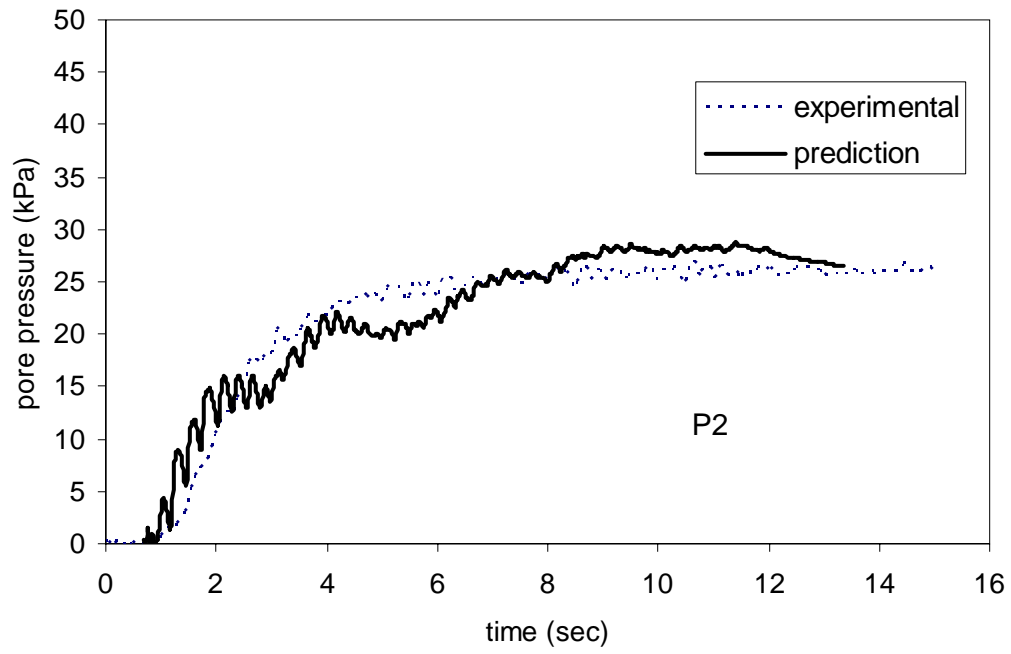


Figure 7-22: Experimental and prediction of pore pressure of transducer P2

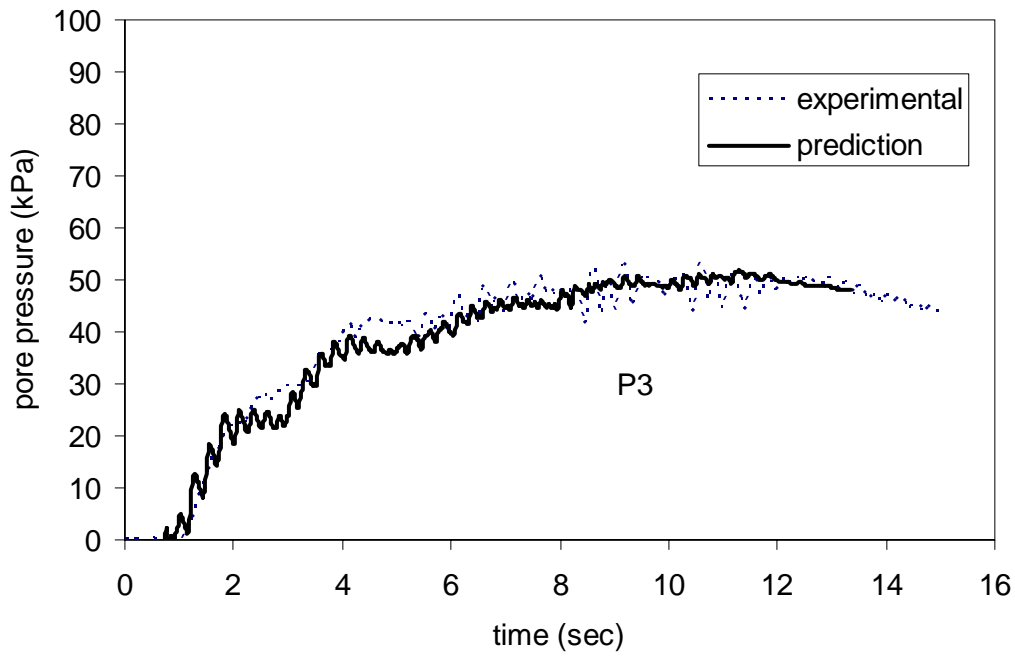


Figure 7-23: Experimental and prediction of pore pressure of transducer P3

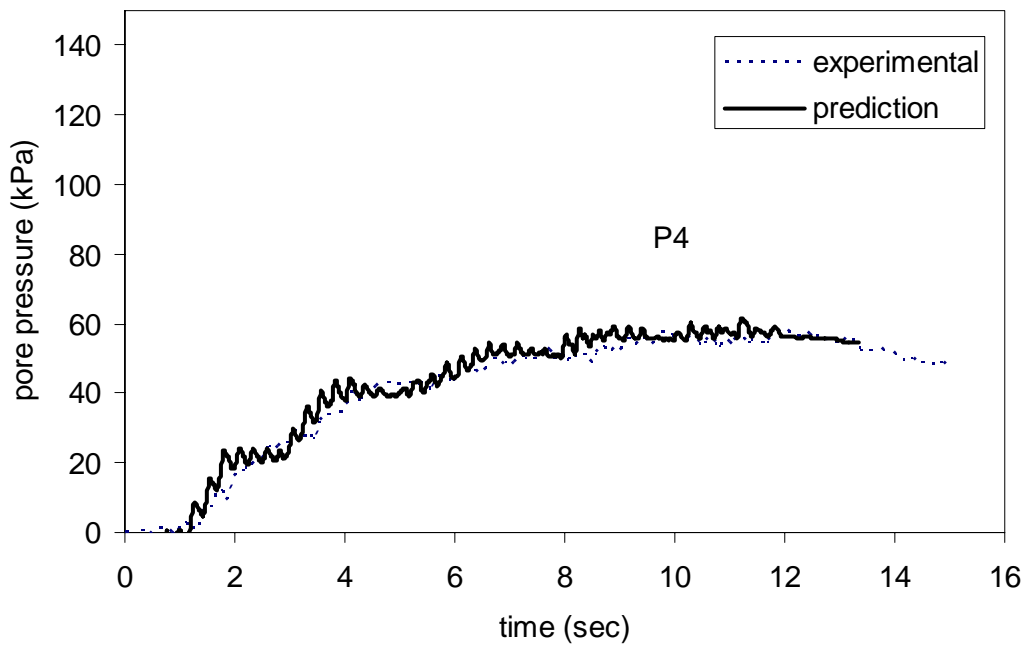


Figure 7-24: Experimental and prediction of pore pressure of transducer P4

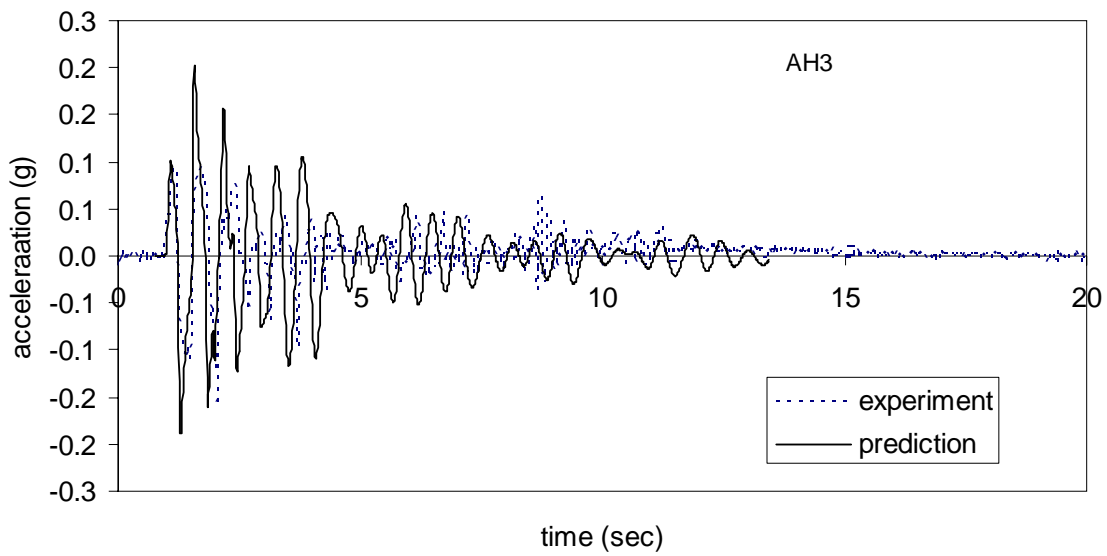


Figure 7-25: Experimental and prediction of acceleration of accelerometer AH3

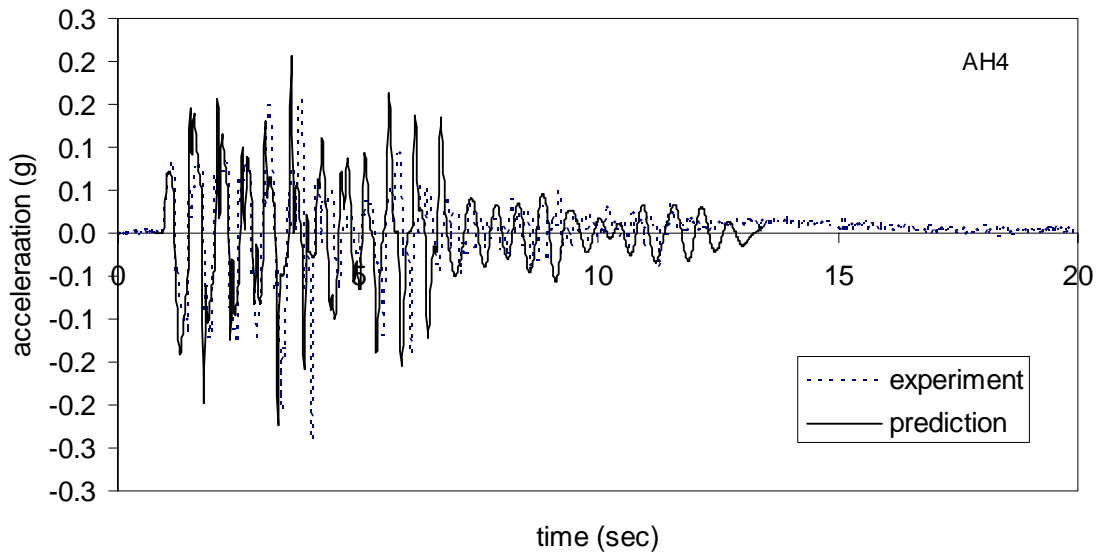


Figure 7-26: Experimental and prediction of acceleration of accelerometer AH4

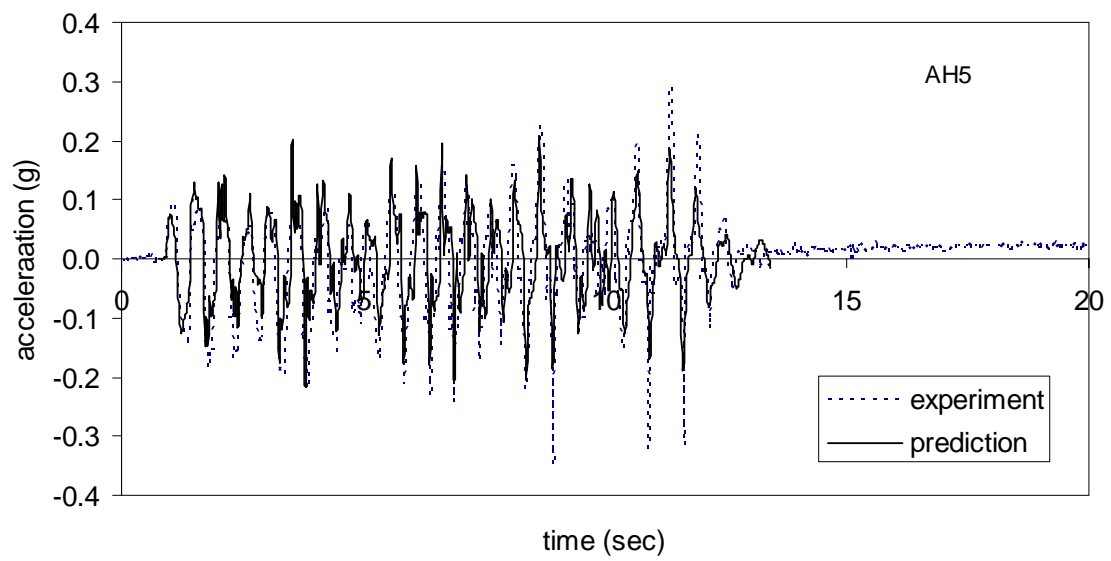


Figure 7-27: Experimental and prediction of acceleration of accelerometer AH5

## *Chapter 8*

### **CONCLUSIONS AND RECOMENDATIONS**

The widely used critical state concepts in constitutive modeling of soils were developed based mainly on the behavior of reconstituted, essentially isotropic, materials. Significant improvements are necessary in order to obtain an acceptable degree of realism in these models for sands. This study presents an extension of the critical model by incorporating the features of granular fabric. The resulting model is a physically attractive and robust anisotropic model for sand. The new anisotropic sand model is generalized into six dimensional spaces using bounding surface plasticity. The model was then implemented into the finite difference code, FLAC3D and used to simulate monotonic and cyclic triaxial tests. A centrifuge test is simulated to verify its predictive capability to liquefaction and attenuation of shear waves. This chapter summarizes first the development of the new model, its features, and its uses towards the constitutive modeling of sands followed by recommendations for further research.

#### **8.1 Conclusions**

Central to the development of the model is the recognition that volumetric strain increments during shear deformation of granular materials result from two sources. The first source  $\dot{\epsilon}_{vi}^p = -\alpha\dot{\epsilon}_q^p$  is as a result of changes in granular fabric and unique to these materials. This relation is purely kinematic, always dilative, and identified to be that of

Reynolds's kind and is termed as fabric induced volumetric strain. It does not contribute to plastic energy dissipation in granular materials. This relation resulted from the characterization of the directional distribution of porosity in sand and its evolution under shear deformation. The second source  $\dot{\epsilon}_{vc}^P$  is a direct response to changes in stress as in a standard elastic/plastic continuum. This component of volumetric strain increment contributes to the plastic energy dissipation and hence is included in the dissipation function. However, these two volume changes are present right from the start of shear loading and the sum of these two is the macroscopic volume change measured in experiments.

The inclusion of the two sources of volume change in the anisotropic model results in three important datum states. When subjected to isotropic strains, the resulting stress state is not isotropic but lies upon the kinematic normal consolidation line with slope  $\alpha$ . There exists a state in which the volumetric strain rate  $\dot{\epsilon}_v^P = 0$  and where it changes its sign from positive to negative. The line on which this occurs is often termed the phase transformation line (PTL) with slope  $\eta = \sqrt{M^2 + \alpha^2}$ . The third datum state is one in which the stress induced volumetric strain rate  $\dot{\epsilon}_{vc}^P$  is zero with slope  $\eta = M + \alpha$ . Note that  $\dot{\epsilon}_{vi}^P$  is non-zero at this state; therefore, dilation is now entirely due to the Reynolds effect. Even though the sand is dilating, the dissipation is entirely due to shear at this state as in Taylor's work dissipation. The latter state is termed the Reynolds-Taylor state. None of these states are deemed necessarily unique.

It is shown that during a plastic shear strain cycle, the  $\dot{\epsilon}_{vi}^P$  is reversible whilst the  $\dot{\epsilon}_{vc}^P$  is permanent. The accumulation of the permanent volumetric strain causes generation of excess pore pressure that under undrained loading leads to liquefaction. Therefore, as the anisotropic model explicitly accounts for the permanent and reversible plastic volumetric strain, the model is implemented into the numerical code FLAC3D for numerical studies on liquefaction. Since  $\dot{\epsilon}_{vi}^P$  is recovered after each cycle of plastic shear strain, it does not explicitly contribute to the pore pressure build up. However, it has a strong effect on post liquefaction behavior such as lateral spreading.

A correlation for the evolution of  $\alpha$  with shear is proposed based on drained triaxial compression test results. It is seen that  $\alpha$  is dependent on the mean effective pressure as well as the initial void ratio. Since the proposal is made based on the triaxial test of samples of Ottawa sand prepared by water sedimentation, it is only applicable to the soils without any collapsible structure or crushable particles.

Micromechanical considerations suggest that  $\alpha$  must vary with shear strain, beginning at zero, since the material is assumed initially isotropic here, growing to a maximum level of anisotropy and thereafter reduce progressively. It is not clear if it would return to zero at higher pressures without the possibility of crushing. In the event  $\alpha$  does return to zero, a critical state as in isotropic theory could be reached.

The discussion here assumed that  $\alpha$  is positive, as would be the case for normal sands. However, for sands with a collapsible structure  $\alpha$  would be negative to begin with. Thus,  $\dot{\epsilon}_{vi}^P$  would be positive and would result in overall volume decrease (Sec. 3.5). Such

sands would contract and reach the RTL first with no possibility of attaining PTL. Upon further deformation the evolution of  $\alpha$  and accordingly the locations of RTL and PTL would essentially follow the pattern as in the case of normal sands. This has been observed in the past by several experiments on ultra loose sands (e.g. Alarcon et al. 1988).

The new anisotropic sand model is implemented into FLAC3D to verify its performance in numerical studies. It is seen that the model simulates the drained and undrained monotonic triaxial tests well. The numerical simulation of cyclic triaxial test matches well with experimental data. The applicability of the model to field problems is verified with the centrifuge test. At first, it is assumed that undrained condition prevails during dynamic excitation. Results showed that there is significant pore pressure dissipation during earthquake loading. Hence, a solid-fluid coupled analysis is performed to capture the pore pressure distribution within the soil layer. It is seen that the model simulations agree well with the experimental results.

## **8.2 Recommendations**

- The fabric induced volumetric strain increment  $\dot{\epsilon}_{v_i}^p$  is a unique phenomenon for granular materials. In this study, it is applied in the improvement of modified Cam Clay. Similar procedures can be carried out to improve other well-known continuum soil models.
- This study presented a systematic way of decomposing macroscopic plastic volumetric strain into two parts; one is cumulative and the other is reversible. It is

shown that proper account of accumulated volumetric strain simulate the build of excess pressure very well. The model can also be used to predict the settlement in sand layer due to drained cyclic loading.

- Although the evolution law for  $\alpha$  is derived from experimental test data, the prediction of very dense sand does not match very well. Therefore, the evolution law will need to be refined. Non-destructive imaging techniques such as X-ray computed tomography could be used for this purpose to characterize the initial fabric arrangement as well as its evolution with shear deformation in order to obtain better forms.
- The model prediction of liquefaction of level ground is verified with the centrifuge test. The model could be applied to sloping ground as well as to soil structures such as dams, levees etc. for the prediction of liquefaction under cyclic loading.
- In the bounding surface plasticity formulation, radial mapping is used to get the flow rule and plastic modulus. Radial mapping is found to be suitable only for monotonic loading. In cyclic loading, at  $\eta = 0$ , radial mapping gives the dilatancy as infinity. This in turn predicts zero pore pressure increment. This is not in accord with the experimental data. Some other mapping rules should be used to get a better prediction of cyclic loading.

## REFERENCES

- Alarcon, A., Chameau, J.L., and Leonards, G.A. (1988). "Undrained monotonic and cyclic strength of sands." *J. Geotech. Engrg.*, ASCE, 114(10), 1089-1109.
- Anandarajah, A. (1994), "Procedures for elastoplastic liquefaction modeling of sands", ASCE, *Journal of Engineering Mechanics*, 120(7):1563-1587
- Arulmoli, K., Muraleetharan, K.K., Hossain, M.M., and Fruth, L.S. (1992), "VELACS: verification of liquefaction analysis by centrifuge studies – laboratory testing program, soil data report. Earth Technology Corporation.
- Bardet, J.P. (1984), "Application of plasticity theory to soil behavior: A new sand model", PhD thesis, Cal. Int. Tech.
- Bardet, J.P. (1986), "A bounding surface model for sands", *Journal of Engineering Mechanics Division*", ASCE, 112(11):1198-1217.
- Bathurst, R.J. and Rothenburg, L. (1990), "Observations on Stress-Force-Fabric Relationships in Idealized Granular Materials", *Mechanics of Materials*, 9: 65-80.
- Byrne, P. (1991), "A Cyclic Shear-Volume Coupling and Pore-Pressure Model for Sand", in proceedings: 2<sup>nd</sup> Int. Conf. on Recent Advances in Geotechnical Earthquake Engineering and Soil Dynamics (St. Louis, Missouri, March, 1991), Paper No. 1.24, 47-55.
- Been, K. and Jefferies, M. G. (1985), "A state parameter for sands", *Geotechnique*, 35(2): 99-112
- Been, K. and Jefferies, M. G. (2004), "Stress-dilatancy in very loose sand", *Ca. Geotech. J.* 41: 972-989
- Benahmed, N (2002) Influence of the structure on the mechanical behaviour of sand. Discussion. *Constitutive and Centrifuge Modelling: Two extremes*. Ed. Sarah Springman, A.A. Balkema, 227-229.
- Boehler, J.P (Ed.), (1987), *Application of Tensor Functions in Solid Mechanics*, Springer Verlag
- Boukpeti, N. and Drescher, A (2000), "Triaxial behavior of refined Superior sand model", *Computers and Geotechnics*, 26(1), 65-81

- Burland, J. B. (1965), Discussion, *Geotechnique* 15: 211-214
- Casagrande, A. (1936), "Characteristics of cohesionless soils affecting the stability of earth fills", *Journal of Boston Society of Civil Engineers*, 23(1), 13-32
- Casagrande, A. (1975), "Liquefaction and cyclic deformation of sands: A critical review", *Proceedings of the 5<sup>th</sup> Pan-American Conference on Soil Mechanics and Foundation Engineering*, Buenos Aires, Argentina, 5, 80-133
- Casagrande, A. (1976). Liquefaction and cyclic deformations of sands – a critical review. *Harvard Soil Mech. Ser.* No. 88, Harvard Univ., Cambridge, Mass.
- Castro (1969). Liquefaction of sands, Ph.D thesis, Harvard Soil Mechanics Series, No. 81, Harvard University, Cambridge, Mass.
- Castro, G. (1975), "Liquefaction and Cyclic Mobility of Saturated Sands", *Journal of the Geotech. Eng. Div., ASCE*, 101(GT6), 551-569.
- Chang, C.S. and Whitman, R.V. (1988), "Drained permanent deformation of sand due to cyclic loading", *ASCE, J. Geotechnical Engineering*, 114(10): 1164-1180.
- Chang, C.S. and Hicher, P-Y., (2005), "An elasto-plastic model for granular materials with microstructural considerations", *Int. J. Solids and Structures* 42, 4258-4277.
- Chen, W.F and Huang, T.K., (1994), "Plasticity analysis in geotechnical engineering: From theory to practice", *Developments in Geotechnical Engineering*, Balasubramaniam, et al. (eds.), Balkema, pp 49-79.
- Chu, J. (1995), "An experimental examination of the critical state and other similar concept for granular soils", *Can. Geotech. J.*, 32, 1065-1075.
- Chu, J. and Lo, R. (1994), "Asymptotic behavior of a granular soil in strain path testing", *Geotechnique*, 44(1), 65-82.
- Chu, J. and Leong, W.K. (2002), "Effect of fines on instability behavior of loose sand", *Geotechnique*, 52(10), 751-755.
- Chandler, H. W. (1985), "A plasticity theory without Drucker's postulate, suitable for granular materials", *J. Mech. Phys. Solids*, 33(3), 215-226.
- Collins, I.F. and Houlby, G.T. (1997). Application of thermomechanical principles to the modelling of geotechnical materials. *Proc. Roy. Soc. Lond. A* 453, 1975-2001.

- Collins, I.F. and Kelly, P.A. (2002), “A thermomechanical analysis of a family of soil models”, *Geotechnique*, 52(7), 507-518.
- Collins, I.F. and Hilder, T. (2002), “A theoretical framework for constructing elastic/plastic constitutive models for triaxial tests”, *Int. J. Numer. Anal. Methods Geomech.*, 26, 1313-1347.
- Collins, I. F. and Muhunthan, B. (2003), “On the relationship between stress-dilatancy, anisotropy, and plastic dissipation for granular materials”, *Geotechnique*, 53(7), 611-618.
- Collins, I. F. (2005), “Elastic/plastic models for soils and sands”, *Int.J.Mech Sci.*, 47: 493-508.
- Collins, I. F., Muhunthan, B., Tai, A.T.T., and Pender, M.J. (2006), “The concept of a “Reynolds Taylor State” and the mechanics of sands, *Submitted to Geotechnique*.
- Coulomb, C.A (1773), “Essai sur une application des regles de maximis et minimis a quelques problemes de statique, relatifs a l’architecture”, *Memoires de Mathematique de l’Academie Royal des Sciences, Paris, Vol.7* : 343-382.
- Cubrinovski, M. and Ishihara, K. (1998). Modelling of sand behaviour based on state concept. *Soils and Foundations*, 38, No 2, 115-127.
- Dafalias, Y. F., and Popov, E. P. 1976, “Plastic internal variables formalism of cyclic plasticity”, *Journal of applied mechanics, ASME*, 43: 645-651.
- Dafalias, Y. F. and Herrmann, L. R. (1982), “Bounding surface formulation of soil plasticity”, In: *Soil mechanics-cyclic and transient loads*, Pande, G.N and Zienkiewicz, O.C. (ed.), Chichester: Wiley: 253-282.
- Dafalias, Y. F. and Herrmann, L. R. (1986), “Bounding surface plasticity II: Application to isotropic cohesive soils”, *Journal of Engineering Mechanics Division, ASCE*, 112(EM12): 1263-1291.
- Dafalias, Y. F. (1986), “Bounding surface plasticity. I: Mathematical foundation and hypoplasticity”, *Journal of Engineering Mechanics*, 112(9), 966-987.
- Dafalias, Y. F. and Manzari, M. T. (2004), “A simple plasticity sand model accounting for fabric change effects”, *Journal of Engineering Mechanics, ASCE*, 130(6): 622-634.
- Desai, C.S. (1995). Constitutive modeling using the disturbed state as microstructure

- self-adjustment concept, In *Continuum Models for Materials with Microstructure*, (ed. H.B.Muhlhaus), John Wiley & Sons.
- Deshpande, V.S and Cebon, D. (1999) Steady state constitutive relationship for idealised asphalt mixes. *Mechanics of Materials*, 31, 271-287.
- di Prisco, C., Nova, R. and Lanier, J.(1993), “A mixed isotropic-kinematic hardening law for sand”, *Modern Approaches to Plasticity*, Ed: D. Kolymbas, Amsterdam: Elsevier, 83-124.
- Drucker, D.C., Greenberg, H.J., and Prager, W. (1951), “The safety factor of an elastic-plastic body in plane strain”, *Journal of Applied Mechanics*, Vol. 18: p.371.
- Drucker, D.C. and Prager, W. (1952). “Soil mechanics and plastic analysis or limit design”, *Quarterly Journal of Applied Mathematics*, Vol. 10 (2):157-165.
- Drucker, D.C., Greenberg, H.J., and Prager, W. (1952), “Extended limit design theorems for continuous media”, *Quarterly Journal of Applied Mathematics*, Vol. 9, p.381.
- Drucker, D.C., Gibson, R.E., and Henckel, D.J. (1957), “Soil mechanics and work-hardening theories of plasticity”, *ASCE Transactions*, 122, 338-346.
- Drucker, D.C (1959), “A definition of stable inelastic material”, *ASME Transactions, Journal of Applied Mechanics*, Vol.26(1):101-106.
- Drucker, D.C. (1991). *Average Flow Stress, Dislocation Motion Impediments Cell Walls, Atomically Disordered Regions*. In *Topics in Plasticity* (ed.W.H.Yang), Am. Press, Ann Arbor, MI, USA
- Duncan, J. M. and Chang, C. Y. (1970), “Non-linear analysis of stresses and deformations, *Journal of Soil Mechanics and Foundation Engineering*, ASCE 96(SM4): 1629-1653. F
- Fardis, M.N., Alibe, B., and Tassoulas, J.L. (1983), “Monotonic and Cyclic Constitutive Law for Concrete”, *Journal of Engineering Mechanics*”, ASCE, 109(EM4):516-536.
- Elgamal, A., Yang, Z., Parra, E., and Ragheb, A. (2003), “Modeling of cyclic mobility in saturated cohesionless soils”, *International Journal of Plasticity*, 19:883-905.

- Gajo, A and Muir Wood, D. (1999), "Severn-Trent sand: a kinematic-hardening model for sands: the q-p formulation", *Geotechnique*, 49(5), 595-614.
- Ghaboussi, J. and Momen, H. (1979), "Plasticity model for cyclic behavior of sands", *Proceedings of the 3<sup>rd</sup> International Conference on Numerical Methods in Geomechanics*, Aache, Vol.1, pp. 423-434.
- Ghaboussi, J. and Momen, H. (1981), "Modeling and analysis of cyclic behavior of sands", *Soil Meachanics-Transient anf Cyclic Loads*, Pande, G.N and Zienkiewicz, O.C. (eds.), John Wiley and Sons, Chapter 12, pp. 313-342.
- Goddard, J.D. and Bashir, Y. M. (1990), "On Reynolds dilatancy" *Recent Developments in Structured Continua*, eds. D. DeKee and P.N. Kaloni, New York, Longmans, 2: 23-35.
- Gudehus, G. (1976), "On constitutive laws for soils and rocks", *Proc. E.F. Conference on Numerical methods in Geomechanics*, Blacksburg, VA, USA, 3, 1305-1320.
- Hart, R. D., and C. Detournay, 2005, *Geotechnical constitutive models in an explicit, dynamic solution scheme*, *Soil constitutive models: evaluation, selection and calibration (Proceeding of geo-frontiers 2005, Austin, Texas, January 2005)*, ASCE geotechnical special publication No. 128, pp. 185-203.
- Hashiguchi, K. and Chen, Z-P. (1998), "Elastoplastic equation of soils with the subloading surface and the rotating hardening", *Int. J. Numerical and Analytical Meth. In Geomechanics*, 22,197-227.
- Hashiguchi, K. (1989), "Subloading surface model in unconventional plasticity", *Int. J. Solids Struct.*, 25, 917-945.
- Hashiguchi, K. (1986), "A mathematical description of elastoplastic deformation in normal-yield and subyield states", *Proceedings of the 2<sup>nd</sup> Int. Conf. on Numerical Model in Geomechanics*, Pande, G.N. and van Impe, W.F. (eds.), M.Jackson and Son, 17-24.
- Hazen, A. (1920), "Hydraulic fill dams", *ASCE Transactions*, 83, 1713-1745.
- Horne, M.R. (1965). *The behaviour of an assembly of rotund, rigid, cohesionless particles II. Proc. Roy. Soc. London, Series A.* 286, No 1404, 79-97.
- Houlsby, G.T. (1993), "Interpretation of dilation as a kinematic constraint", *Modern approaches to plasticity*, ed. D. Kolymbas, New York, Elsevier: 119-38.
- Iai, S. (1993). *Concept of effective strain in constitutive modeling of granular materials.*

- Soils and Foundations, 33, No. 2, 171-180
- Iai, S. (1994). A new look at the stress dilatancy relation in cam-clay model. *Soils and Foundations*, 34, No. 2, 1-13
- Itasca Consulting Group, Inc. *FLAC3D, Fast Lagrangian Analysis of Continua in 3 Dimensions User's Guide, Version 2.1*, 2002.
- Ishihara (1978). Stability of natural deposits during earthquakes, *Proc. XI Int. Conf. Soil Mech. Found. Engrg, San Francisco, CA, Vol. 1*, 321-376.
- Ishihara, K. (1993), "Liquefaction and flow failure during earthquakes", *Geotechnique*, 43(3), 351-415.
- Iwan, W.D. (1967), "On a class of models for the yielding behavior of continuous and composite systems", *Journal of Applied Mechanics, ASME*, 34(E3): 612-617.
- Jefferies, M.G. (1993), "Nor – Sand: a simple critical state model for sand", *Geotechnique*, 43(1): 1037-1042.
- Jefferies, M.G. (1997), "Plastic work and isotropic hardening in unloading", *Geotechnique*, 47(5): 91-103.
- Jefferies, M.G. and Shuttle, D.A., (2002), "Dilatancy in General Cambridge-Type Models", *Geotechnique*, 52(9): 625-638.
- Kabilamany, K. and Ishihara, K. (1990). Stress dilatancy and hardening laws for rigid granular model for sand. *Soil dynamics and Earthquake Engineering*, 9(2):66-77.
- Kanatani, K. (1982), "Mechanical foundation of the plastic deformation of granular materials", *Proc. IUTAM Conf. on Deformation and Failure of granular materials, Delft*, 119-127.
- Kanatani, K. (1984), "Stereological determination of structural anisotropy", *International Journal of Engineering Science*, 22(5): 531-546.
- Kanatani, K. (1985), "Procedures for stereological estimation of structural anisotropy", *International Journal of Engineering Science*, 23(5): 587-598.
- Khalili, N., Habte, M.A, and Valliappan, S. (2005), "A bounding surface plasticity model for cyclic loading of granular soils", *Int. J. Numerical and Analytical Meth. In Geomechanics*, 63:1939-1960.

- Klotz, E.U and Coop, M.R. (2002), "On the identification of critical state lines for sands", *Geotechnical Testing Journal*, 25(3), 1-13.
- Koiter, W.T. (1953), "Stress-strain relations, uniqueness, and variational theorems for elasto-plastic materials with a singular yield surface, *Quart.Appl.Math.* 11(3):350.
- Krieg, R.D. (1975), "A practical two-surface plasticity theory", *Journal of Applied Mechanics, Transactions of ASME*, Vol. 42, 641-646.
- Lade, P. V. and Duncan (1973), "Cubical triaxial test on cohesionless soil", *Journal of Soil Mechanics and Foundation Division*", ASCE, 99(SM10): 793-812.
- Lade, P. V. and Duncan (1975), "Elasto-plastic stress-strain theory for cohesionless soil", *Journal of the Geotechnical Engineering Division, ASCE*, 101(GT10):1037-1-53.
- Lade, P. (1977), "Elasto-plastic stress-strain theory for cohesive soil with curved yield surfaces", *Int. Journal of Solids and Structures*, 13(11): 1019-1035.
- Lade, P. V. (1997), "Rotational kinematic hardening model for sand. Part 1: Concept of rotating yield and potential surfaces", *Computers and Geotechnics*, 21, 183-216.
- Lade, P.V. and Pradel, D. (1990), "Instability and plastic flow of soils, 1: Experimental observations", *J. Engineering mechanics, ASCE*, 116(11), 2532-2550.
- Leroueil, S. (1997), "Critical state soil mechanics and the behavior of real soils", *Symposium on Recent Developments in Soil and Pavement mechanics, Rio de Janeiro, Brazil*, 1-40.
- Li, X.S. and Dafalias, Y.F. and Wang, Z-L. (1999), "State dependent dilatancy in critical state constitutive modeling of sand", *Can. Geotech. J.* 36, 599-611.
- Li, X. S. and Dafalias, Y. F. (2000), "Dilatancy for cohesionless soils", *Geotechnique*, 50(4): 449- 460.
- Li, X. S. and Dafalias, Y. F. (2002), "Constitutive modeling of inherently anisotropic sand behavior", *Journal of Geotechnical and Geoenvironmental Engineering, ASCE*, 128(10): 868-880.
- Li, X.S. and Dafalias, Y.F. (2004), "A constitutive framework for anisotropic sand including non-proportional loading", *Geotechnique*, 54(1), 41-55.
- Luong, M.P. and Sidaner, J.F. (1981), "Undrained behavior of cohesionless soils under cyclic and transient loading", *Proc., Int. Conf. on Recent Advances in Geotech. Earthquake Eng. And Soil Dynamics*, Vol. 1, 215-221.

- Manzari, M. T. and Dafalias, Y. F., 1997, A critical state two-surface plasticity model for sand,  
*Geotechnique*, 47(2), 255-272.
- Martin, G.R., Finn, W.D.L., and Seed, H.B. (1975), “Fundamentals of Liquefaction Under Cyclic Loading”, *Journal of Geotechnical Engineering Division, ASCE*, 101(GT5): 423-438.
- Masad, E., Muhunthan, B., Chameau, J. (1998), “Stress-strain model for clays with anisotropic void ratio distribution”, *Int. J. Numerical and Analytical Meth. In Geomechanics*, 22(5), 393-416.
- Masad, E., and Muhunthan, B. (2000), “Three-dimensional characterization and simulation of anisotropic fabric”, *Journal of Geotechnical and Geoenvironmental Engineering*, 126(3):199-207.
- Masing, G. (1920), “Eigenspannungen and verfestigung beim messing”, *Proceedings of the Int. Cong. of Appl. Mech., Zurich, Switzerland*.
- Mehrabadi, M. M. and Nemat-Nasser, S. (1983), “Stress, Dilatancy, and Fabric in granular materials”, *Mechanics of Materials*, 2 :155-161.
- Mehrabadi, M. M., Nemat-Nasser, S., and Oda, M. (1982), “On statistical description of stress and fabric in granular materials”, *Int. Jour. Num. Anal. Meth. Geomech.* 6(1): 95-108.
- Mindlin, R.D. (1949), “Compliance of Elastic Bodies in Contact”, *Journal of Applied Mechanics, Trans. ASME*, 71:255-229.
- Molenkamp, F. (1981), *Elasto-plastic double hardening model MONOT*, LGM Report CO-218595, Delft Soil Mechanics Laboratory.
- Mooney, M.A, Viggiani, G., and Finno, R.J. (1997), “Undrained shear band deformation in granular media”, *Journal of Engineering Mechanics, ASCE*, 123(6):577-585.
- Mooney, M.A., Finno, R.J. and Viggiani, M.G. (1998), “A unique critical state for sands?”, *ASCE, J. Geotech. And Geoenv. Eng.*, 124 (11), 1100-1107.
- Mroz, Z. (1967), “On the description of anisotropic work-hardening”, *Journal of the Mechanics and Physics of Solids*, 15: 163-175.
- Mroz, Z. (1969), “An attempt to describe the behavior of metals under cyclic loads using a more general work-hardening model”, *Acta Mechanica*, 7: 199-212.

- Mroz, Z. and Norris, V.A. (1982), “Elastoplastic and viscoplastic constitutive models for soils with application to cyclic loading”, *Soil Mechanics – Transient and Cyclic Loads*, Pande, G.N. and Zienkiewicz, O.C. (eds.), John Wiley and Sons, Chapter 8, 173-217.
- Mroz, Z., Norris, V.A., and Zienkiewicz, O.C. (1979), “Application of an anisotropic hardening model in the analysis of elastoplastic deformation of soils”, *Geotechnique*, 29(1): 451-469.
- Mroz, Z., Norris, V.A., and Zienkiewicz, O.C. (1981), “An anisotropic, critical state model for soils subjected to cyclic loading”, *Geotechnique*, 31, 451-469.
- Mroz, Z. (1998), “Elastoplastic and viscoplastic constitutive models for granular materials behavior of granular materials”, Cambou, B (ed) *CISM courses and lectures No 385*, Springer, Wien, New York, 269-337.
- Muhunthan, B., Chameau, J., and Masad, E. (1996), “Fabric effects on the yield behavior of soils”, *Soils and Foundations*, 36(3), 85-97.
- Muhunthan, B. and Schofield, A.N. (2000), “Liquefaction and Dam Failures”, In: *Slope Stability 2000*, ASCE Geotechnical special publication No.101, Proc. of sessions of Geo-Denver 2000, 266-280.
- Muhunthan, B., and Olcott, D. (2002), “Elastic energy and shear work”, *Geotechnique*, 52(7), 541-544.
- Muhunthan, B., Pillai, V.S. and Olcott, D. (2004). Measurement of energy and strength of sand at critical state. *ASTM. Geotechnical Testing Journal*, 27, No 2, 1-7.
- National Research Council (1985), “Liquefaction of soils during earthquakes”, Committee on Earthquake Engineering, Commission on Engineering and Technical Systems.
- Niemunis, A., Wichtmann, T. and Triantafyllidis, Th. (2005), “A high-cycle accumulation model for sand”, *Computers and Geotechnics*, 32, 245-263.
- Nixon, S.A. and Chandler, H.W. (1999), “On the elasticity and plasticity of dilatant granular materials”, *J. Mech. Phys. Solids*, 47: 1397-1408.
- Noorzad, A. (1998), “Cyclic behavior of cohesionless granular media using the compact state concept”, PhD thesis, Concordia University.

- Nova, R and Wood, D.M. (1979), "A constitutive model for sand in triaxial compression", *Int. J. Numerical and Analytical Meth. In Geomechanics*, 3, 255-278.
- Nova, R. (1982), "A constitutive model for soil under monotonic and cyclic loading", In: *Soil mechanics- cyclic and transient loads*, Pande, G.N and Zienkiewicz, O.C. (ed.), Chichester: Wiley: 343-376.
- Oda, M. (1972), "The mechanism of fabric changes during compressional deformation of sand", *Soils and Foundations*, 12(2):1-18.
- Oda, M. (1975), "On stress-dilatancy relation of sand in simple shear test", *Soils and Foundations*, 15(2):17.
- Oda, M., Nemat-Nasser, S., and Mehrabadi, M.M., (1982), "A Statistical Study of Fabric in a Random Assembly of Spherical Granulates", *Int. Jour. Num. Anal. Meth. Geomech.* 6(1): 77-94.
- Oda, M., Nemat-Nasser, S. and Konishi, J. (1985), "Stress-induced anisotropy in granular masses", *Soils and Foundations*, 25(3): 85-97.
- Oda, M. (1993), "Inherent and induced anisotropy in plasticity theory of granular soils", *Mechanics of Materials*, 16:35-45.
- Ohmaki, S. (1979), "A mechanical models for the stress-strain behavior of normally consolidated cohesive soil", *Soils and Foundations* 3(19): 29-44.
- Olcott, D.L (2001). *Energy dissipation and critical state strength of sand*, M.Sc. Thesis, Washington State University
- Papadimitriou, A.P., Dafalias, Y.F. and Yoshimine, M. (2005), "Plasticity modeling of the effect of sample preparation method on sand response", *Soils and Foundations*, 40(2), 109-124.
- Pastor, M., Zienkiewicz, O.C., and Leung, K.H (1985), "Simple model for transient soil loading in earthquake analysis, Part II: Non-associative models for sands", *Int. J. Numerical and Analytical Meth. In Geomechanics*, 9, pp.151-190.
- Pastor, M., Zienkiewicz, O.C., and Chan, A.H.C. (1990), "Generalized plasticity and the modeling of soil behavior", *Int. J. Numerical and Analytical Meth. In Geomechanics*, 14, pp.151-190.

- Philofsky, E.M. and Finn, J.E. (1967), "A New method for Measuring Strain Distribution", In: Stereology, Proc. 2<sup>nd</sup> Int. Congress for Stereology, Chicago, Springer, Berlin.
- Pietruszczak, S., Krucinski, D. (1989), "Description of anisotropic response of clays using a tensorial measure of structural disorder", *Mechanics of Materials*, 8: 237-249.
- Poorooshasb, H.B., Holubec, I., and Sherbourne, A.N. (1967), "Yielding and flow of sand in triaxial compression", *Canadian Geotechnical Journal*, 4(4), Part II and III: 376-399.
- Poorooshasb, H. B. (1989), "Description of flow of sand using state parameters", *Computers and Geotechnics*, 8, 195-218.
- Prager, W. (1955), "The theory of plasticity – A survey of recent achievements", *Proceedings of the Institution of Mechanical Engineers*, London, vol. 169, 41-57.
- Prager, W. (1956), "A new method of analyzing stresses and strains in work-hardening plastic solids", *Journal of Applied Mechanics*, ASME, Vol.23, 493-496.
- Prevost, J.H. and Hoeg, K. (1975), "Effective stress-strain-strength model for soils, *Journal of Geotechnical Engineering*, 101(3):257-288.
- Prevost, J.H. (1977), "Mathematical modeling of monotonic and cyclic undrained clay behavior", *Int. J. Numerical and Analytical Meth. In Geomechanics*, 1(2):195-216.
- Prevost, J.H. (1985), "A simple plasticity theory for frictional cohesionless soils", *Journal of Soil Dynamics and Earthquake Engineering*, 4(1):9-17.
- Radjai, F., Wolf, D.E., Jean, M., and Roux, S., and Moreau, J-J. (1997). Force networks in dense granular media. In *Powders and grains* (eds R.P. Behringer and J.T. Jenkins), pp. 211- 214. Rotterdam: Balkema.
- Reynolds, O. (1885), "On the dilatancy of media composed of rigid particles in contact. With experimental illustrations", *Phil. Mag.* 20, 469-482.
- Reynolds, O. (1885), "On an Inversion of Ideas as to the Structure of the Universe", Rede Lecture, Cambridge University Press, Cambridge.
- Richart, F. E. Jr., Hall, J. R. & Woods, R. D. (1970), *Vibrations of soils and foundations*, International Series in Theoretical and Applied Mechanics, Englewood Cliffs, NJ: Prentice-Hall.

- Riemer, M.F. and Seed, R.B. (1997), "Factors affecting apparent position of steady-state line", *Journal of Geotechnical and Geoenvironmental Engineering*, ASCE, 123(3):281-288.
- Roscoe, K. H., Schofield, A. N. & Wroth, C. P. (1958). On the yielding of soils. *Geotechnique* 8, No. 1, 22-53.
- Roscoe, K. H. and Schofield, A. N. (1963), "Mechanical behavior of an idealized 'wet-clay'", In: Proc. of the European conference on SMFE, Wiesbaden: 47-54.
- Roscoe, K. H., Schofield, A. N. & Thurairajah, A. (1963), "Yielding of clays in states wetter than critical", *Geotechnique* 13(3), 211-240.
- Roscoe, K. H. and Burland, J. B. (1968), "On the generalized stress-strain behavior of wet clays", *Engineering Plasticity*, University Press, Cambridge, 535-609.
- Rowe, P.W. (1962). The stress-dilatancy relation for static equilibrium of an assembly of particles in contact. *Proc. Roy. Soc. A*. 269:500-527.
- Santamarina, J.C. and Cho, G.C. (2001), "Determination of critical state parameters in sandy soils – simple procedure", *Geotechnical Testing Journal*, 24(2), 185-192.
- Satake, M. (1989). Stress and strain in granular materials, *Mechanics of granular materials*, Japanese Society of Soil Mechanics and Foundation Engineering, 1-15
- Schofield A.N. and Wroth, P. (1968), *Critical State Soil Mechanics*, McGraw-Hill.
- Schofield, A.N. (1980), "Cambridge Geotechnical Centrifuge Operations", *Geotechnique*, 30(3), 227-268.
- Schofield, A.N. (1982), "Dynamic and earthquake geotechnical centrifuge modeling", *Proc. Int. Conf. on Recent Advances in Geotech. Earthquake Eng. and Soil Dynamics*, Vol.3, St.Louis, 1081-1100.
- Schofield, A.N. (2000), "Behavior of soil paste continuum", In: *Developments in Theoretical Geo-mechanics*, The John Booker memorial symposium, Balkema, Rotterdam, 253-266.

- Schofield A.N (2005), *Disturbed soil properties and geotechnical design*, Thomas Telford.
- Scott, R.F (1987), “Constitutive relations for soil: Present and future”, in Saada and Bianchini(ed.), Proc. Int. Workshop on Constitutive Equations for Granular Non-Cohesive soils, Balkema, Rotterdam, 723-726.
- Seed, H.B. and Lee, K.L (1966), “Liquefaction of saturated sands during cyclic loading”, J. Soil mechanics and Foundation division, ASCE, 92, SM9, 1249-1273.
- Seed, H.B. (1979), “Soil liquefaction and cyclic mobility evaluation for level ground during earthquakes”, Journal of Geotechnical Engineering, 105(2):201-255.
- Shamoto, Y., Zhang, J-M, and Goto, S. (1997), “Mechanism of large post-liquefaction deformation in saturated sand”, Soils and Foundations, 37(2), 71-80.
- Shu Shanzhi (2005), “Sand state and performance analysis of micro piles”, PhD thesis, Washington State University.
- Sribalaskandarajah, K. (1996), “A Computational Framework for Dynamic Soil-Structure Interaction Analysis, PhD thesis, University of Washington.
- Sladen, J.A, D’Hollander, R.D, and Krahn, J. (1985), “The liquefaction of sands, a collapse surface approach”, Can. Geotech. J., 22: 522-526.
- Stroud, M. A. (1971). “The behavior of sand at low stress levels in the simple shear apparatus”, PhD thesis, Cambridge University.
- Suiker, A.S.J and Fleck, N.A (2004), “Frictional collapse of granular assemblies”, Journal of Applied Mechanics, ASME, 71:350-358.
- Tatsuoka, F. and Ishihara, K. (1974), “Yielding of sand in triaxial compression”, Soils and Foundations, 14(2): 63-76.
- Taylor, D.W. (1948), *Fundamentals of soil mechanics*, John Wiley, New York.
- Terzaghi, K, Peck, R. B., & Mesri, G. (1996). *Soil mechanics in engineering practice 3<sup>rd</sup> Ed.* John Wiley & Sons, Inc.
- Thurairajah, A. (1961), “Some properties of kaolin and of sand”, PhD thesis, University of Cambridge.

- Tobita, Y. (1989), "Fabric tensors", *Mechanics of Granular Materials*, Report from TC-13, ISSMFE, M. Satake ed., Rio de Janeiro, 6-9.
- Tseng, N.T., and Lee, G.C. (1983), "Simple Plasticity Model of Two-Surface Type", *Journal of Engineering Mechanics*, ASCE, 109:795-810.
- Tsutsumi, S., and Hashiguchi, K. (2005), "General non-proportional loading behavior of soils", *International Journal of Plasticity*, 21(10): 1941-1969
- Vaid, Y.P., Sivathayalan, S. and Stedman, D. (1999), "Influence of specimen-reconstituting method on the undrained response of sand", *Geotechnical Testing Journal*, 22(3), 187-195.
- Verdugo (1992). Discussion of "The critical state of sand". *Geotechnique* 42, 655-658.
- Vemmer (1978), "A double hardening model for sand", *Geotechnique* 28(4), 413-433.
- Wan, R.G. and Guo, P.J. (2001), "Drained cyclic behavior of sand with fabric dependence", *Journal of Engineering Mechanics*, 127 (11): 1106-1116.
- Wan, R.G. and Guo, P.J. (2004), "Stress dilatancy and fabric dependencies on sand behavior", *Journal of Engineering Mechanics*, 130 (6): 635-645.
- Wang, Z.L., Dafalias, Y.F., Li, X.S. and Maksidi, F.I. (2002), "State pressure index for modeling sand behavior", *ASCE. J. Geotech. and Geoenviron. Eng.*, 128, 511-519.
- Wood, D. M. (1990), *Soil behavior and critical state soil mechanics*, University Press, Cambridge.
- Wood (2001). Discussion of "Influence of the structure on the mechanical behaviour of sand."  
In *Constitutive and Centrifuge Modelling: Two extremes*. Ed. Sarah Springman, A.A. Balkema, 227-229.
- Wood, D.M (2004), "Experimental inspiration for kinematic hardening soil models", ASCE.  
*Journal of Eng. Mechanics*, 130(6), 656-664.
- Wood, D. M., Belkher, K. and Liu, D. F., (1994). "Strain softening and state parameters for sand modeling", *Geotechnique*, 44(2), 335-339

- Wroth, C.P. and Bassett, R.H. (1965), "A stress-strain relationship for the shearing behavior of a sand", *Geotechnique* 15(1), 32-56
- Yang, Z., Elgamal, A. and Parra, E. 2003, "Computational model for cyclic mobility and associated shear deformation", *ASCE. J. Geotech. and Geoenviron. Eng.*, 129(12): 1119-1127.
- Yoshimine, M., Ishihara, K. and Vargas, W. (1998), "Effects of principal stress direction and intermediate principal stress on undrained shear behavior of sand", *Soils and Foundations*, 38(3): 177-186.
- Yasufuku, N. (1990), "Yielding characteristics and constitutive equation of anisotropically consolidated sand in wide range of loading, PhD Thesis, Kyu-syu University.
- Zienkiewicz, O.C. and Mroz, Z. (1984), "Generalized plasticity formulation and applications to geomechanics", *Mechanics of Engineering Materials*, Desai, C.S. and Gallagher, R.H. (eds.), John Wiley, Chapter 33, pp. 655-679.
- Zhang, J-M, Shamoto, Y. and Tokimatsu, K. (1997), "Moving critical and phase-transformation stress state lines of saturated sand during undrained cyclic shear", *Soils and Foundations*, 37(2), 51-59.
- Zhang, J-M, Shamoto, Y. and Tokimatsu, K. (1999), "Cyclic critical stress states of sand with non frictional effects", *ASCE, J. Eng. Mech.* 125(10), 1106-1114.
- Zhu, H., Mehrabadi, M.M., and Massoudi, M. (2006), "Three-dimensional constitutive relations for granular materials based on the dilatant double shearing mechanism and the concept of fabric", *Journal of Plasticity*, 22(5): 826-857.
- Ziegler, H. (1959), "A modification of Prager's hardening rule", *Quarterly Applied Mathematics*, Vol. 17, 55-65.